

27/6 616
28/6/83
Indian J Pure & Appl Phys, Vol 21 No 2, pp 69-132
February 1983

293
27/6/83
CODEN : IJOPAU ISSN : 0019-5596
21(2) 69-132 (1982)

INDIAN JOURNAL OF PURE & APPLIED PHYSICS



Published by
PUBLICATIONS & INFORMATION DIRECTORATE, CSIR
NEW DELHI

in association with
THE INDIAN NATIONAL SCIENCE ACADEMY, NEW DELHI



EVER ONWARD

India is the recipient of congratulations from all over the world for the success achieved by us as hosts of the 9th Asian Games.

Stadia were built in record time. Colour television brought the games live into millions of homes all over the country and abroad. Computers, electronic exchanges, micro-wave and satellite links were smoothly and efficiently utilised in a mammoth network of services.



An apt example of what united endeavour and hard work can achieve.

Similar success can be achieved in other spheres of national development if we work in the same spirit.

LET US ALL JOIN HANDS TO BUILD A STRONG NATION

Indian Journal of Pure & Applied Physics

EDITORIAL BOARD

Prof. D Basu
Indian Association for
the Cultivation of Science
Calcutta

Prof. Probir Roy
Tata Institute of Fundamental
Research
Bombay

Prof. B Buti
Physical Research Laboratory
Ahmedabad

Prof. E S Raja Gopal
Indian Institute of Science
Bangalore

Prof. S C Dutta Roy
Indian Institute of Technology
New Delhi

Prof. G Rajasekaran
Madras University
Madras

Dr R Hradaynath
Instruments Research & Development
Establishment Dehra Dun

Dr A P B Sinha
National Chemical Laboratory
Pune

Prof. D Premaswarup
Nagarjuna University
Nagarjuna Nagar

Prof. C V Vishveshwara
Raman Research Institute
Bangalore

Prof. A N Mitra
Indian National Science Academy
New Delhi/University of Delhi
Delhi

Prof. M S Sodha
Indian National Science Academy
New Delhi/Indian Institute of
Technology New Delhi

Shri Y R Chadha, *Ex-officio* Secretary & Chief Editor

EDITORIAL STAFF

• Editors

D S Sastry, K S Rangarajan & R P Goel

Assistant Editors

G N Sarma, J B Dhawan & Tarun Banerjee

Scientific Assistant

(Mrs) Poonam Bhatt

Published by the Publications & Information Directorate, CSIR, Hillside Road, New Delhi 110012

Chief Editor: Y R Chadha

The Indian Journal of Pure & Applied Physics is issued monthly. The Directorate assumes no responsibility for the statements and opinions advanced by contributors. The editorial staff in its work of examining papers received for publication is assisted, in an honorary capacity, by a large number of distinguished scientists, working in various parts of India.

Communications regarding contributions for publication in the journal should be addressed to the Editor, Indian Journal of Pure & Applied Physics, Publications & Information Directorate, Hillside Road, New Delhi 110012.

Correspondence regarding subscriptions and advertisements should be addressed to the Sales & Distribution Officer, Publications & Information Directorate, New Delhi 110012.

Annual Subscription

Rs. 120.00 £20.00 \$45.00

Single Copy

Rs. 12.00 £2.00 \$4.50

50% Discount is admissible to research workers and students and 25% discount to non-research individuals, on annual subscription. Payments in respect of subscriptions and advertisements may be sent by cheque, bank draft, money order or postal order marked payable *only* to **Publications & Information Directorate, New Delhi 110012**. Claims for missing numbers of the journal will be allowed only if received within 3 months of the date of issue of the journal plus the time normally required for postal delivery of the journal and the claim.

Indian Journal of Pure & Applied Physics

VOLUME 21

NUMBER 2

FEBRUARY 1983

CONTENTS

Solid State Physics

- X-ray, Crystal Data, Magnetic Susceptibility & Electrical Conductivity of Hydrated Trinickel Pentasulphide 69
J P Mishra & Mrs Lakshmi*
- Modified Two-Phase Model for the Mechanical Properties of the Semicrystalline Polymer—Polyethylene 73
P K Biswas*, S Sengupta & A N Basu
- Hydrogen Pretreatment of CdS Films and Properties of CdS/NaOH/Pt Cells 78
C D Lokhande, M D Uplane & S H Pawar*

Chemical Physics

- Force Field for In-Plane Vibrations of *trans-cis*-Diacetamide: Use of CNDO/Force Method 82
A Annamalai & Surjit Singh*
- Spectral Studies on New Dioxouranium(VI) Complexes of Tridentate Schiff Bases Derived from Salicylhydrazide & Salicylaldehyde or Substituted Salicylaldehydes 87
A Syamal* & D Kumar
- Reference Interaction Site Model (RISM) for the Liquid Structure of Oxygen, Chlorine & Iodine 92
R V Gopala Rao* & B M Satpathy

Theoretical & Mathematical Physics

- Interacting Bosons and Properties of Liquid ^4He II 97
K M Khanna, S Chauba Singh* & O P Sinha
- Bound *s*-State Energies for Superposed Screened Coulomb Potential in Ecker-Weizel Approximation 103
A P Kajwadkar & L K Sharma*

Nuclear Physics

- Low Energy Spectrum & Directional Correlation Measurements in ^{187}Re 107
K Singh, B S Grewal, Raj Mittal & H S Sahota*

Spectroscopy

- Vibrational Spectra of Phosphotungstate Ion— $\text{PW}_{12}\text{O}_{40}^{3-}$ 112
S Sheik Saleem & G Aruldas*

NOTES

- Crystallization of Amorphous Mercury Selenide Films 116
K N Sharma & K Barua*
- Viscosity of Binary Liquid Mixtures in Hard-Sphere Approximation 119
Harminder*

Continued overleaf

CONTENTS

Force Field Study of Some Non-linear XY_2 -type Molecules	121
S Mohan*, S Gunasekaran & K G Ravikumar	
Dipole Moments of Dichlorotoluenes in Benzene Solution	123
Jai Prakash*, Bashishth Rai & Rahul	
Uranium Estimation in Mussoorie Phosphorites using Solid State Nuclear Track Detector	125
Surinder Singh & H S Virk*	
Electronic Spectral Study of Praseodymium (III) Complexes with Cysteine & Diols ...	127
Ashol Kothari, Sudhindra N Misra* & M P Bhutra	
Spectroscopic Studies of Oxovanadium (IV) Complexes of Biguanide, Dibiguanides & o-Methyl-1- amidinourea	130
A Syamal*	

The Author to whom all correspondence is to be addressed is indicated by the () mark.

X-ray, Crystal Data, Magnetic Susceptibility & Electrical Conductivity of Hydrated Trinickel Pentasulphide

J P MISHRA & Mrs LAKSHMI*

Department of Chemistry, University of Gorakhpur, Gorakhpur

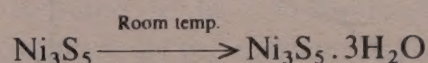
Received 28 December 1981; revised received 29 October 1982

The compound, hydrated trinickel pentasulphide, has been prepared in solid state condition. X-ray powder diffraction pattern of the compound shows cubic structure with $a = 8.503 \text{ \AA}$ and $Z = 3$. The magnetic susceptibility measurement shows that the compound is paramagnetic in the temperature range 305-715 K with Curie constant $C = 1.62 \text{ K emu/mol}$ and effective magnetic moment $p = 3.60 \mu_B$ (Bohr magneton). The electrical conductivity measurement explains the impurity levels and intrinsic semiconducting behaviour in the temperature range 313-433 K and 533-713 K with activation energy 0.05 and 0.60 eV respectively. Above 713 K, the compound becomes metallic. Thermogravimetric analysis and differential thermal analysis data indicate the presence of nonstoichiometric compound and dehydration step. The density of the compound is found to be $3.20 \pm 0.10 \text{ g/cc}$.

1 Introduction

The compound hydrated trinickel pentasulphide shows very interesting solid state properties of transition metal sulphides. The compound has been prepared¹ in solid state condition and analyzed to confirm the stoichiometric formula. Crystal structure, magnetic properties, thermal analysis, density measurement and electrical conductivity measurement of this compound have been reported in this paper. The compound is black and is stable up to 440°C . In the range $440-660^\circ\text{C}$ it becomes nonstoichiometric having the formula $\text{Ni}_3\text{S}_{5-x}$ ($x = 0.3$) which is stable up to 900°C . Above 900°C it again becomes $\text{Ni}_3\text{S}_{5-(x+y)}$ ($x = 0.3, y = 0.1$). The compound is paramagnetic and semiconducting up to 713 K and above 713 K it becomes metallic. By X-ray analysis of the compound, it is found to be cubic with a unit cell dimension (a) of 8.503 \AA and number of molecules per unit cell (z) equal to 3. Agreement between observed and calculated $\sin^2 \theta_{hkl}$ values (Table 1) was found to be satisfactory. The density of the compound is $3.20 \pm 0.10 \text{ g/cc}$.

$x \approx 1$, surplus oxygen



The identification of hydrated trinickel pentasulphide¹ was carried out by chemical analysis of Ni and S, 47 and 39% (observed value) against 45.1 and 41% (calculated value) respectively. Further, the compound was identified by powder X-ray diffraction pattern of reactants (S_8 and $\text{NiO}_{1+x} \cdot \frac{1}{3}\text{H}_2\text{O}$) and product ($\text{Ni}_3\text{S}_5 \cdot 3\text{H}_2\text{O}$). On comparing the intensities and the d -values, neither the strong, medium lines of sulphur nor the strong, medium lines of nickel oxide are present in the X-ray powder diffraction pattern of $\text{Ni}_3\text{S}_5 \cdot 3\text{H}_2\text{O}$. New strong and medium lines, appearing in the X-ray powder diffraction pattern of the product, given in Table 1, show the formation of new compound $\text{Ni}_3\text{S}_5 \cdot 3\text{H}_2\text{O}$.

2 Experimental Details

Fresh nickel oxide¹, $\text{NiO}_{1+x} \cdot \frac{1}{3}\text{H}_2\text{O}$ ($x \approx 1$, surplus oxygen) (100 mesh), prepared from basic nickel carbonate $[\text{NiCO}_3\text{Ni}(\text{OH})_2 \cdot 4\text{H}_2\text{O}]$ (100 mesh), (Sarabhai) and cyclo-octasulphur, S_8 (100 mesh), (BDH) were mixed in 3:1 molar ratio and crushed in agate mortar. The mixture was heated in an air oven at $105 \pm 1^\circ\text{C}$ for 17 hr till its weight became constant. The process of heating and crushing was repeated several times in order to get the homogeneous compound (hydrated trinickel pentasulphide). The reaction takes place as shown in the following:

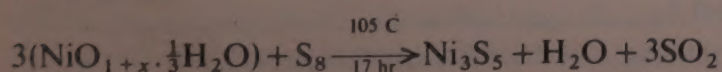


Table 1—Crystal Data for $\text{Ni}_3\text{S}_5 \cdot 3\text{H}_2\text{O}$

$d(\text{\AA})$	$\sin^2 \theta_{hkl}$		hkl	I/I_0
	Obs.	Calc.		
4.5521	0.0286	0.0246	111	37.5
4.2502	0.0328	0.0328	200	100
3.3885	0.0517	0.0492	211	13.1
2.9688	0.0674	0.0656	220	22.4
2.8400	0.0736	0.0738	300	29.2
2.7223	0.0801	0.0820	310	15.4
2.5707	0.0899	0.0902	311	17.0
2.5425	0.0919	0.0984	222	17.0
2.3382	0.1086	0.1066	320	22.4
2.1270	0.1313	0.1312	400	9.2
2.0018	0.1483	0.1476	411	8.9
1.7217	0.2004	0.1968	422	16.5
1.7098	0.2032	0.2050	430	19.0

The powder X-ray diffraction pattern has been taken with X-ray diffractometer using Cu-K α radiation at the Bhabha Atomic Research Centre, Bombay. The pattern was indexed by Hesse-Lipson's method².

The molar magnetic susceptibility (χ_m) was measured by Faraday's method³ employing a sensitive magnetic balance of least count 10⁻⁵ g and an electromagnet with pole pieces. The experimental technique has been given in detail⁴. The variation of inverse magnetic susceptibility with temperature is shown in Fig. 1.

For the electrical conductivity (σ) measurement, powdered samples were pelletized at the high pressure (8 \times 10³ kg cm⁻²) using a hydraulic pressure and a suitable die. The conductance was measured with a Toshniwal

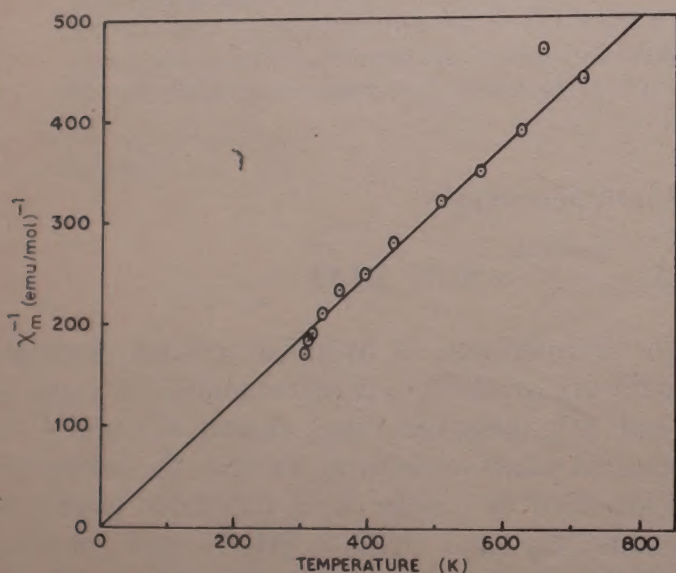


Fig. 1—Inverse molar magnetic susceptibility χ_m^{-1} versus T for $\text{Ni}_3\text{S}_5 \cdot 3\text{H}_2\text{O}$

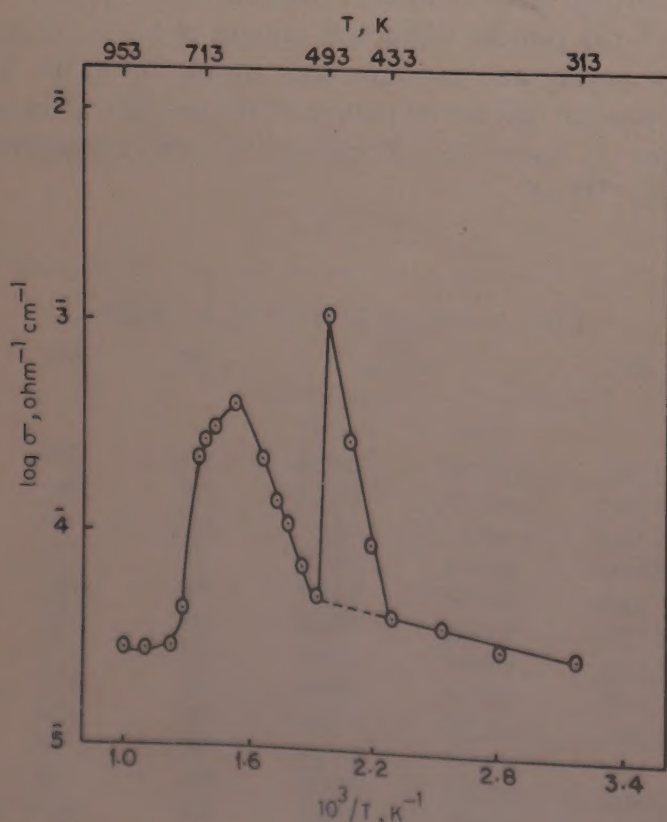


Fig. 2—Variation of $\log \sigma$ versus $10^3/T$, for $\text{Ni}_3\text{S}_5 \cdot 3\text{H}_2\text{O}$ pellet at a pressure 8 \times 10³ kg. cm⁻²

Conductivity Bridge, type CLo1/01A, whose internal operating frequency was 50 Hz using platinum electrodes. The variation of the logarithm of conductance with inverse temperature, presented in Fig. 2, shows the semiconducting and metallic behaviour of the compound. Differential thermogravimetric analysis (DTG), differential thermal analysis (DTA) and thermogravimetric analysis (TGA) of the compound were performed using a recording thermal analyzer (Paulik-Paulik-Erdey MoM derivatograph, Hungary) at the Indian Institute of Technology, Kanpur at a heating rate of 10°C/min. The data obtained by TGA, given in Fig. 3, show a better response against the data of differential thermogravimetric analysis (DTGA) and DTA.

The density measurement was performed by pycnometer of 25 cc capacity using toluene as displacing liquid. The value of observed density is in good agreement with the calculated value (obtained by X-ray powder diffraction pattern).

3 Discussion

The chemical analysis of binary sulphide of nickel has shown the stoichiometry $\text{Ni}_3\text{S}_5 \cdot 3\text{H}_2\text{O}$ which has been

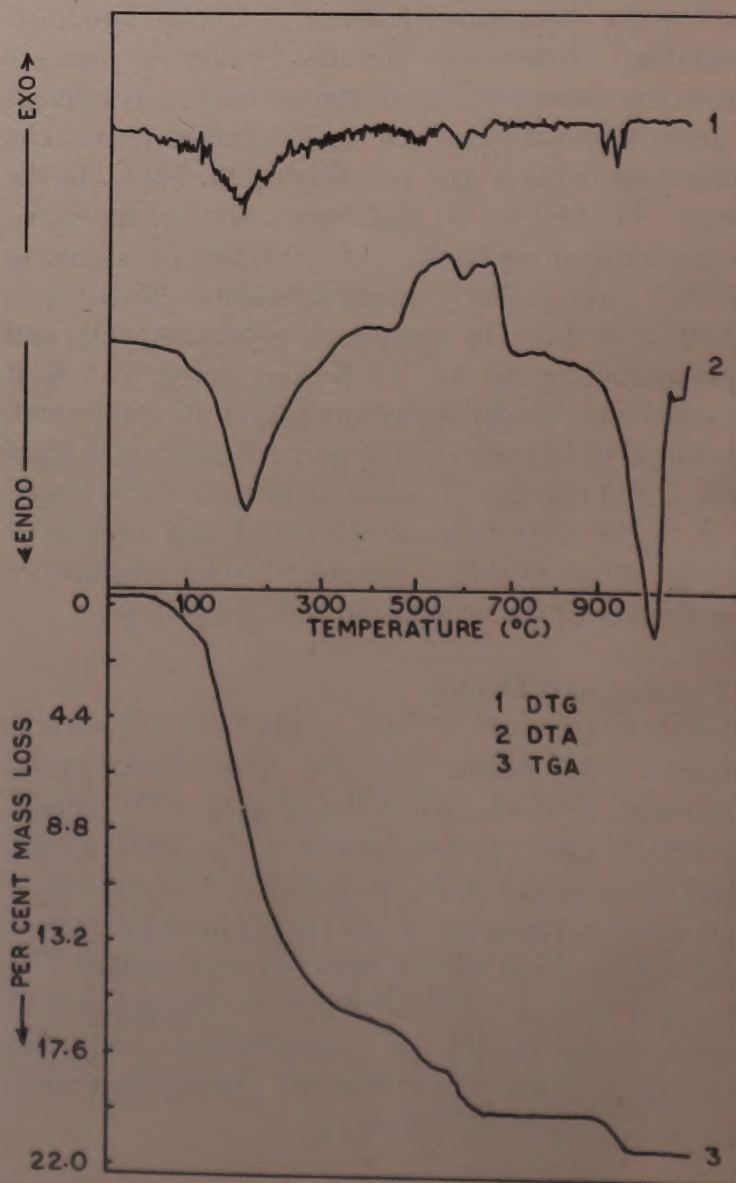
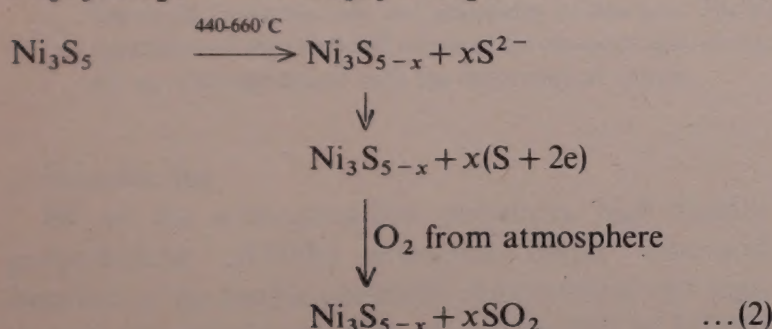
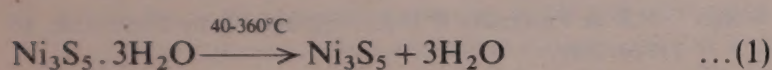


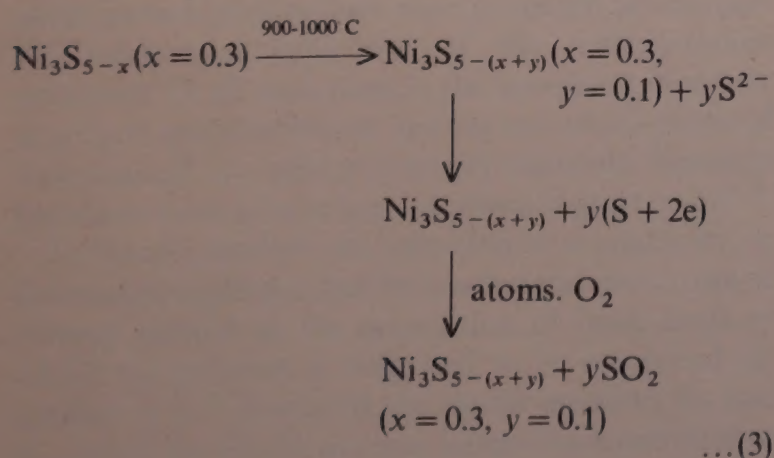
Fig. 3—DTG, DTA and TGA of $\text{Ni}_3\text{S}_5 \cdot 3\text{H}_2\text{O}$

reported¹ earlier. The presence of three moles of water has been confirmed with the help of TGA. TGA of $\text{Ni}_3\text{S}_5 \cdot 3\text{H}_2\text{O}$ indicates the loss of three moles of water up to 300°C, which has further been confirmed by an endotherm at 160°C and the peak at 160°C in DTG given in Fig. 3. Further, a peak at 520°C in DTG, an endotherm at 520°C indicates a weight loss due to escape of sulphur. This has further been confirmed when the pellet of $\text{Ni}_3\text{S}_5 \cdot 3\text{H}_2\text{O}$ was prepared at high pressure ($8 \times 10^3 \text{ kg cm}^{-2}$) and heated from 440-620°C; the pellet became yellow on surface due to the sulphur coming out. This clearly indicates that the weight loss in TG curve in the temperature range 440-660°C might be due to escape of sulphide ions in the form of sulphur and consequently the evolution of SO_2 takes place⁵, which is as follows:



(where $x = 0.3$).

This nonstoichiometric compound $\text{Ni}_3\text{S}_{5-x}$ ($x = 0.3$) remains stable up to 900°C. Further, a weight loss in the temperature range 900-1000°C in TG curve has been confirmed by a peak in DTG as well as an endotherm at 900°C. These observations also indicate that a second type of nonstoichiometric compound $\text{Ni}_3\text{S}_{5-(x+y)}$ (where $x = 0.3$, $y = 0.1$) has been obtained, according to the following scheme as:



The chemical analyses of both nonstoichiometric compounds are in good agreement with the theoretical value.

X-ray powder diffraction pattern of the compound shows new strong peaks on comparing the spectra of reactants. The $\sin^2 \theta_{hkl}$ values have been calculated from

the powder X-ray diffraction pattern. A comparison of observed and calculated $\sin^2 \theta_{hkl}$ values, given in Table 1 indicates that the compound is cubic with unit cell dimension, $a = 8.503 \text{ \AA}$. The number of molecules per unit cell (Z) has been found to be 3, using the following expression:

$$Z = \frac{D \cdot V \cdot N}{M}$$

where D is the observed density, V the volume of cubic system, N the Avogadro number and M the molecular weight of the compound. The value of Z has been obtained in order to calculate X-ray density. The observed density (3.20 g/cc) is found to be comparable against the calculated X-ray density (3.16 g/cc).

A straight line obtained in the plot of inverse molar magnetic susceptibility versus temperature, given in Fig. 1, indicates the presence of paramagnetic centres⁶ within the temperature range 305-713 K.

From this straight line, the value of Curie constant (C) is found to be 1.62 K emu/mol. Effective magnetic moment (p) per molecule, is found to be $3.60 \mu_B$ (Bohr magneton) using the following expression⁶

$$p^2 = \frac{3kC}{N\beta^2}$$

where k is the Boltzmann constant, N the Avogadro number and β the Bohr magneton.

The variation of $\log \sigma$ versus $\frac{10^3}{T}$ is shown in Fig. 2.

This curve can be represented as the resultant of three straight lines, and thus the conductivity (σ) can be expressed as the sum of three contributions σ_1 , σ_2 and σ_3 as follows:

$$\sigma = \sigma_1 + \sigma_2 + \sigma_3$$

$$\begin{aligned} \text{or } \sigma &= C_1 \exp\left(-\frac{W_1}{kT}\right) + C_2 \exp\left(-\frac{W_2}{kT}\right) \\ &+ C_3 \exp\left(-\frac{W_3}{kT}\right) \end{aligned}$$

From the experimental curve, the values (in $\text{ohm}^{-1}\text{cm}^{-1}$) of constants are $C_1 = 7.58 \times 10^{-5}$, $C_2 = 79.43$, $C_3 = 1.66 \times 10^{-2}$ and activation energies (in eV) are $W_1 = 0.05$, $W_2 = 0.95$ and $W_3 = 0.60$. As W_1 is very small, it indicates the presence of impurity band of extrinsic type due to presence of water in the temperature range 313-433 K. Due to dehydration energy, conductivity increases in the temperature range 433-493 K and the energy associated (W_2) is found to be 0.95 eV. As soon as the compound becomes dehydrated, the nonstoichiometric compound $\text{Ni}_3\text{S}_{5-x}$ ($x = 0.3$) shows an intrinsic type of semiconductivity with activation energy $W_3 = 0.60 \text{ eV}$ in the temperature range 533-713 K which can be explained by band

theory⁷. The relevant bands for conduction in this solid are empty ($\text{Ni}^{2+}:3d$) band and filled ($\text{S}^{2-}:3p$) band, where $\text{S}^{2-}:3p$ band is probably the valence band and $\text{Ni}^{2+}:3d$ band is the conduction band of solid. As the temperature is increased from 533 to 713 K, the charge transfer excitation of electron, from the valence band ($\text{S}^{2-}:3p$) to $3d$ conductivity band ($\text{Ni}^{2+}:3d$), takes place and crosses a band gap within the reported⁸ range (1-10 eV). The experimentally observed energy band gap is found to be 1.20 eV. The compound shows metallic behaviour within the temperature range 713-953 K, i.e. conductivity decreases with increase of temperature and becomes constant.

Acknowledgment

The authors are thankful to Prof R P Rastogi, Head, Chemistry Department, University of Gorakhpur and Dr H B Lal, Department of Physics, University of

Gorakhpur for providing necessary facilities. Thanks are also due to the CSIR, New Delhi for financial assistance.

References

- 1 Mishra J P & Mrs Lakshmi, *J Solid State Chem (USA)*, **45** (1982) in press.
- 2 Lipson H & Steeple H, *Interpretation of X-ray powder diffraction patterns* (Macmillan, London) 1970, 155.
- 3 Bates L F, *Modern magnetism* (University Press, Cambridge) 1951.
- 4 Lal H B, Dar N & Kumar A, *J Phys & Chem Solids (GB)*, **7** (1974) 4335.
- 5 Cotton F A & Wilkinson G, *Advanced inorganic chemistry*, (John Wiley, New York) 2nd Edn 1966, 526.
- 6 Martin D H, *Magnetism in solids* (Iliffe Books, London), 1967.
- 7 *Transfer and storage of energy by molecules*, Vol. 4, edited by G M Burnett, A M North and J N Sherwood, (John Wiley, London) 1974.
- 8 Rao C N R & Pisharody K P R, *Prog Solid State Chem (GB)*, **10** (1976) 208.

Modified Two-Phase Model for the Mechanical Properties of the Semicrystalline Polymer—Polyethylene

P K BISWAS* & S SENGUPTA

Solid State Physics Research Centre, Physics Department, Presidency College, Calcutta 700 073

and

A N BASU

Physics Department, Jadavpur University, Calcutta 700 032

Received 28 December 1981; revised received 6 October 1982

A phenomenological model for semicrystalline polymer is proposed which takes into account both variation of crystallinity and orientation of the molecular chains with the direction of draw. The elastic properties of the polymer are calculated in terms of those of the constituent phases as in Takayanagi's model. At the drawn state it has been shown that a partially oriented crystalline phase may be considered as a superposition of a perfectly aligned crystalline portion on a polycrystalline phase. The model contains only two adjustable parameters. The model is applied in the case of high density polyethylene and the agreement of the predicted values of the elastic moduli along the direction of draw and perpendicular to it and shear modulus are in close agreement with the experimental values.

1 Introduction

Of all the semicrystalline polymers, high-density polyethylene (HDPE) attracted major attention because of its simple chemical composition and high degree of crystallinity. The elastic moduli of HDPE along the direction of draw (E_0) and perpendicular to it (E_{90}) and shear modulus (G) have been measured up to a moderately high draw ratio¹.

Recently Mead *et al.*² have measured E_0 up to a very high draw ratio for various temperatures of draw. They have also studied the variation of crystallinity with rate of draw in detail². The theoretical situation, however, remains very unclear. During the last twenty years, several attempts were made and different phenomenological models were proposed to interpret the mechanical behaviour of the semicrystalline polymers. Of all such models the one-phase model or aggregate model of Ward³ and the two-phase model of Takayanagi⁴ are most extensively discussed. Recently the above models have been reviewed in great detail^{5,6}.

In Ward's model³, the variation of crystallinity on drawing is neglected and the mechanical anisotropy is directly related to the orientation of basic units of which the polymer is supposed to be composed of. Hadley *et al.*¹ measured the elastic modulus E_0 and E_{90} and G for HDPE at room temperature and tried to interpret the data in terms of the aggregate model. But the range of predicted values is too large to be meaningful and the experimental values do not even lie in the predicted range in most of the cases (see Figs 1-3). In trying to apply Ward's model in the case of HDPE^{1,2} we investigated if suitable values of C_{11} , C_{33} and $(C_{13} + 2C_{44})$ or S_{11} , S_{33} and $(2S_{13} + S_{44})$ can be

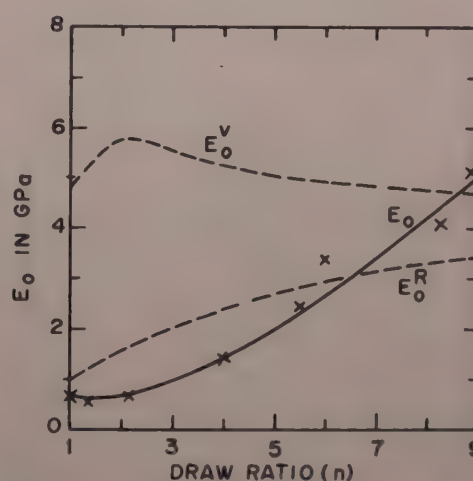


Fig. 1—Comparison of the calculated values of E_0 with experimental values¹ at room temperature [Solid line represents calculated values and experimental values are indicated by \times . E_0^V and E_0^R denote the Voigt and Reuss average as calculated by using the Ward model¹.]

chosen which will fit the experimental values of elastic modulus for different draw ratios. We have found that no consistent set of values exists which can reproduce the experimental results. Moreover, if we try to fit the data for any three draw ratios, the values of the elastic constants (the solution for C_{11} etc. and S_{11} etc.) which we get are absurd as given in Table 1. From Table 1 it can be easily seen that Ward's concept of units with fixed elastic constants seems to breakdown.

The poor agreement found with the Ward model is not surprising, since the model assumes a single phase in contradiction with the experimental observation (see page 310 of Ref. 6). Here Takayanagi model⁴ has relevance in trying to calculate the elastic moduli of the

polymer in terms of those of its constituents. But this model was proposed to explain qualitatively the cross rule of E_0 and E_{90} for highly oriented and well annealed samples in the vicinity of T_g . The model does

not deal with the development of mechanical anisotropy on drawing.

It is well known^{3,7} that crystallinity and orientation are the two most important factors which influence the mechanical properties of polymers. It is also established from experiments^{2,7} that both the factors change on drawing.

We have already proposed^{8,9} a modified two-phase model for polypropylene in which the variation of crystallinity and orientation with rate of draw has been taken into account. A general theoretical procedure for calculating the mechanical anisotropy for a two-phase system has also been proposed by Maeda *et al.*¹⁰ Three-phase models for highly oriented semicrystalline polymers have also been proposed by Takayanagi¹¹ and Prevorsek¹².

In the next section we propose a modified two-phase model in which the variation of crystallinity and orientation has been taken into account. It will be seen from the detailed analysis of the proposed model that at the fully oriented state, the structural features of the proposed model and the Takayanagi model⁴ are identical.

2 Modified Two-Phase Model

In the proposed model the change of crystallinity and the orientation of the molecular chains have been taken into account in the light of structural information available up to date. It is a well known experimental fact that at the undrawn state a polymer is mechanically isotropic. At this stage a polymer is composed of two phases⁷. Of the two phases, the amorphous phase is isotropic. So the universal experimental fact that a polymer is elastically isotropic at the undrawn state demands the crystalline phase to be isotropic as well. Following the discussion of Holliday (see page 258 of Ref. 6), we consider that a semicrystalline polymer at the undrawn state consists of two phases—isotropic polycrystalline phase and isotropic amorphous phase. The only Young's modulus (E) it possesses is given by

$$\frac{1}{E} = \frac{\chi_0}{E_p} + \frac{1 - \chi_0}{E_a} \quad \dots (1)$$

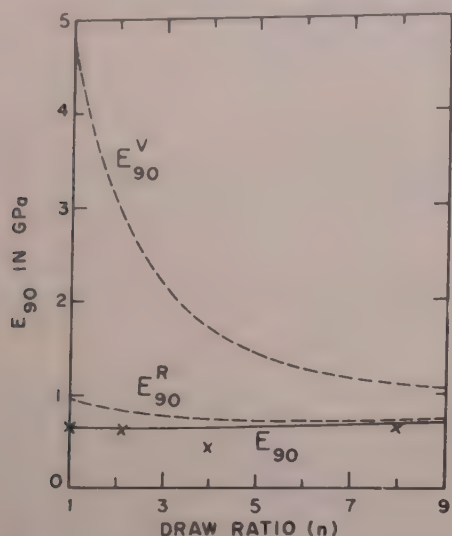


Fig. 2—Comparison of the calculated values of E_{90} with experimental values¹ [Symbols as in Fig. 1]

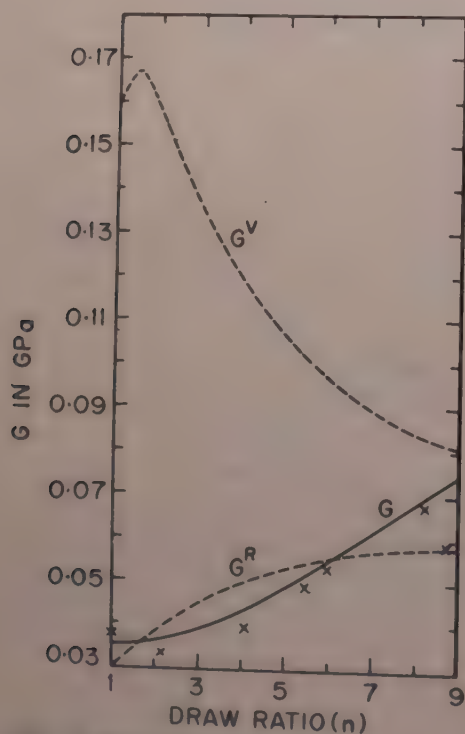


Fig. 3—Comparison of the calculated values of shear modulus G with experimental values¹ [Symbols as in Fig. 1]

Table 1—Elastic Constants Obtained by Fitting E_0 Values for Any Three Draw Ratios in Aggregate Model for HDPE (Semicrystalline Polymer)

Polymer	Draw ratios used	C_{11}	C_{33}	$(C_{13} + 2C_{44})$	S_{11}	S_{33}	$(2S_{13} + S_{44})$
		(in GPa)			(in GPa) ⁻¹		
HDPE ¹	1, 4, 8	16.85	6.75	-36.45	-0.348	-0.361	13.800
HDPE ²	8.5, 18, 27.5	30164.7	79.6	-18035.7	31.574	0.0034	-29.167
(Draw temp = 120°C)							

where E_p and E_a are the Young's modulus of the polycrystalline phase and amorphous phase respectively and χ_0 denotes the volume fraction of crystallinity at the undrawn state.

In the same manner, the value of the shear modulus at the undrawn state is given by

$$\frac{1}{G} = \frac{\chi_0}{G_p} + \frac{1 - \chi_0}{G_a} \quad \dots (2)$$

where G_p and G_a are the shear modulus for the polycrystalline and amorphous phase respectively.

Next we consider the polymer at the drawn state. The X-ray studies⁷ reveal the presence of preferred orientation in the direction of draw. Recent studies¹³ on stretched PVC films indicate that the major contribution to the observed orientation on extrusion originates from the crystalline region of the polymer.

In the Ward model, the elastic constants of the ensemble of partially oriented units have been expressed in terms of the elastic constants of the basic units. A similar procedure cannot be applied in the case of a two-phase system. The real situation in this case is very complex and there is as yet no sufficiently rigorous and consistent theory of the elastic properties incorporating the effect of orientation of the crystalline phase in a two-phase model. We take account of the effect of orientation in a partially oriented crystalline region of the polymer in a simplified manner. It can be easily shown⁸ that so far as the effective elastic behaviour is concerned, the partially oriented crystalline phase of the polymer may be supposed to be the combination of one part consisting of perfectly aligned chains along the draw direction and the remaining portion composed of crystallites arranged at random. From Takayanagi's model⁴ (Fig. 4) it is seen that the stress-strain relation of the whole crystalline phase with the amorphous phase is not the same. A portion of the crystalline phase is in parallel combination with the amorphous phase and this combination is in series with the rest of the crystalline phase. Here we also assume that the amorphous phase is at constant stress condition with the polycrystalline portion of the crystalline phase and this combination is at constant strain condition with the portion of the crystalline phase consisting of crystalline chains having c -axis within a small angle with the draw direction. If χ be the crystallinity at any arbitrary draw ratio n and p be the fraction of the crystalline phase supposed to be composed of perfectly aligned chains, then the volume concentration of amorphous phase and the two fractions of the crystalline phase will be as shown in Fig. 5. A comparison of Figs 4 and 5 reveals that at the highly drawn state when the crystalline chains are almost perfectly aligned to the draw direction, the distribution

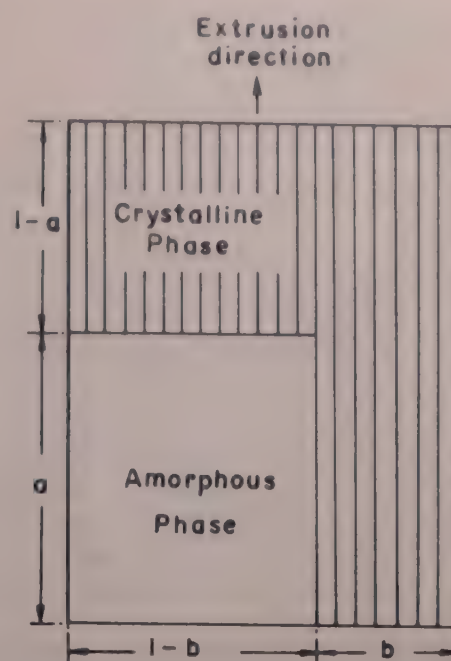


Fig. 4—Schematic diagram of crystalline chains and amorphous phase in Takayanagi's model⁴

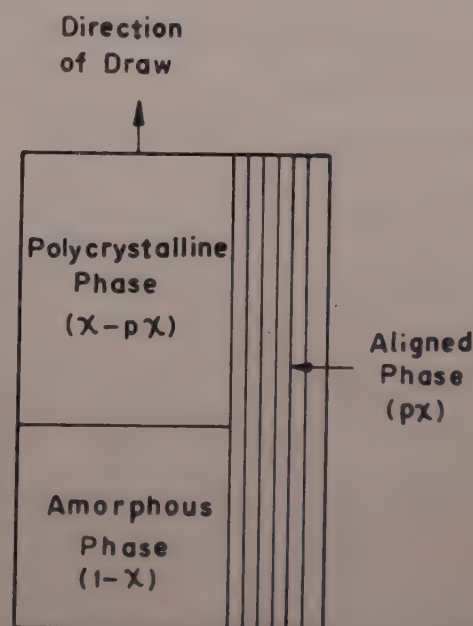


Fig. 5—Symbolic representation of the three phases envisaged in the present model at the drawn state

of different phases in the proposed model and the Takayanagi model will be identical.

Now, so far as the value of p is concerned, it is obvious that it will be some function of the draw ratio (n) with $p = 0$ for $n = 1$. It is also clear³ that p will increase with n and ultimately will reach a maximum value. Unfortunately, the direct experimental information is not available at present. As an alternative we suggest a two-parameter empirical relation obtained by trial and error, given by

$$p = A[1 - \exp\{-(n-1)^2/\beta\}] \quad \dots (3)$$

where A and β are two constants. A represents the maximum value of the fraction of the crystalline

Table 2—Input Data

Elastic moduli ¹⁴ (in GPa)						
$E_{ }^{(c)}$	$E^{(c)}$	$G^{(c)}$	E_p	G_p	E_a	G_A
240	4.00	2.00	5.05	2.00	0.215	0.012

Table 3—The Best Fit Values of Parameters A and β [Eq. (3)] for Different Samples

Substance	Draw temp., °C	A	β	Data Ref.
Rigidex	Not stated	0.05	100	1
Alathon 7050	80	0.16	100	2
	120	0.50	1000	2
	132	0.37	1000	2
	134	0.32	1000	2
	136	0.25	1000	2

portion which may get perfectly aligned along the draw direction and β determines the rapidity with which the maximum value is reached through drawing.

In the light of the above discussion, we can write the expressions for E_0 , E_{90} and G for any n in the same manner as in the Takayanagi model, as given below:

$$E_0 = p\chi E_{||}^{(c)} + (1 - p\chi)E' \quad \dots(4)$$

$$E_{90} = p\chi E_{\perp}^{(c)} + (1 - p\chi)E' \quad \dots(5)$$

$$G = p\chi G^{(c)} + (1 - p\chi)G' \quad \dots(6)$$

$$\text{where } \frac{1}{E'} = \left(\frac{\chi - p\chi}{E_p} + \frac{1 - \chi}{E_a} \right) \cdot \frac{1}{1 - p\chi} \quad \dots(7)$$

$$\text{and } \frac{1}{G'} = \left(\frac{\chi - p\chi}{G_p} + \frac{1 - \chi}{G_A} \right) \cdot \frac{1}{1 - p\chi} \quad \dots(8)$$

where $G^{(c)} = C_{44}^{(c)}$ is the shear modulus for the crystallites.

3 Application

The proposed model is applied for the case of HDPE. The input data and parameters for using Eqs (1) to (6) are given in Tables 2 and 3 respectively. For polyethylene the values of E_p , $E_{||}^{(c)}$, $E_{\perp}^{(c)}$ and G_p are taken from experimental values quoted by Odajima and Maeda¹⁴. The value of E_a is also estimated in accordance with the order of magnitude given by Holliday (see page 261 of Ref. 6). The value of G_A is estimated to give an exact fit at the undrawn state.

The crystallinity corresponding to different draw ratios has been experimentally studied by Mead *et al.*² for different temperatures of draw. Now in order to interpret the E_0 , E_{90} and G values of Hadley *et al.*¹, we have used crystallinity values corresponding to a draw temperature of 60°C in the absence of the actual information of the temperature of draw. The comparison of the experimental values, at room temperature, of E_0 , E_{90} and G and the corresponding

predicted values by the present model and by Ward model¹ is shown in Figs 1-3.

Mead *et al.*² have measured E_0 for HDPE for different temperatures of draw. The experimental values of χ corresponding to 90°C have been used for calculation of E_0 for a draw temperature of 80°C; for E_0 values at draw temperatures 120, 132, 134 and 136°C, we have used crystallinity values corresponding to a draw temperature 134°C. The comparison of the predicted values and the experimental values of E_0 for different values of n , corresponding to different temperatures of draw is shown in Fig. 6.

4 Discussion

From Figs 1-3 it can be seen that at room temperature the predicted values of E_0 , E_{90} and G by the present model are in close agreement with the experimental values¹ and the agreement is much better than those given by Ward model¹ except for the fact that it cannot explain a small dip in E_0 at the initial stage of drawing. This may be due to some decrease of crystallinity at the initial stage of drawing as observed¹⁵ in the case of polypropylene and low density polyethylene¹⁶. In the case of HDPE the experimental values² of crystallinity are not reported for the initial stage of drawing. From Fig. 6 it can be seen that the general agreement between the calculated and experimental values for all the five different temperatures of draw is satisfactory. This model has already been used^{8,9} with success in the case of polypropylene.

The morphology of the polymer is so complex that at this stage all models including the present one are too approximate to tackle the minute peculiarities in different cases. From the moderate success of this model it emerges that both orientation of chains and crystallinity are equally important. These are only two adjustable parameters A and β , whereas in the aggregate model all the five elastic constants of the unit

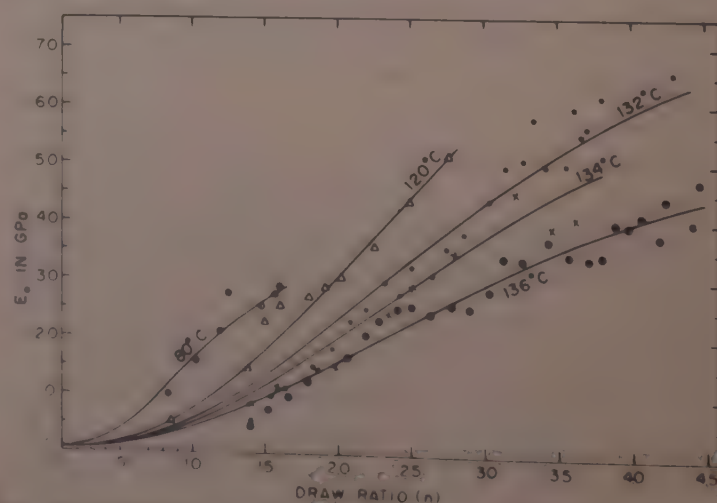


Fig. 6 Comparison of the calculated values of E_0 with experimental values for different temperatures of drawing [Solid lines represent calculated values]

are practically input parameters. At present, it is not possible to comment on the nature of variation of A and β with temperature and other experimental parameters. If this model is applied for different polymers over a wide range of temperature it may be possible to predict quantitatively how A and β vary with other experimental parameters.

In this model we have tried to calculate the elastic modulus of the polymer in terms of those of its constituents as in the Takayanagi's model. It is well known that a clear quantitative picture of the different components present in semicrystalline polymers and the specific way in which they are interlinked is yet to emerge. It was our motivation to develop a suitable model that will incorporate at least the compelling empirical findings.

We have cast the model in such a form that it may have some predictability. The assumptions and the physical picture envisaged in this model may thereby be modified and revised when tested against more refined data to be obtained in future. Finally, we conclude that while the two important models by Ward and Takayanagi are suitable for the glassy polymers and for the high-drawn polymers respectively, the present model emphasizing the role of morphology and its variation with draw ratio embraces the entire range. The proposed model will not offer a complete understanding of the problem but

will stimulate systematic experimental and theoretical investigations.

References

- 1 Hadley D W, Pinnock P R & Ward I M, *J Mater Sci (GB)*, **4** (1969) 152.
- 2 Mead W T, Desper C R & Porter R S, *J Polym Sci Polym Phys Ed (USA)*, **17** (1979) 859.
- 3 Ward I M, *Proc Phys Soc (GB)*, **80** (1962) 1176.
- 4 Takayanagi M, Imada K & Kajiyama T, *J Polym Sci (USA)*, **C15** (1966) 263.
- 5 Hadley D W & Ward I M, *Rep Prog Phys (GB)*, **38** (1975) 1143.
- 6 Ward I M, *Structure and properties of oriented polymers*, edited by I M Ward (Applied Science Publishers, London) 1975.
- 7 Alexander L E, *X-ray diffraction methods in polymer science* (Wiley Interscience, New York), 1969.
- 8 Biswas P K, Sengupta S & Basu A N, *Pramana (India)*, **19** (1982) 215.
- 9 Biswas P K & Basu A N, *Proceedings of Nuclear and Solid State Physics Symposium* (Department of Atomic Energy, Government of India, Bombay) 1980.
- 10 Maeda M, Hibi S, Itoch F, *et al.* *J Polym Sci (USA)*, **A2** (1970) 1303.
- 11 Takayanagi M & Kajiyama T, *J Macromol Sci (GB)*, **B8** (1973) 1.
- 12 Preversek D C, *J Polym Sci (USA)*, **C32** (1971) 343.
- 13 Dasgupta D K, Donghty K & Sheer D B, *J Electrostat (Netherlands)*, **1** (1979) 267.
- 14 Odajima A & Maeda T, *J Polym Sci (USA)*, **C15** (1966) 55.
- 15 Chan O K, Chen F C, Choy C L & Ward I M, *J Phys D (GB)*, **11** (1978) 617.
- 16 DeCandia F, Russo R & Vittoria V, *J Polym Sci Polym Phys Ed (USA)*, **20** (1982) 269.

Hydrogen Pretreatment of CdS Films and Properties of CdS/NaOH/Pt Cells

C D LOKHANDE, M D UPLANE & S H PAWAR*

Energy Conversion Laboratory, Department of Physics, Shivaji University, Kolhapur 416 004

Received 8 April 1982

Cadmium sulphide films have been deposited on both glass and stainless steel substrates by chemical bath deposition technique. The post-preparation heat treatment in hydrogen atmosphere is given to the films and CdS/NaOH/Pt cells are formed. The influence of hydrogen treatment to CdS film electrode on the electrical and optical properties of these cells is studied. The variation of I_{sc} and V_{oc} is explained as due to the diffusion of sulphur vacancies and due to the increase in crystallinity in the CdS film both being caused by the heat treatment.

1 Introduction

During the last decade, the energy crisis has stimulated enormous interest to search for alternative energy resources to replace our dwindling conventional energy reserves. Of the many attempts for the conversion of solar energy into electricity, the semiconductor-liquid junction photovoltaic cells (SLJ PCs) have been preferred as an economical solar energy conversion device. These cells have some potential advantages over the conventional solid state devices, e.g. in minimizing problems arising from lattice mismatch, in controlling the barrier heights, easy method of fabrication, direct penetration of solar radiation to the active semiconductor surface and no requirement of antireflection coating. The efficiency of the SLJPCs is reported as high as 12% with a single crystal semiconductor material as photoanode¹. With the polycrystalline semiconductors, however, the efficiency is found to be very poor. The reasons are many. It is recently reported that the controlled pretreatment of polycrystalline CdS layer in the hydrogen atmosphere before the barrier height formation improves the performance of CdS/Cu₂S solar cells². Such data are few in the case of SLJPCs. In the present investigation, an attempt has been made to reveal the role of hydrogen pretreatment on the electrical properties of CdS/NaOH/Pt cells.

2 Experimental Details

Cadmium sulphide films were prepared by closely following the chemical bath deposition technique³⁻⁵. For each deposition 20 cc of 1 M CdSO₄ solution and 100 cc of 2 M ammonia solution were mixed in a 250 cc beaker to form a complex compound. The substrates were kept rotating in the reaction vessel with the rotation speed of 150 rev/min and the temperature of the reaction bath was raised to 85°C. Then 20 cc of 1 M thiourea were added drop by drop at the rate of 0.7 cc/min to provide the sulphur ions. Cadmium sulphide

films of uniform thickness were obtained on both the glass and stainless steel substrates. The stainless steel substrates used were of mirror grade polish.

The films were annealed in hydrogen atmosphere at 200°C and 300°C for different time intervals up to 90 min. The hydrogen gas employed was purified by passing it through the successive stages of glass wool, NaOH, KMnO₄ and pyrogallol solutions. Some films were furnace cooled after the 90-min heat treatment.

The SLJC was formed by dipping CdS film formed on stainless steel substrate as photoanode and platinum wire as counterelectrode in a quartz Cauvet containing 1 M NaOH solution. The reference electrode employed was saturated calomel electrode (SCE). The electrical properties of SLJCs were measured both in the presence and absence of light with the help of Aplab TFM 13 FET nanoammeter and Phillips DC microvoltmeter (PP-1004). The light source used was 500 W tungsten filament lamp. The optical absorption study of the films was made with specol (Carl Zeiss, Jena) in the wavelength range 4000-7000 Å.

3 Results and Discussion

Cadmium sulphide film formed on the stainless steel substrate was tested for its nature of contact by studying the $I-V$ curves of the film sandwiched between the stainless steel and indium. From the observed nature of $I-V$ curve the stainless steel substrate was found to give ohmic contact to CdS. In the present study, therefore, the stainless steel substrate was used as the contact electrode for the CdS film employed in the SLJCs.

The $I-V$ characteristic of a typical CdS/NaOH/Pt cell in the dark is shown in Fig. 1. The nonlinear nature of $I-V$ curve predicts that the CdS film electrode makes rectification contact with the liquid electrolyte NaOH. This is in agreement with the results reported earlier⁶⁻⁹. The semiconductor-liquid junction is

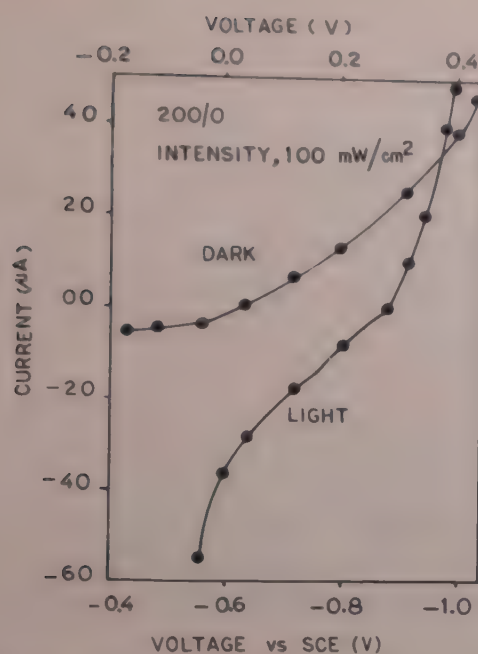


Fig. 1—Dynamic current-voltage (I - V) characteristics in dark and light for 200/0 cell

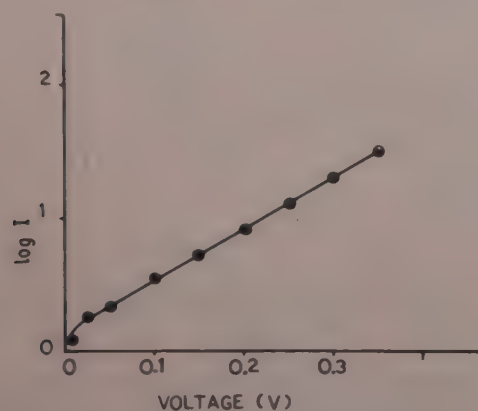


Fig. 2—Log I versus V plot for 200/0 cell in dark

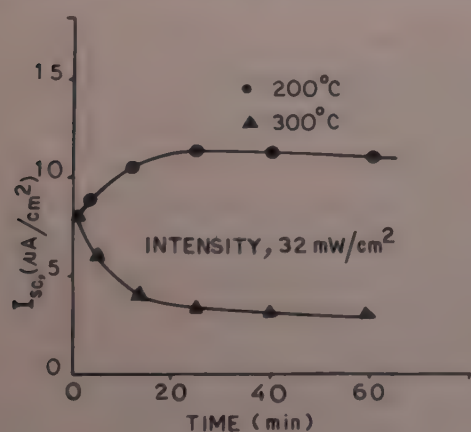


Fig. 3—Variation of I_{sc} of the cell with the duration of post-preparation heat treatment of CdS electrode at 200 and 300°C

analogous to the Schottky barrier junction¹⁰ and the observed linear nature of $\log I$ versus V plot (Fig. 2) supports the prediction. The I - V curve of CdS/NaOH/Pt cell is modified (Fig. 1) under white light illumination of the CdS electrode. This observation reveals that the CdS/NaOH/Pt cell shows the photovoltaic effect and confirms the formation of barrier layer at CdS/NaOH interface.

From Fig. 1 it is seen that even when the external voltage is zero, the PEC cell in dark gives some voltage.

The polarity of the voltage is positive towards CdS electrode. The origin of the voltage is attributed to the difference between the two half cell potentials in the PEC cell and can be written as

$$E = (E)_{CdS} - (E)_{Pt} \quad \dots (1)$$

where $(E)_{CdS}$ and $(E)_{Pt}$ are the half cell potentials developed respectively when the electrodes of CdS and Pt are introduced in an electrolyte. From the polarity of E observed, one can write that

$$(E)_{CdS} > (E)_{Pt} \quad \dots (2)$$

This observation is in agreement with the results reported earlier¹¹.

Eleven CdS/NaOH/Pt cells were formed with different post-preparation heat treatment CdS films, and the short circuit currents (I_{sc}) of the cells under white light intensity of 100 mW/cm² were measured. It is found that, I_{sc} is dependent on both the temperature and duration of post-preparation heat treatment of the CdS films. The variation of I_{sc} with the duration of post-preparation heat treatment is shown in Fig. 3. It is noted that the I_{sc} of the cells formed with 200°C heat treated CdS films, increases with the duration of heat treatment up to about 30 min, remains nearly constant up to about 60 min and then slightly decreases with further increase in duration of heat treatment. In case of the cells formed with 300°C heat treated films, however, the I_{sc} is found to decrease continuously with increase in the duration of heat treatment.

The magnitude of I_{sc} of the SLJC is dependent on various parameters like contact resistance, resistance of photoanode, shunt resistance and the different electrolyte properties namely, reduction-oxidation potential, electron transfer rates of oxidized and reduced species, photo and thermal stabilities, substrate compatibility, optical transparency, fluidity, solubility, conductance and reactivity to the environment¹⁰. In the present investigation, all these parameters, except the bulk resistance of photoanode, were kept constant, and hence the decrease in I_{sc} of the cell is attributed to the increase in bulk resistance of the CdS electrode film. For 300°C heat treated films as well as for long duration of 200°C heat treated films, the increase in the resistance of the CdS film formed on stainless steel substrate can be attributed to the diffusion of some impurities into the film from the substrate. The increase in I_{sc} of CdS/NaOH/Pt, as shown in Fig. 3, is attributed to the decrease in resistance of the photoanode. The decrease in resistance of CdS film can be understood as follows: During the heat treatment of the CdS films in hydrogen atmosphere, the sulphur from the top layer chemically reacts with hydrogen and gets removed resulting in the sulphur vacancies. This leads to the diffusion of loosely bound sulphur atoms along the grain boundary

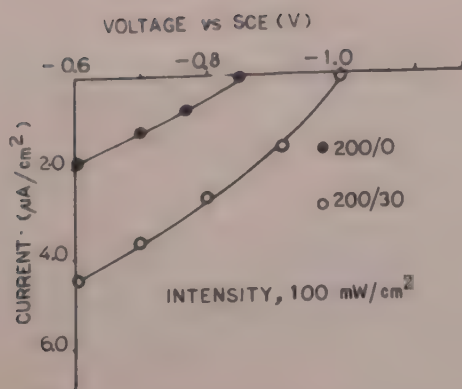


Fig. 4—Photovoltaic current-voltage curves of 200/0 and 200/30 cells (intensity of white light illumination is 100 mW/cm²)

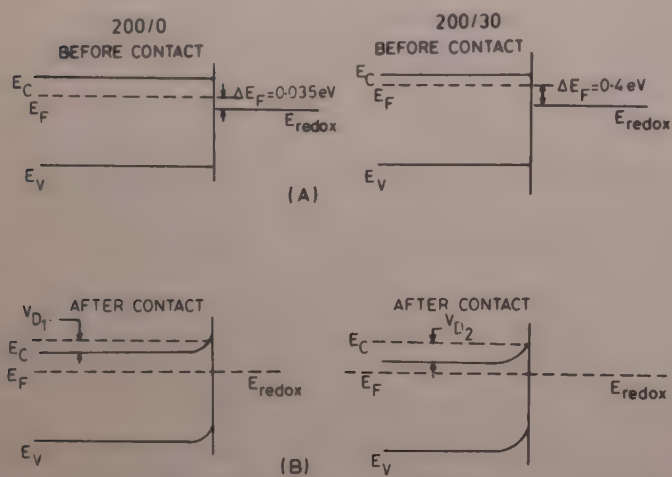


Fig. 5—Energy level diagrams for 200/0 and 200/30 cells [(A), before contact and (B), after contact (diagram is not to the scale.)]

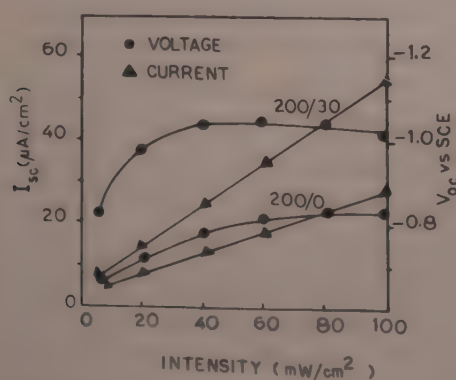


Fig. 6—Variation of short circuit current (I_{sc}) and open circuit voltage (V_{oc}) with intensity levels for 200/0 and 200/30 cells

towards the surface. Conversely, sulphur vacancies may be assumed to diffuse into the interior of the film¹². This gives rise to the additional donor levels in the film causing decrease in the resistance. The increase in I_{sc} of CdS/NaOH/Pt cell can also be partly due to the increase in crystallinity in the CdS film¹³.

Out of eleven different CdS/NaOH/Pt cells studied, the results of only two representative cells, one the CdS film unheated and the other (CdS film) heated at 200°C for 30 min, are presented here. The cells are respectively called 200/0 and 200/30. The photovoltaic output characteristics of the cells are studied and the variations of I with V are shown in Fig. 4. It is found that the magnitudes of both, I_{sc} and V_{oc} for the 200/30

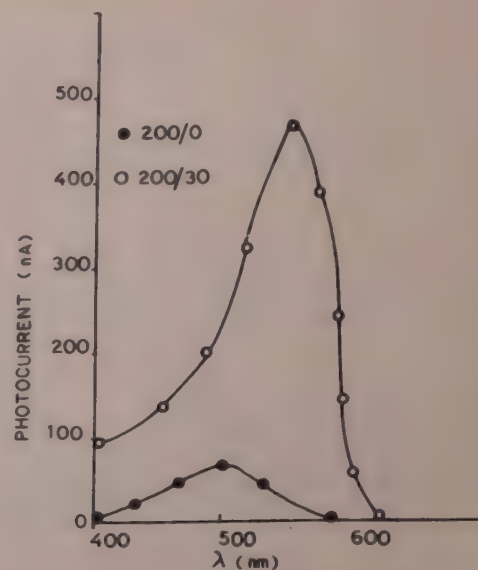


Fig. 7—Spectral response of 200/0 and 200/30 cells

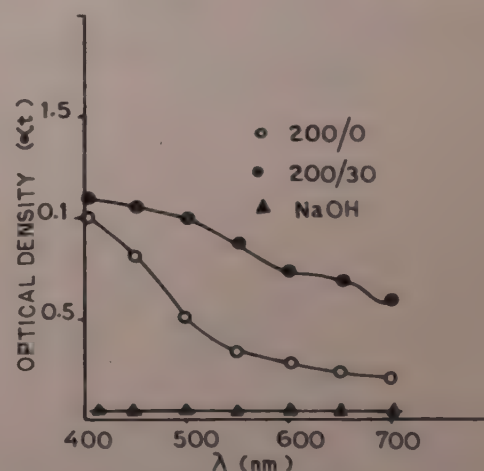


Fig. 8—Variation of optical density (αt) with wavelength for CdS and 200°C heat treated CdS film for 30 min [The optical absorption spectrum for NaOH electrolyte is also given.]

cell are larger than those of the values for the 200/0 cell. The possible reasons for larger I_{sc} for the 200/30 are already given in the paragraph above. The explanation for the large magnitude of V_{oc} can also be understood on the basis of the removal of sulphur atoms from the grain boundary and generation of S vacancies in the film as predicted above. The Fermi level of redox system for 200/0 and 200/30 cells is constant. However, the Fermi level for H₂ heat treated CdS film shifts upward due to increase in the concentration of donor levels. This situation causes the band bending in the case of 200/30 to be more than for the 200/0 cell. The schematic picture of energy level diagram is shown in Fig. 5. The variations of I_{sc} and V_{oc} with (illumination) light intensity for both 200/0 and 200/30 cells are shown in Fig. 6. The nature of the plots is similar to those given by other workers¹⁴⁻¹⁶ and fairly in good agreement with the theory of photovoltaic effect¹⁷.

The photovoltaic spectral response of 200/0 and 200/30 cells is shown in Fig. 7. It is seen that the spectral response of 200/30 cell differs from that of 200/0, both in magnitude of I_{sc} and wavelength response. This can be understood with the help of the plots of variation of

optical density (αt) with wavelength for CdS and heat treated CdS films (Fig. 8). It is seen that heat treated film has relatively higher optical density and the wavelength cut off is shifted towards the red region. Both of these effects are responsible for the stronger absorption of light in the depletion region of semiconductor liquid junction and hence subjected to alteration both in magnitude and the wavelength response of the 200/30 cell.

Acknowledgement

Two of the authors (CDL & MDU) are indebted to the CSIR, New Delhi for the awards of Junior Research Fellowships. They are also thankful to Profs R N Patil and J K Zope for their constant encouragement.

References

- 1 Parkinson B A, Heller A & Miller B, *Appl Phys Lett (USA)*, **33** (1978) 521.
- 2 Mitchell K, Fabrenbruch A L & Bube R H, *J Vac Sci Technol (USA)*, **12** (1975) 910.
- 3 Pavaskar N R, Menezes C A & Sinha A P B, *J Electrochem Soc (USA)*, **124** (1977) 743.
- 4 Shikalgar A G & Pawar S H, *Solid State Commun (USA)*, **32** (1979) 361.
- 5 Kaur I, Pandya D K & Chopra K L, *J Electrochem Soc (USA)*, **127** (1980) 943.
- 6 Ellis A B, Kaiser S W & Wrighton M S, *J Am Chem Soc (USA)*, **98** (1976) 6855.
- 7 Ellis A B, Kaiser S W & Wrighton M S, *J Am Chem Soc (USA)*, **98** (1976) 1635.
- 8 Miller B & Heller A, *Nature (GB)*, **262** (1976) 680.
- 9 Memming R, *Proceedings of the conference on the electrochemistry and physics of semiconductor liquid interfaces under illumination*, Airlie, Virginia, May 3-5, edited by A Heller (The Electrochemical Society Inc., N. J. USA), 1977, 38.
- 10 Gale R J & Dubew J, *Solar Energy Materials (USA)*, **4** (1981) 135.
- 11 Heller A & Miller B, *Electrochimica Acta (GB)*, **25** (1980) 29.
- 12 Mukherjee M K & Das S K, *Proc National solar energy convention*, Annamalai University, Annamalainagar (Allied Publishers, New Delhi, India) 1980, 326.
- 13 Vecht A, *Physics of thin films*, Vol. 3, edited by George Hass & R E Thun (Academic Press, New York), 1966, 165.
- 14 Russak M A, Reichman J, Witzke H *et al.*, *J Electrochem Soc (USA)*, **127** (1980) 725.
- 15 Chin-Hsin Jason & Jui H Wang, *Appl Phys Lett (USA)*, **36** (1980) 852.
- 16 Gerischer H, *Electroanalytical Chemistry and Interfacial Electrochemistry (Netherlands)*, **58** (1975) 263.
- 17 Jain G C & Berry W B, *Transport properties of solids and solid state energy conversion* (Tata McGraw-Hill, Bombay), 1972, 203.

Force Field for In-Plane Vibrations of *trans-cis*-Diacetamide Use of CNDO/Force Method

A ANNAMALAI & SURJIT SINGH*

Structural Chemistry Group, Department of Chemistry, Indian Institute of Technology, Madras 600 036

Received 25 May 1982

Using the CNDO/Force and the least squares refinement calculations, the redundancy-free internal valence force field is evaluated for the in-plane vibrations of *trans-cis*-diacetamide. The initial force field considered is based on the bending and interaction force constants obtained from the CNDO/Force calculations, and the stretching force constants transferred from chemically related molecules. The vibrational frequencies of $\text{CH}_3\text{CONHCOCH}_3$, $\text{CH}_3\text{CONDCOCH}_3$, $\text{CD}_3\text{CONHCOCD}_3$ and $\text{CD}_3\text{CONDCOCD}_3$ are employed in refining the force field. The refined force field obtained is found to be reasonable.

1 Introduction

It is well known that diacetamide exists in two crystalline forms^{1,2}. In the usually occurring crystalline modification, form A, diacetamide prefers the *trans-cis* conformation in which one of the two carbonyl groups is *trans* and the other is *cis* with respect to the central NH bond. In the metastable crystalline modification, called form B, the molecules take the more symmetric *trans-trans* conformation. The form B crystals change to form A on long standing at room temperature¹. Uno *et al.*³⁻⁶ reported the Urey-Bradley force fields for both the conformers. Kanakavel⁷ calculated the valence force constants for the metastable *trans-trans* conformer using CNDO/Force method. In the present work, the redundancy-free internal valence force field (RFIVFF) is evaluated for the in-plane vibrations of the stable *trans-cis* conformer using the CNDO/Force as well as the least squares refinement calculations. The stretching force constants derived from the CNDO/Force calculations are known to be overestimated by a factor of 2-3.5. The CNDO stretch-stretch interaction constants are found to be about 50% higher than the experimental values. However, the magnitudes obtained for the other interaction and bending force constants are, in general, reasonable. Mostly, the signs obtained for the interaction constants are correct. Hence, the CNDO/Force calculations provide us with a convenient way of choosing the bending and interaction force constants to frame the initial force constant matrix for the least squares refinement calculations. In the present study, to construct the initial force constant matrix, the stretching force constants are transferred as usual from chemically related molecules; bending and interaction force constants are taken from the CNDO Force field after scaling down the stretch-stretch interaction constants by a factor of 0.65 (Ref. 8). It is not easy,

otherwise, to guess reasonably the interaction force constants. The force field is then refined using the vibrational frequencies.

2 Computational Details and Results

The CNDO SCF energies and geometries are computed for the conformers having the methyl group hydrogen atoms eclipsed or staggered with respect to the adjacent carbonyl groups. It is found that the rotational conformer having the hydrogen atoms of the two methyl groups eclipsed with respect to the adjacent

Table 1—Redundancy-free Internal Coordinates for *trans-cis*-Diacetamide

1. $\nu_{\text{N-H}}$	= d	N—H stretch.
2. $\nu_{\text{N-C}}$	= L_1	N—C stretch.
3. $\nu_{\text{N-C}}$	= L_2	N—C stretch.
4. $\nu_{\text{C=O}}$	= R_1	C=O stretch.
5. $\nu_{\text{C=O}}$	= R_2	C=O stretch.
6. $\nu_{\text{C-C}}$	= D_1	C—C stretch.
7. $\nu_{\text{C-C}}$	= D_2	C—C stretch.
8. $\nu_s(\text{CH}_3)$	= $3^{-1/2}(r_1 + r_2 + r_3)$	CH_3 stretch.
9. $\nu_s(\text{CH}_3)$	= $3^{-1/2}(r_4 + r_5 + r_6)$	CH_3 stretch.
10. $\nu'_s(\text{CH}_3)$	= $6^{-1/2}(2r_1 - r_2 - r_3)$	CH_3 stretch.
11. $\nu'_s(\text{CH}_3)$	= $6^{-1/2}(2r_4 - r_5 - r_6)$	CH_3 stretch.
12. δ_{CNC}	= $6^{-1/2}(2\theta_1 - \theta_2 - \theta_3)$	CNC deform.
13. ρ_{NH}	= $2^{-1/2}(\theta_2 - \theta_3)$	N—H rock
14. δ_{NCC}	= $6^{-1/2}(2\delta_1 - \delta_2 - \delta_3)$	NCC deform.
15. δ_{NCC}	= $6^{-1/2}(2\delta_4 - \delta_5 - \delta_6)$	NCC deform.
16. ρ_{CO}	= $2^{-1/2}(\delta_2 - \delta_3)$	C=O rock.
17. ρ_{CO}	= $2^{-1/2}(\delta_5 - \delta_6)$	C=O rock.
18*. $\delta_s(\text{CH}_3)$	= $[3(1+b^2)]^{-1/2}[b(\alpha_1 + \alpha_2 + \alpha_3) - (\beta_1 + \beta_2 + \beta_3)]$	CH_3 deform.
19*. $\delta_s(\text{CH}_3)$	= $[3(1+b^2)]^{-1/2}[b(\alpha_4 + \alpha_5 + \alpha_6) - (\beta_4 + \beta_5 + \beta_6)]$	CH_3 deform.
20. $\delta_s(\text{CH}_3)$	= $6^{-1/2}(2\alpha_1 - \alpha_2 - \alpha_3)$	CH_3 deform.
21. $\delta_s(\text{CH}_3)$	= $6^{-1/2}(2\alpha_4 - \alpha_5 - \alpha_6)$	CH_3 deform.
22. $\rho_{\parallel}(\text{CH}_3)$	= $6^{-1/2}(\beta_1 - \beta_2 - \beta_3)$	CH_3 rock.
23. $\rho_{\parallel}(\text{CH}_3)$	= $6^{-1/2}(2\beta_4 - \beta_5 - \beta_6)$	CH_3 rock.

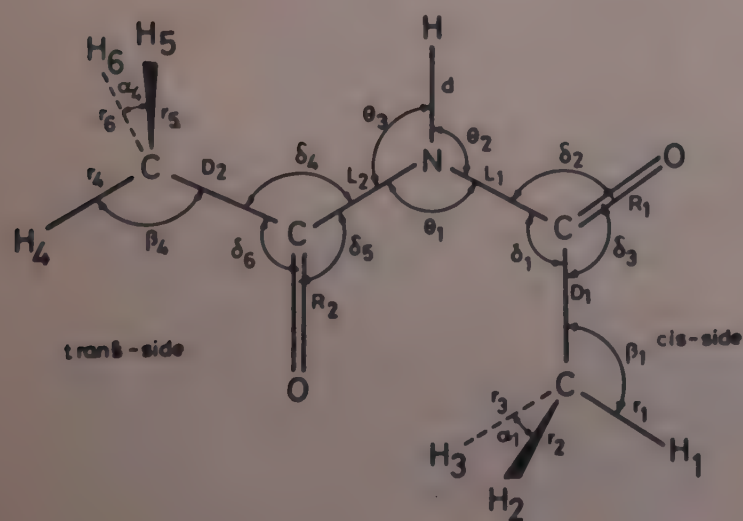
$$*b = -3\sin\beta \cos\beta \sin\alpha$$

Table 2—Force Fields of *trans-cis*-Diacetamide*

Force constant	CNDO/Force	Refined	Force constant	CNDO/Force	Refined	Force constant	CNDO/Force	Refined	Force constant	CNDO/Force	Refined
$F_{1,1}$	14.321	5.848	$F_{5,7}$	1.290	0.8(C)	$F_{8,14}$	0.031	—	$F_{14,18}$	-0.026	—
$F_{1,2}$	0.484	0.262	$F_{4,12}$	0.067	0.035	$F_{8,16}$	-0.023	—	$F_{14,20}$	0.044	0.028
$F_{1,3}$	0.489		$F_{4,13}$	0.024	—	$F_{8,18}$	0.175	—	$F_{15,21}$	0.038	
$F_{1,12}$	-0.268	-0.153	$F_{4,14}$	-0.481	-0.289	$F_{9,9}$	12.245	5.030	$F_{14,22}$	0.081	0.08(C)
$F_{1,14}$	0.067	0.008	$F_{4,15}$	-0.482		$F_{9,17}$	-0.027	—	$F_{15,23}$	0.108	
$F_{1,17}$	0.049	—	$F_{4,16}$	0.088	0.093	$F_{9,19}$	0.187	—	$F_{15,15}$	0.846	1.280
$F_{2,2}$	19.327	6.855	$F_{4,17}$	0.041	—	$F_{10,10}$	11.799	4.683	$F_{15,16}$	0.017	—
$F_{2,3}$	1.044	0.65(C)	$F_{4,18}$	-0.057	—	$F_{10,14}$	0.056	0.04(C)	$F_{15,17}$	-0.098	-0.238
$F_{2,4}$	2.440	1.6(C)	$F_{4,20}$	0.028	—	$F_{11,15}$	0.057	—	$F_{15,19}$	-0.030	—
$F_{3,5}$	2.433		$F_{4,22}$	-0.099	-0.112	$F_{10,16}$	0.030	—	$F_{15,22}$	0.010	—
$F_{2,5}$	-0.289	-0.273	$F_{5,23}$	-0.086		$F_{10,20}$	-0.260	-0.03(C)	$F_{16,16}$	1.032	1.340
$F_{3,4}$	-0.233		$F_{5,5}$	29.061	10.976	$F_{11,21}$	-0.258		$F_{16,18}$	0.039	—
$F_{2,6}$	0.926	0.6(C)	$F_{5,6}$	0.075	—	$F_{10,22}$	0.298	0.03(C)	$F_{16,22}$	0.051	—
$F_{3,7}$	0.951		$F_{5,12}$	0.029	—	$F_{11,23}$	0.291		$F_{17,17}$	1.000	1.039
$F_{2,12}$	0.197	0.344	$F_{5,13}$	-0.047	—	$F_{11,11}$	11.770	4.683	$F_{17,19}$	0.033	—
$F_{2,13}$	0.285	0.309	$F_{5,16}$	0.069	0.127	$F_{11,17}$	0.032	—	$F_{17,10}$	0.016	—
$F_{2,14}$	0.197	0.283	$F_{5,19}$	-0.056	—	$F_{12,12}$	0.574	0.717	$F_{17,22}$	0.019	—
$F_{2,15}$	0.071	0.089	$F_{6,6}$	16.096	4.329	$F_{12,13}$	0.010	—	$F_{17,23}$	0.047	—
$F_{2,16}$	0.516	0.643	$F_{6,8}$	0.590	0.4(C)	$F_{12,14}$	0.031	0.114	$F_{18,18}$	0.731	0.562
$F_{2,17}$	-0.028	—	$F_{7,9}$	0.584		$F_{12,15}$	0.054	0.073	$F_{18,20}$	-0.015	—
$F_{2,18}$	-0.072	-0.056	$F_{6,13}$	0.044	—	$F_{12,16}$	0.034	0.021	$F_{18,22}$	-0.038	—
$F_{3,19}$	-0.069		$F_{6,14}$	0.225	0.028	$F_{12,20}$	0.035	—	$F_{19,23}$	-0.032	-0.03(C)
$F_{2,20}$	0.043	—	$F_{7,15}$	0.259		$F_{12,22}$	-0.049	—	$F_{19,19}$	0.739	0.558
$F_{2,22}$	0.020	—	$F_{6,16}$	-0.424	-0.136	$F_{12,23}$	0.013	—	$F_{19,21}$	-0.019	—
$F_{3,3}$	19.335	6.846	$F_{7,17}$	-0.423		$F_{13,13}$	0.610	0.600	$F_{20,20}$	0.719	0.494
$F_{3,6}$	-0.066	—	$F_{6,18}$	-0.420	-0.333	$F_{13,14}$	0.069	0.131	$F_{20,22}$	-0.052	—
$F_{3,12}$	0.052	0.036	$F_{7,19}$	-0.427		$F_{13,15}$	0.013	—	$F_{21,21}$	0.743	0.500
$F_{3,13}$	-0.324	-0.243	$F_{6,20}$	-0.032	—	$F_{13,16}$	-0.019	—	$F_{21,23}$	-0.066	—
$F_{3,15}$	0.236	0.262	$F_{6,22}$	0.092	—	$F_{13,17}$	-0.053	—	$F_{22,22}$	0.766	0.694
$F_{3,17}$	0.448	0.627	$F_{7,7}$	16.066	4.592	$F_{13,22}$	0.016	—	$F_{23,23}$	0.779	0.625
$F_{3,21}$	0.025	—	$F_{7,12}$	0.022	—	$F_{14,14}$	0.890	1.218			
$F_{3,22}$	-0.029	—	$F_{7,13}$	-0.039	—	$F_{14,15}$	-0.017	—			
$F_{3,23}$	0.056	—	$F_{7,16}$	0.020	—	$F_{14,16}$	-0.138	-0.133			
$F_{4,4}$	29.151	10.939	$F_{7,23}$	0.081	—	$F_{14,17}$	0.033	0.091			
$F_{4,5}$	0.170	0.1(C)	$F_{8,8}$	12.270	5.031						
$F_{4,6}$	1.292	0.8(C)	$F_{8,12}$	0.026	—						

*Units: Stretch-stretch in $\text{mdyne}\text{\AA}^{-1}$, stretch-bend in mdyne rad^{-1} and bend-bend in $\text{mdyne}\text{\AA rad}^{-2}$

(C) Constrained force constant values

Fig. 1—Internal coordinates of *trans-cis*-diacetamide

carbonyl groups are more stable than the other conformers considered. This observation is similar to the experimental findings for various acetyl compounds^{9,10}. The geometry optimization is carried out using the steepest descent method^{11,12}. The CNDO/Force calculations are performed using the computer program CNINDO of Pople and Beveridge¹³ after suitable modifications¹². The CNDO/Force field is calculated using the optimized geometry as reference. The molecule is distorted slightly in the positive and negative directions of various redundancy-free internal coordinates and the forces are computed for the distorted configurations. From these forces, the CNDO/Force constants are obtained using numerical differentiation^{11,12}. The redundancy-free internal coordinates used in the present study are given in Table 1 in terms of the internal coordinates given in Fig. 1. The CNDO/Force field is listed in Table 2.

Table 3 - Calculated and Observed Frequencies (in cm^{-1}) and PEDs for *trans-cis*-Diacetamide

	Obs.	Calc.	$\Delta\nu$	PED	
				$\text{CH}_3\text{CONHCOCH}_3$	
A'	3225	3240	-15	F1, 1(101)	
	3000	2963	37	F10, 10(78)	F11, 11(22)
	3000	2963	37	F11, 11(78)	F10, 10(22)
	2945	2945	0	F8, 8(100)	
	2945	2945	0	F9, 9(100)	
	1736	1742	-6	F5, 5(56)	F4, 4(21) F13, 13(16)
	1701	1702	-1	F4, 4(56)	F5, 5(23)
	1506	1502	4	F13, 13(63)	F4, 4(20) F3, 3(14)
	1426	1425	1	F21, 21(61)	F20, 20(24)
	1426	1422	4	F20, 20(58)	F21, 21(58)
	1376	1372	4	F18, 18(82)	F19, 19(16) F6, 18(-12)
	1376	1371	5	F19, 19(84)	F18, 18(15) F7, 19(-11)
	1310	1323	-13	F2, 2(63)	F3, 3(52) F2, 3(-11)
	1223	1223	0	F3, 3(25)	F6, 6(21) F2, 2(19) F16, 16(17)
				F13, 13(16)	F7, 7(13)
	1034	1053	-19	F22, 22(46)	F7, 7(36)
	1034	1016	18	F23, 23(65)	
	1014	1000	14	F22, 22(34)	F7, 7(31)
	836	840	-4	F6, 6(39)	F2, 2(17) F23, 23(14)
	649	642	7	F17, 17(32)	7, 7(24) F14, 14(15)
	563	560	3	F16, 16(65)	F15, 15(15) F6, 6(13)
	419	417	2	F17, 17(54)	F14, 14(26) F15, 15(11) F15, 17(-10)
	375	377	-2	F15, 15(43)	F14, 14(36)
	164	162	2	F12, 12(71)	F14, 14(10) F15, 15(14)
				$\text{CH}_3\text{CONDCCOCH}_3$	
A'	2995	2963	22	F10, 10(75)	F11, 11(25)
	2995	2963	22	F11, 11(75)	F10, 10(25)
	2940	2945	-5	F8, 8(100)	
	2940	2945	-5	F9, 9(100)	
	2385	2373	12	F1, 1(100)	
	1728	1723	5	F5, 5(80)	F7, 7(10)
	1694	1691	3	F4, 4(83)	F14, 14(11)
	1416	1427	-11	F21, 21(71)	F20, 20(11)
	1416	1422	-6	F20, 20(70)	F21, 21(14)
	1376	1374	2	F19, 19(57)	F18, 18(24) F3, 3(13)
	1376	1372	4	F18, 18(71)	F19, 19(27) F6, 18(-12)
	1360	1362	-2	F3, 3(54)	F19, 19(16) F13, 13(17)
	1290	1295	-5	F2, 2(69)	F6, 6(31) F16, 16(24)
				F2, 2, 16(-17)	F2, 6(-10)
	1111	1101	10	F7, 7(33)	F13, 13(21) F17, 17(16)
				F3, 3(12)	F23, 23(11)
	1024	1034	-10	F22, 22(57)	F23, 23(14)
	1024	1012	12	F23, 23(37)	F22, 22(17) F7, 7(13)
	919	934	-15	F13, 13(42)	F7, 7(12) F23, 23(11)
	811	828	-17	F6, 6(41)	F2, 2(18) F23, 23(11)
	646	637	9	F17, 17(33)	F7, 7(24) F14, 14(15)
				F12, 12(10)	
	557	556	1	F16, 16(66)	F15, 15(15) F6, 6(12)
	418	417	1	F17, 17(54)	F14, 14(25) F15, 15(11)
				F15, 17(-10)	
	374	375	-1	F15, 15(43)	F14, 14(36)
	164	162	2	F12, 12(72)	F15, 15(14) F14, 14(10)
				$\text{CD}_3\text{CONHCOCD}_3$	
A'	3225	3240	-15	F1, 1(101)	
	2175	2210	-35	F11, 11(67)	F10, 10(32)
	2175	2209	-34	F10, 10(67)	F11, 11(32)
	2115	2112	3	F8, 8(100)	
	2115	2112	3	F9, 9(99)	

(Contd)

Table 3—Calculated and Observed Frequencies (in cm^{-1}) and PEDs for *trans-cis*-Diacetamide—Contd.

Obs.	Calc.	$\Delta\nu$	PED		
$\text{CD}_3\text{CONHCOCD}_3$					
1732	1738	-6	F5, 5(57)	F4, 4(15)	F13, 13(16)
1693	1696	-3	F4, 4(59)	F5, 5(22)	
1505	1501	4	F13, 13(63)	F4, 4(21)	F3, 3(14)
1325	1325	0	F2, 2(64)	F3, 3(35)	F6, 6(12) F2, 3(-11)
1228	1225	3	F6, 6(25)	F3, 3(24)	F2, 2(17) F7, 7(16)
			F13, 13(16)	F16, 16(16)	
1092	1110	-18	F19, 19(56)	F7, 7(34)	F7, 19(-21)
1068	1070	-2	F18, 18(76)	F6, 18(-12)	
1037	1024	13	F21, 21(93)		
1037	1020	17	F20, 20(91)		
955	961	-6	F19, 19(30)	F17, 17(16)	F7, 7(12)
A' 870	870	0	F23, 23(25)	F6, 6(17)	F15, 15(17)
827	815	12	F22, 22(71)		
711	736	-25	F23, 23(54)	F6, 6(17)	
587	594	-7	F17, 17(28)	F7, 7(23)	F22, 22(10)
523	524	-1	F16, 16(62)	F6, 6(13)	
397	397	0	F17, 17(52)	F14, 14(27)	F15, 15(10)
			F15, 17(-10)		
337	335	2	F15, 15(44)	F14, 14(31)	
(164)	151	-	F12, 12(68)	F15, 15(14)	F14, 14(12)
$\text{CD}_3\text{CONDCOCD}_3$					
A' 2400	2373	27	F1, 1(100)		
2155	2210	-55	F11, 11(70)	F10, 10(29)	
2155	2209	-54	F10, 10(70)	F11, 11(29)	
2115	2112	3	F8, 8(100)		
2115	2112	3	F9, 9(99)		
1727	1719	8	F5, 5(81)	F7, 7(11)	
1687	1684	3	F4, 4(85)	F14, 14(11)	
1365	1368	-3	F3, 3(76)	F13, 13(22)	F3, 18(-10)
1308	1297	11	F2, 2(67)	F6, 6(36)	F16, 16(23)
			F2, 16(-17)	F2, 6(-11)	
1137	1130	7	F7, 7(52)	F19, 19(45)	F7, 19(-20)
1067	1072	-5	F18, 18(87)	F6, 6(13)	F6, 18(-15)
1035	1039	-4	F19, 19(32)	F13, 13(29)	F3, 3(12)
1015	1023	-8	F21, 21(82)	F20, 20(11)	
1015	1020	-5	F20, 20(80)		
934	926	8	F13, 13(22)	F19, 19(17)	F5, 5(13)
845	847	-2	F23, 23(25)	F6, 6(19)	F15, 15(12)
			F13, 13(11)		
822	815	7	F22, 22(72)		
—	732	-	F23, 23(52)	F3, 3(17)	
587	591	-4	F17, 17(29)	F7, 7(23)	F22, 22(10)
521	522	-1	F16, 16(63)	F6, 6(13)	
395	396	-1	F17, 17(52)	F14, 14(27)	F15, 15(10)
			F15, 17(-10)		
335	334	1	F15, 15(44)	F14, 14(32)	
(164)	151	-	F12, 12(66)	F15, 15(15)	F14, 14(12)

Note: The frequency enclosed within parentheses is not used in calculating the force constants. The figures given in parenthesis under PED are per cent contributions.

The initial force field is constructed as suggested above. Since, in the present problem, the independent force constants to be evaluated are too large in number, several mathematical constraints are required to be imposed on the force field. In some cases, on the basis of the CNDO/Force results, the interaction constant for the *trans*-part (Fig.1) and the corresponding force

constant for the *cis*-part are made equal to each other. Some of the stretch-stretch interaction constants are kept fixed at the values obtained by scaling down the corresponding CNDO/Force estimated, by a factor of 0.65 (Ref. 8). Other constraints imposed are based on the force fields of related molecules¹⁴. The G matrix elements are calculated based on the structural

parameters reported by Kuroda *et al.*¹⁵ The N—H and C—H bond distances are assumed to be 1.02 and 1.08 Å respectively; tetrahedral angles are assumed around the methyl group C atoms, and the CNH bond angles are taken as 120°. Based on C_s symmetry of *trans-cis*-diacetamide, the 36 normal modes are divided into 23 in-plane (A') and 13 out-of-plane (A'') vibrations. The in-plane frequencies reported by Uno *et al.*⁵ for $\text{CH}_3\text{CONHCOCH}_3$, $\text{CH}_3\text{CONDCOCH}_3$, $\text{CD}_3\text{CONHCOCD}_3$ and $\text{CD}_3\text{CONDCOCH}_3$ are used in the force field calculations. The force field refinements are carried out using the FPERT program of Schachtschneider¹⁶ after including the damped least squares subroutines. The absolute weighting factors¹⁷ are used for the frequency parameters. Of the 64 parameters considered for the experimental force field, 53 are refined using 89 frequencies. All the calculations are carried out on an IBM 370/155 computer. The refined force field is included in Table 2. The observed and calculated frequencies are summarized in Table 3 along with potential energy distributions (PEDs).

3 Discussion

The carbonyl stretching force constants (F_{CO}) obtained in this work for *trans-cis*-diacetamide are very close to those of *trans-trans*-diacetamide⁷ and acetamide¹⁸ in the solid phase. The F_{CO} values in these molecules are between 10.69 and 11.05 mdyne Å⁻¹ for the solid phase. These values are smaller than the F_{CO} value in formaldehyde (12.9 mdyne Å⁻¹)¹⁹ because of the strong π -electron delocalization present in amides leading to a decrease in the C—O bond order. The C—O bond is further weakened in the condensed phase by hydrogen bonding. The force constants for the CN and CC stretching vibrations and the methyl group vibrations are also close to the corresponding force constants of acetamide¹⁸.

The PEDs obtained for *trans-cis*-diacetamide and its deuterated derivatives suggest that most of the bands have mixing of several different modes. The carbonyl stretching modes corresponding to both the *trans*- and *cis*-parts mix together in the imide I bands at 1736 and 1710 cm⁻¹ in the spectrum of $\text{CH}_3\text{CONHCOCH}_3$, which is quite reasonable. In the imide III bands at 1310 and 1223 cm⁻¹, the two CN stretching modes show strong coupling. Also in the deformation and asymmetric stretching frequencies of CH_3 groups the corresponding vibrational modes belonging to *trans*- and *cis*-parts mix to some extent. The tendencies to mix the vibrational modes are more or less similar in deuterated diacetamides also. In the spectrum of $\text{CH}_3\text{CONHCOCH}_3$, the imide III band at 1223 cm⁻¹ shows considerable contributions from the two CC stretching as well as the *cis* C—O rocking modes. The N—H rocking mode also contributes slightly to this

band. In the imide II band at 1506 cm⁻¹, the major contribution comes from N—H rocking mode. This band has slight contributions from *cis* C=O and *trans* C—N stretching modes. The mixing of N—H rocking and *trans* C—N stretching modes in 1506 and 1223 cm⁻¹ bands is similar to the observations made earlier^{5,20} that N-monosubstituted amides with the *trans*—CONH— group show the amide II and amide III bands arising from the coupling between C—N stretching and N—H in-plane deformation modes. The coupling of this type was also found for the —CONHCO— group having *trans* structure in it^{3,7}. In the fundamental bands appearing below 650 cm⁻¹, the skeletal deformation modes are found to mix intimately. Apart from these modes, the *cis* and *trans* C—C stretching modes contribute significantly to the bands at 563 and 649 cm⁻¹ respectively. The frequency fit obtained in the present work shows less deviations, particularly in imide characteristic frequencies, than those obtained earlier⁵. The NCC deformation force constants for the *cis*- and *trans*-parts differ significantly. In the C—O and C—N stretching force constants the differences between the *cis*- and *trans*-parts are found to be very little.

Acknowledgement

The financial assistance to one of the authors (AA) by the CSIR, New Delhi, and the Department of Atomic Energy, Government of India, is gratefully acknowledged.

References

- 1 Uno T & Machida K, *Bull Chem Soc Jpn (Japan)*, **34** (1961) 545.
- 2 Uno T & Machida K, *Bull Chem Soc Jpn (Japan)*, **35** (1962) 1226.
- 3 Uno T & Machida K, *Bull Chem Soc Jpn (Japan)*, **36** (1963) 427.
- 4 Kuroda Y, Saito Y, Machida K & Uno T, *Bull Chem Soc Jpn (Japan)*, **45** (1972) 2413.
- 5 Kuroda Y, Saito Y, Machida K & Uno T, *Spectrochim Acta (GB) Vol A*, **27** (1971) 1481.
- 6 Kuroda Y, Saito Y, Machida K & Uno T, *Spectrochim Acta Vol A (GB)*, **29** (1973) 411.
- 7 Kanakavel M, *Vibrational analysis and evaluation of force fields of polyatomic molecules*, PhD thesis, Indian Institute of Technology, Madras, 1976.
- 8 Annamalai A & Singh S, *J Mol Struct Theochem (Netherlands)*, **87** (1982) 169.
- 9 Allinger N L, *Adv Phys Org Chem (GB)*, **13** (1976) 1.
- 10 Caminati W, Scappini F & Corbelli G, *J Mol Spectrosc (USA)*, **75** (1979) 327.
- 11 Pulay P & Torok F, *Mol Phys (GB)*, **25** (1973) 1153.
- 12 Kanakavel M, Chandrasekhar J, Subramanian S & Singh S, *Theoret Chim Acta (Germany)*, **43** (1976) 185.
- 13 Pople J A & Beveridge D L, *Approximate molecular orbital theory* (McGraw-Hill, New York), 1970.
- 14 Annamalai A, *Force field studies of carbonyl compounds*, PhD thesis, Indian Institute of Technology, Madras, 1981.
- 15 Kuroda Y, Taira Z, Uno T & Osaki N, *Cryst Struct Comm (Italy)*, **4** (1975) 325.
- 16 Schachtschneider J H, *Technical Reports No. 57-65* (Shell Development Co., California), 1964.
- 17 Overend J & Scherer J R, *J Chem Phys (USA)*, **32** (1960) 1720.
- 18 Annamalai A & Singh S, *J Chem Phys (USA)*, **77** (1982) 860.
- 19 Duncan J L & Mallinson P D, *Chem Phys Lett (Netherlands)*, **23** (1973) 597.
- 20 Miyazawa T, Shimanouchi T & Mizushima S, *J Chem Phys (USA)*, **29** (1958) 611.

Spectral Studies on New Dioxouranium(VI) Complexes of Tridentate Schiff Bases Derived from Salicylhydrazide & Salicylaldehyde or Substituted Salicylaldehydes

A SYAMAL*

Department of Applied Sciences and Humanities, Kurukshetra University, Kurukshetra 132 119

and

D KUMAR

Department of Chemistry, Regional Engineering College, Kurukshetra 132 119

Received 19 August 1981; revised received 3 September 1982

New dioxouranium(VI) complexes of the type $\text{UO}_2\text{L} \cdot \text{CH}_3\text{OH}$ (where LH_2 = Schiff base 1) have been synthesized and characterized on the basis of elemental analysis, quantitative determination of ligand, conductance, molecular weight, magnetic susceptibility, IR, NMR and electronic spectra. The reactivity of the complexes towards bidentate ligands has been tested and dioxouranium(VI) heterochelates of the type $\text{UO}_2\text{L}(\text{AA})$ (where AA = bidentate NN donor ligand) have been synthesized. The complexes are non-electrolytes, diamagnetic and monomers. The $\text{UO}_2\text{L} \cdot \text{CH}_3\text{OH}$ complexes are six-coordinated and the heterochelates are seven-coordinated:

1 Introduction

The coordination complexes of arylhydrazones are known to possess biological activity as they act as inhibitors for enzymes¹. The Schiff base, N-salicylidene-N'-salicylhydrazide(1) is a potential quadridentate ligand and forms²⁻⁵ complexes with copper(II), nickel(II), cobalt(II), titanium(IV) and tin(IV). The structure of Schiff base 1 is shown in Fig. 1. Although there is a report of a 1:2 complex⁶ of UO_2 (VI) with 1(X = H), the 1:1 complex has not been synthesized. In continuation of our work on oxometal cations⁷⁻¹¹, we report here dioxouranium(VI) complexes of 1. Two different types of complexes, viz. $\text{UO}_2\text{L} \cdot \text{CH}_3\text{OH}$ and $\text{UO}_2\text{L}(\text{AA})$ (where L = Schiff base, AA = bidentate NN donor ligand) have also been prepared. The newly prepared complexes have been characterized on the basis of elemental analysis, conductance, molecular weight, IR, electronic and NMR spectra, and magnetic susceptibility measurements.

2 Experimental Details

2.1 Chemicals

Dioxouranium(VI) acetate dihydrate was obtained from M/s Hopkins and Williams (UK). Salicylaldehyde and ethylenediamine were the products of M/s Sarabhai M Chemical Co. Samples of 5-bromosalicylaldehyde, 5-methoxysalicylaldehyde, 3-ethoxysalicylaldehyde, 3-aminopyridine, 2,2'-dipyridyl and orthophenanthroline were obtained from M/s Aldrich Chemical Co. (USA). Sample of 3,5-dichlorosalicylaldehyde was the product of M/s

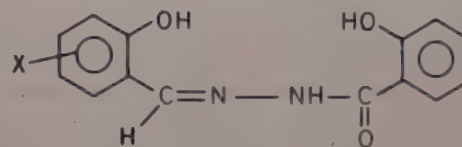


Fig. 1—Structural formula of Schiff base 1 (X represents H, 5-chloro, 5-bromo, 5-methoxy, 3-methoxy, 3-ethoxy, 3,5-dichloro and 5,6-benzo)

Eastman Kodak Co. (USA). Samples of 3-methoxysalicylaldehyde, 2-hydroxy-1-naphthaldehyde, trimethylenediamine, tetramethylenediamine, hexamethylenediamine and orthophenylenediamine were procured from M/s Fluka AG (Switzerland). Samples of 5-chlorosalicylaldehyde¹² and the Schiff bases⁴ were prepared according to the published procedures. The sample of sodium methoxide was a product of SD's Lal-Chem Industry.

2.2 Physical Measurements

Uranium was determined gravimetrically as U_3O_8 after decomposing the complexes with concentrated nitric acid and igniting the residue. Nitrogen was determined microanalytically. Quantitative determination of ligands was carried out by bromometric titration technique. Electrolytic conductance measurements were carried out in dimethylsulphoxide using a Toshniwal conductivity bridge (type CL01-02A) calibrated with potassium chloride solutions. Molecular weights were determined by the Rast method¹³ using diphenyl as the solvent. Infrared spectra were recorded in KBr pellets using Beckman IR-20 spectrophotometer calibrated with polystyrene.

Electronic spectra were recorded on a Unicam SP-1600 spectrophotometer. Nuclear magnetic resonance spectra were recorded on a Varian NMR spectrometer (T-60 60 mH) in DMSO- d_6 using tetramethylsilane as the internal standard. Magnetic susceptibility measurements were done by the Guoy method using $Hg[Co(NCS)_4]$ as the standard.

2.3 General Method of Syntheses of Dioxouranium(VI) Complexes

Complexes of the type $UO_2L \cdot CH_3OH$ —A methanolic solution of dioxouranium(VI) acetate dihydrate (0.84 g, 0.002 mol in 10 ml) was added to a methanolic solution of the appropriate Schiff base (0.002 mol in 200–300 ml). The mixture was refluxed on a waterbath for 2 hr. A methanolic solution of sodium methoxide (0.22 g, 0.004 mol in 30 ml) was added to this solution. The mixture was refluxed for 1 hr on a waterbath. The separated precipitate was suction filtered, washed with methanol and dried in vacuum at room temperature (yield = 70%).

Heterochelates of the type $UO_2L(AA)$ —A methanolic solution of dioxouranium(VI) acetate dihydrate (0.84 g, 0.002 mol in 10 ml) was added to a methanolic solution of the Schiff bases (1) ($X = H$, 0.52 g, 0.002 mol in 200 ml). The mixture was refluxed on a waterbath for 2 hr. A methanolic solution of the appropriate bidentate ligand (0.002 mol in 10 ml) was added to this mixture and was refluxed on a waterbath for 1 hr. The separated compounds were suction filtered, washed with methanol and were dried in vacuum at room temperature (yield = 80%).

3 Results and Discussion

3.1 Synthesis

The Schiff bases (1) react with dioxouranium (VI) acetate dihydrate in methanol in 1:1 ratio and form complexes of the type $UO_2L \cdot CH_3OH$. These complexes exhibit a broad band around 3400 cm^{-1} which can be assigned to the $\nu(OH)$ stretch of methanol. The $\nu(C—O)$ (alcoholic) stretch of methanol occurring¹⁴ at 1034 cm^{-1} shifts to $\sim 970\text{ cm}^{-1}$ and this is indicative of oxygen coordination of methanol. The complexes do not decompose or lose weight on heating at 120°C for hours and this indicates that (i) methanol is not lost at this temperature, and (ii) it is coordinated to uranium. The complexes react with NN donor bidentate ligands in methanol and heterochelate complexes of the type $UO_2L(AA)$ (where $L = N$ -salicylidene- N' -salicylhydrazide, $AA =$ ethylenediamine, trimethylenediamine, tetramethylenediamine, hexamethylenediamine, orthophenylenediamine, orthophenanthroline, 2,2'-dipyridyl or 3-aminopyridine) are formed. The heterochelates have been prepared *in situ* without isolating

the homochelate. We wish to point out that the *in situ* method of synthesis of heterochelates described here is simpler and less time-consuming as it does not involve the isolation of the homochelate in solid state. It is seen from Table 1 that all the complexes show non-electrolytic behaviour ($\Lambda_M = 1.2\text{--}8.8\text{ ohm}^{-1}\text{ cm}^2\text{ mol}^{-1}$). The complexes are monomers and are diamagnetic as expected for a $5f^0$ system.

3.2 Infrared Spectra

Although the Schiff bases (1) are potential tetradentate ligands, these have been found to behave as tridentate ligands and not as tetradentate ligands^{2–5}. The Schiff bases exhibit the $\nu(C=O)$ stretch at $1645\text{--}1660\text{ cm}^{-1}$ and this band is absent in the complexes indicating the destruction of $(C=O)$ group due to enolization (Table 2). A strong band in the ligands at $1620\text{--}1630\text{ cm}^{-1}$ is assigned to the $\nu(C=N)$ stretch. On complex formation, this band shifts to lower energy by $5\text{--}30\text{ cm}^{-1}$ indicating coordination through the nitrogen atom of the azomethine group of the Schiff bases¹⁵. The $\nu(C—O)$ (phenolic) stretch of the Schiff bases (1) occurs at $1535\text{--}1560\text{ cm}^{-1}$ and this band shifts to higher energy by $5\text{--}30\text{ cm}^{-1}$ in complexes, indicating oxygen coordination of these ligands¹⁶. The shift of the $\nu(C—O)$ (phenolic) band to higher energy is expected due to the maintenance of a ring current arising out of electron delocalization in the chelate ring. A new strong band at $1240\text{--}1250\text{ cm}^{-1}$ in the complexes is assigned to the $\nu(C—O)$ (enolic) stretch^{17,18}. The analytical data and the consideration of valence requirement of uranium indicate that the Schiff bases are behaving as dibasic ligands. There are two phenolic hydroxyl groups in the Schiff bases and on the basis of previous work^{2–4} in the field we suggest that the phenolic oxygen atom of salicylaldehyde moiety is coordinated. A broad band at $3300\text{--}3400\text{ cm}^{-1}$ in the complexes confirms the presence of non-coordinated OH group of ligands. Although this band may also be due to $\nu(OH)$, $\nu(CH_3OH)$ and $\nu(NH)$ of aliphatic or aromatic amines, the presence of this band in $UO_2L(AA)$ (where $AA =$ orthophenanthroline or 2,2'-dipyridyl) supports the above assignment. The $\nu(C=N)$ (ring) stretch of 2,2'-dipyridyl, orthophenanthroline and 3-aminopyridine occurs at 1582 , 1558 and 1590 cm^{-1} respectively^{19–21}. In the heterochelates, this band shifts to higher energy by $5\text{--}15\text{ cm}^{-1}$ and merges with the $\nu(C=N)$ (azomethine) stretch indicating nitrogen coordination of these bidentate ligands. The NH_2 bending vibration of ethylenediamine, trimethylenediamine, tetramethylenediamine, hexamethylenediamine, orthophenylenediamine and 3-aminopyridine occurs at 1620 , 1620 , 1620 , 1620 , 1640 and 1590 cm^{-1} respectively^{21,22}. In the dioxouranium(VI) hetero-

Table 1—Analytical, Conductance and Molecular Weight Data of Dioxouranium(VI) Complexes with the Schiff Bases^a

Compound ^(a)	Stoichiometry	Λ_M (ohm ⁻¹ mol ⁻¹ cm ²)	Mol. weight ^(b)	U, %	N, %	Ligand %
UO ₂ (sal-SHZ).CH ₃ OH	C ₁₅ H ₁₄ N ₂ O ₆ U	4.8	542	42.5	5.2	45.3
UO ₂ (5-chlorosal-SHZ).CH ₃ OH	C ₁₅ H ₁₃ N ₂ O ₆ ClU	8.8	(556)	(42.80)	(5.04)	(45.68)
UO ₂ (5-bromosal-SHZ).CH ₃ OH	C ₁₅ H ₁₃ N ₂ O ₆ BrU	2.8	610	40.2	4.5	49.1
UO ₂ (5-methoxysal-SHZ).CH ₃ OH	C ₁₆ H ₁₆ N ₂ O ₇ U	2.3	(590.5)	(40.30)	(4.74)	(48.86)
UO ₂ (3-methoxysal-SHZ).CH ₃ OH	C ₁₆ H ₁₆ N ₂ O ₇ U	5.8	649	37.2	4.7	52.1
UO ₂ (3-ethoxysal-SHZ).CH ₃ OH	C ₁₇ H ₁₈ N ₂ O ₇ U	5.2	(635)	(37.48)	(4.41)	(52.44)
UO ₂ (3,5-dichlorosal-SHZ).CH ₃ OH	C ₁₅ H ₁₂ N ₂ O ₆ Cl ₂ U	7.2	573	40.3	4.5	48.6
UO ₂ (hydroxy-SHZ).CH ₃ OH	C ₁₉ H ₁₆ N ₂ O ₆ U	6.7	(586)	(40.61)	(4.78)	(48.46)
UO ₂ (sal-SHZ).en	C ₁₆ H ₁₈ N ₄ O ₅ U	6.8	604	40.8	4.9	48.3
UO ₂ (sal-SHZ).tn	C ₁₇ H ₂₀ N ₄ O ₅ U	5.2	(600)	(39.67)	(4.67)	(49.67)
UO ₂ (sal-SHZ).bn	C ₁₈ H ₂₂ N ₄ O ₅ U	1.2	616	39.5	4.7	49.8
UO ₂ (sal-SHZ).hn	C ₂₀ H ₂₆ N ₄ O ₅ U	5.0	(606)	(39.27)	(4.62)	(50.17)
UO ₂ (sal-SHZ).phen	C ₂₀ H ₁₈ N ₄ O ₅ U	1.2	567	40.9	9.4	43.5
UO ₂ (sal-SHZ).dipy	C ₂₄ H ₁₈ N ₄ O ₅ U	3.7	(584)	(40.75)	(9.59)	(43.49)
UO ₂ (sal-SHZ).ampy	C ₁₉ H ₁₆ N ₄ O ₅ U	2.2	573	39.4	9.1	42.6
UO ₂ (sal-SHZ).ophen	C ₂₆ H ₁₈ N ₄ O ₅ U	3.9	(598)	(39.80)	(9.36)	(42.47)
			635	38.5	9.4	41.7
			(612)	(38.89)	(9.15)	(41.50)
			627	37.4	8.5	39.3
			(640)	(37.19)	(8.75)	(39.69)
			625	37.4	8.6	56.8 ^(c)
			(632)	(37.66)	(8.86)	(57.28)
			696	34.9	8.0	60.2 ^(c)
			(680)	(35.00)	(8.24)	(60.29)
			603	38.2	9.3	56.7 ^(c)
			(618)	(38.51)	(9.06)	(56.31)
			728	33.6	7.6	61.4 ^(c)
			(704)	(33.80)	(7.95)	(61.65)

^(a) Abbreviation: sal = salicylaldehyde, 5-chlorosal = 5-chlorosalicylaldehyde, 5-bromosal = 5-bromosalicylaldehyde, 5-methoxysal = 5-methoxysalicylaldehyde, 3-methoxysal = 3-methoxysalicylaldehyde, 3-ethoxysal = 3-ethoxysalicylaldehyde, 3,5-dichlorosal = 3,5-dichlorosalicylaldehyde, hydroxy = 2-hydroxy-1-naphthaldehyde, SHZ = salicylaldehydrazide, en = ethylenediamine, tn = trimethylenediamine, bn = tetramethylenediamine, hn = hexamethylenediamine, phen = orthophenylenediamine, dipy = 2,2'-dipyridyl, and ophen = orthophenanthroline

^(b) Values in parentheses in the last four columns are calculated values.

^(c) Schiff base and aromatic amine

chelates, this band shifts to lower energy by 20-30 cm⁻¹ and in some cases merges with the $\nu(\text{C}=\text{N})$ (azomethine) stretch. This is indicative of nitrogen coordination of these ligands.

The $\nu_s(\text{O}=\text{U}=\text{O})$ and $\nu_{as}(\text{O}=\text{U}=\text{O})$ stretching vibrations of the complexes occur at 800-840 and 870-910 cm⁻¹ respectively and these are in the usual range (ν_s , 780-885; ν_{as} , 870-950 cm⁻¹) as reported for the majority of dioxouranium(VI) complexes²³⁻²⁵. The introduction of bidentate ligands in UO₂L.CH₃OH leads to the shift of the ν_s and ν_{as} frequencies to lower energy. This is due to the fact that an increase in electron density at the uranium atom would enhance the repulsive forces with non-bonding electrons of the

atoms of UO₂ and, as a result, the weakening of the U—O bond occurs. The plot of ν_s versus ν_{as} gives a straight line and the data satisfy the equation, $\nu_s = -70 + 1.0\nu_{as}$. ν_s and ν_{as} are related by the equation²⁶: $\nu_s = (1 + 2M_{\text{O}}/M_{\text{U}})\nu_{as} = 0.94\nu_{as}$ (where M_{O} and M_{U} are the atomic masses of oxygen and uranium) in case of linear O = U = O moiety with no interaction of the ligands. The observed higher value of the slope and the negative value of the intercept are due to the strong interaction of equatorial ligands on UO₂ moiety. The force constant (f) for U = O bond has been calculated by the method of McGlynn *et al.*²⁶ and the values (Table 2) agree well with those for similar dioxouranium(VI) complexes. The U—O bond length

Table 2 Infrared Spectral Data of Dioxouranium(VI) Complexes with the Schiff Bases

Compound	Complex (ligand) $\nu(\text{C}=\text{N})$ cm^{-1}	$\nu(\text{C}=\text{O})$ (phenolic) cm^{-1}	ν_{as} ($\text{O}=\text{U}=\text{O}$) cm^{-1}	ν_s ($\text{O}=\text{U}=\text{O}$) $\nu_{\text{U}-\text{O}}$ cm^{-1}	mdyne/Å	$R_{\text{U}-\text{O}}$ Å
$\text{UO}_2(\text{sal-SHZ}) \cdot \text{CH}_3\text{OH}$	1605 (1620)	1565 (1545)	910	840	6.88	1.74
$\text{UO}_2(5\text{-chlorosal-SHZ}) \cdot \text{CH}_3\text{OH}$	1605 (1630)	1570 (1550)	895	825	6.65	1.74
$\text{UO}_2(5\text{-bromosal-SHZ}) \cdot \text{CH}_3\text{OH}$	1600 (1630)	1565 (1535)	895	825	6.65	1.74
$\text{UO}_2(5\text{-methoxysal-SHZ}) \cdot \text{CH}_3\text{OH}$	1595 (1620)	1560 (1555)	885	810	6.51	1.75
$\text{UO}_2(3\text{-methoxysal-SHZ}) \cdot \text{CH}_3\text{OH}$	1605 (1620)	1570 (1560)	895	825	6.65	1.74
$\text{UO}_2(3\text{-ethoxysal-SHZ}) \cdot \text{CH}_3\text{OH}$	1600 (1620)	1570 (1555)	890	820	6.58	1.75
$\text{UO}_2(3,5\text{-dichlorosal-SHZ}) \cdot \text{CH}_3\text{OH}$	1595 (1620)	1560 (1555)	890	810	6.58	1.75
$\text{UO}_2(\text{hydroxy-SHZ}) \cdot \text{CH}_3\text{OH}$	1585 (1620)	1550 (1535)	880	810	6.43	1.75
$\text{UO}_2(\text{sal-SHZ}) \cdot \text{en}$	1600	1550	870	800	6.29	1.75
$\text{UO}_2(\text{sal-SHZ}) \cdot \text{tn}$	1600	1555	880	810	6.43	1.75
$\text{UO}_2(\text{sal-SHZ}) \cdot \text{bn}$	1600	1555	885	815	6.51	1.75
$\text{UO}_2(\text{sal-SHZ}) \cdot \text{hn}$	1600	1555	900	830	6.73	1.74
$\text{UO}_2(\text{sal-SHZ}) \cdot \text{phen}$	1595	1550	890	805	6.58	1.75
$\text{UO}_2(\text{sal-SHZ}) \cdot \text{bipy}$	1600	1550	900	830	6.73	1.74
$\text{UO}_2(\text{sal-SHZ}) \cdot 3\text{-Ampy}$	1600	1550	895	825	6.65	1.74
$\text{UO}_2(\text{sal-SHZ}) \cdot \text{ophen}$	1600	1550	900	830	6.73	1.74

 Table 3 Proton NMR Spectral Data (δ in ppm) of Schiff Bases and Dioxouranium (VI) Complexes

Compound	Alcoholic proton	Alkyl protons	Alkoxy protons	Aromatic protons	Azomethine protons	Phenolic protons	N H proton
Sal-SHZ	—	—	—	6.96-8.02 (m, 8H)	8.76 (s, 1H)	10.86 (s, 2H)	11.64 (s, 1H)
$\text{UO}_2(\text{sal-SHZ}) \cdot \text{CH}_3\text{OH}$	2.57 (s, 1H)	3.50 (s, 3H)	—	6.76-7.70 (m, 8H)	8.42-8.48 (s, 1H)	9.38 (s, 1H)	—
5-chlorosal-SHZ	—	—	—	6.94-8.02 (m, 7H)	8.74 (s, 7H)	10.94 (s, 2H)	11.70 (s, 1H)
$\text{UO}_2(5\text{-chlorosal-SHZ}) \cdot \text{CH}_3\text{OH}$	2.58 (s, 1H)	3.48 (s, 3H)	—	6.90-8.00 (m, 7H)	8.42-8.52 (s, 1H)	9.38 (s, 1H)	—
5-bromosal-SHZ	—	—	—	6.92-8.02 (m, 7H)	8.72 (s, 1H)	10.82 (s, 2H)	11.67 (s, 1H)
$\text{UO}_2(5\text{-bromosal-SHZ}) \cdot \text{CH}_3\text{OH}$	2.59 (s, 1H)	3.50 (s, 3H)	—	6.90-7.90 (m, 7H)	8.42-8.50 (s, 1H)	9.38 (s, 1H)	—
5-methoxysal-SHZ	—	—	3.74 (s, 3H)	6.90-8.00 (m, 7H)	8.68 (s, 1H)	10.84 (s, 2H)	12.18 (s, 1H)
$\text{UO}_2(5\text{-methoxysal-SHZ}) \cdot \text{CH}_3\text{OH}$	2.54 (s, 1H)	3.46 (s, 3H)	3.78 (s, 3H)	6.88-7.94 (m, 7H)	8.41-8.46 (s, 1H)	9.28 (s, 1H)	—
3-methoxysal-SHZ	—	—	3.88 (s, 3H)	6.90-8.00 (m, 7H)	8.76 (s, 1H)	10.94 (s, 2H)	12.06 (s, 1H)
$\text{UO}_2(3\text{-methoxysal-SHZ}) \cdot \text{CH}_3\text{OH}$	2.59 (s, 1H)	3.60 (s, 3H)	3.92 (s, 3H)	6.84-7.88 (m, 7H)	8.44-8.54 (s, 1H)	9.34 (s, 1H)	—
3-ethoxysal-SHZ	—	—	1.41-1.48 (t, 3H)	6.80-8.03 (m, 7H)	8.78 (s, 1H)	10.90 (s, 2H)	12.02 (s, 1H)
$\text{UO}_2(3\text{-ethoxysal-SHZ}) \cdot \text{CH}_3\text{OH}$	2.58 (s, 1H)	3.58 (s, 3H)	4.02-4.23 (q, 2H)	6.72-7.82 (m, 7H)	8.44-8.51 (s, 1H)	9.38 (s, 1H)	—
3,5-dichlorosal-SHZ	—	—	4.30-4.79 (q, 2H)	6.90-7.92 (m, 6H)	8.62 (s, 1H)	10.88 (s, 2H)	11.68 (s, 1H)
$\text{UO}_2(3,5\text{-dichlorosal-SHZ}) \cdot \text{CH}_3\text{OH}$	2.50 (s, 1H)	3.52 (s, 3H)	—	6.88-7.68 (m, 6H)	8.41-8.44 (s, 1H)	9.32 (s, 1H)	—

Values given in parentheses under the δ values indicate the type of signal and the nature of the proton causing the signal: s, singlet; t, triplet; q, quartet; and m, multiplet.

(R) has been calculated using the equation²⁷ $R = 1.08f^{1/3} + 1.17$, and the values are in the range 1.74-1.76 Å and these occur in the usual range (1.60-1.92 Å) as reported for the majority of dioxouranium(VI) complexes²⁸.

3.3 Electronic Spectra

The Schiff base 1 (X = H) exhibits four bands at 30030, 33780, 40650 and 45660 cm^{-1} due to the $n \rightarrow \pi^*$, hydrogen bonding and association, $\pi \rightarrow \pi^*$ and $\text{Ph} \rightarrow \text{Ph}^*$ transitions respectively^{5,29}. In the complexes, the $n \rightarrow \pi^*$ transition shifts to lower energy ($\sim 27,800 \text{ cm}^{-1}$). The band due to hydrogen bonding and association is absent in the complexes, as expected. The band due to $\pi \rightarrow \pi^*$ transition does not undergo appreciable shift on complex formation. The complexes exhibit a new band at around 21,000 cm^{-1} which is assigned to the $^1E_g^+ \rightarrow ^3\Pi_u$ transition typical of OOU symmetric stretch frequency for the first excited state³⁰.

3.4 NMR Spectra

The NMR spectra of the Schiff bases (1) and the complexes $\text{UO}_2\text{L} \cdot \text{CH}_3\text{OH}$ were recorded in $\text{DMSO}-d_6$. The chemical shifts (δ) are expressed in Table 3 in ppm downfield from tetramethylsilane. The ligands exhibit a multiplet at 6.72-8.00 ppm due to aromatic protons, a singlet at 8.62-8.78 ppm due to azomethine proton, a broad signal at 10.82-10.94 ppm due to phenolic hydroxylic protons, and a singlet at 11.64-12.18 ppm due to the N—H proton^{5,31,32}. The NMR data of the ligands indicate the presence of the keto form of the ligands in $\text{DMSO}-d_6$. Methanol exhibits alcoholic protons at 4.84 ppm and methyl protons at 3.35 ppm³³. The appearance of alcoholic proton (singlet, 1H) at 2.50-2.59 ppm and methyl protons (singlet, 3H) at 3.46-3.60 ppm in the spectra of the complexes confirms the presence of methanol in the complexes³⁴. In the spectra of the complexes, the signal due to the azomethine proton appears at 8.21-8.54 ppm (singlet, 1H). The downward shift of this signal indicates the coordination of the nitrogen atom of the azomethine group^{5,31,35}. The uncoordinated phenolic hydroxyl proton occurs at 9.28-9.38 ppm. The absence of N—H proton in the spectra of the complexes indicates the enolization of the keto group. The Schiff bases 1 (X = 3-methoxy and 5-methoxy) exhibit a signal (singlet, 3H) due to the methoxy group at 3.88 and 3.74 ppm respectively. In the complexes, these signals suffer a small shielding: 4.10 ppm for X = 3-methoxy and 3.78 ppm for X = 5-methoxy. The Schiff base 1 (X = 3-ethoxy) exhibits a triplet at 1.41-1.48 ppm due to methyl protons and a quartet at 4.02-4.23 ppm due to methylene protons. In the dioxouranium (VI) complexes, these bands appear at 1.58-1.74 (triplet) and 4.30-4.79 ppm (quartet).

It is apparent from the evidence presented that the complexes $\text{UO}_2\text{L} \cdot \text{CH}_3\text{OH}$ are octahedral and the heterochelates $\text{UO}_2\text{L}(\text{AA})$ are seven coordinated.

Acknowledgement

The authors are indebted to the Department of Atomic Energy, Government of India, Bombay, for financial support to this study.

References

- 1 Craliz J C, Rub J C, Willis D & Edger J, *Nature (GB)*, **34** (1955) 176.
- 2 Narang K K & Aggarwal A, *Inorg Chim Acta (Switzerland)*, **9** (1974) 137.
- 3 Iskander M F, Sayed L El & Lasheen M A, *Inorg Chim Acta (Switzerland)*, **16** (1976) 147.
- 4 Syamal A & Kale K S, *Indian J Chem*, **16A** (1978) 46.
- 5 Pardhy S A, Gopinathan S & Gopinathan C, *Indian J Chem*, **18A** (1979) 239.
- 6 Biradar N S & Angadi S D, *J Inorg Nucl Chem (GB)*, **38** (1976) 1405.
- 7 Syamal A, *Coord Chem Rev (Netherlands)*, **16** (1975) 309.
- 8 Syamal A & Kale K S, *J Mol Structure (Netherlands)*, **38** (1977) 195.
- 9 Syamal A & Kale K S, *Inorg Chem (USA)*, **18** (1979) 992.
- 10 Syamal A & Singhal O P, *Transition Metal Chem (Germany)*, **4** (1979) 179.
- 11 Syamal A & Kumar D, *J Less Common Metals (Netherlands)*, **71** (1980) 113.
- 12 Welcher F J, *Organic analytical reagents*, Vol. 3 (Van Nostrand, New York) 1947, 254.
- 13 Mann F G & Saunders B C, *Practical organic chemistry* (Longmans, London) 1961, 435.
- 14 Herzberg G, *Molecular spectra and molecular structure*, Vol. 2 (Van Nostrand, New York) 1959, 335.
- 15 Teyssi P & Charrette J J, *Spectrochim Acta (GB)*, **19** (1963) 1407.
- 16 Battley G E & Graddon D P, *Aust J Chem (Australia)*, **20** (1967) 875.
- 17 Ueno K & Martell A E, *J Phys Chem (USA)*, **59** (1955) 998.
- 18 Freedman H H, *J Am Chem Soc (USA)*, **83** (1961) 2900.
- 19 Schilt A A & Taylor R C, *J Inorg Nucl Chem (GB)*, **9** (1959) 211.
- 20 Inskeep R G, *J Inorg Nucl Chem (GB)*, **24** (1962) 763.
- 21 Matritzky A R, Hands A R & Jones R A, *J Chem Soc (GB)*, (1958) 3165.
- 22 Segal L & Eggerton F V, *Appl Spectrosc (USA)*, **15** (1961) 112.
- 23 Comyns A E, Gatehouse B M & Wait E, *J Chem Soc (GB)*, (1958) 4655.
- 24 Jones M M, *J Chem Phys (USA)*, **23** (1955) 2105.
- 25 Caldow G L, Cleave A B V & Eager R L, *Can J Chem (Canada)*, **38** (1960) 772.
- 26 McGlynn S P, Smith J K & Neely W C, *J Chem Phys (USA)*, **35** (1961) 105.
- 27 Jones L H, *Spectrochim Acta (GB)*, **10** (1958) 395; **11** (1959) 409.
- 28 Zachariasen W H, *Acta Crystallogr (Denmark)*, **8** (1954) 347.
- 29 Syamal A & Singhal O P, *Transition Metal Chem (Germany)*, **4** (1979) 179.
- 30 McGlynn S P & Smith J K, *J Mol Spectrosc (USA)*, **6** (1961) 164.
- 31 Hsieh A T T, Sheashan R M & West B O, *Aust J Chem (Australia)*, **28** (1975) 885.
- 32 Silverstein R M & Bassler G C, *Spectrometric identification of organic compounds* (Wiley, New York), 2nd Edn, 1967, 122.
- 33 Ref. 32, p 135.
- 34 Syamal A, Fricks D H, Pantaleo D C et al., *J Less Common Metals (Netherlands)*, **19** (1969) 141.
- 35 Sharma R K, Singh R V & Tandon J P, *Indian J Chem*, **18A** (1979) 360.

Reference Interaction Site Model (RISM) for the Liquid Structure of Oxygen, Chlorine & Iodine

R V GOPALA RAO* & B M SATPATHY

Physical Chemistry Section, Department of Chemistry, Jadavpur University, Calcutta 700032

Received 14 December 1981

The reference interaction site model (RISM) equations have been used for fused hard spheres as well as Lennard-Jones (LJ) interaction sites fluids to obtain the site-site distribution functions and the structure function of liquid oxygen, chlorine and iodine. The use of LJ interaction sites improves the result over that of hard sphere calculations of Hsu *et al.* [*Chem Phys (Netherlands)*, **14** (1976) 213] for oxygen. In chlorine a three (hard sphere interaction)-site model with an auxiliary site at the centre of the molecule works better than a two (LJ)-site model. Liquid iodine has been studied with a three-site model. In the case of oxygen, the agreement is excellent and in the other two cases the RISM theory fails to give a good account of the experimental results and the agreement is only qualitative. The intermolecular potential functions have been obtained for these liquids from the RISM structure function.

1 Introduction

The reference interaction site model (RISM) theory¹⁻³ has been applied to study the equilibrium structure of a number of fused hard-sphere molecular liquids⁴⁻⁶, and it has been found to predict good results for the distribution functions. Recently, Johnson and Hazoume⁷ have extended the study to include Lennard-Jones (LJ) interaction site fluids and have concluded that the RISM distribution functions of LJ interaction site fluids are as accurate as RISM distribution functions for hard sphere (HS) interaction site fluids. In this paper, the formalism of Johnson and Hazoume⁷ has been used to study the liquid structure of oxygen, chlorine and iodine taking both HS and LJ interaction sites.

2 Theory

In the RISM theory, each molecule is assumed to have a specified number of interaction sites. The RISM equations relating the site-site total correlation function, $h_{\alpha\gamma}(r)$, to the site-site direct correlation function, $C_{\alpha\gamma}(r)$ and the site-site indirect correlation function, $y_{\alpha\gamma}(r)$ are as follows:

$$\hat{h}(k) = \hat{\omega}(k) \hat{C}(k) [I - \rho \hat{\omega}(k) \hat{C}(k)]^{-1} \hat{\omega}(k) \quad \dots (1)$$

$$C_{\alpha}(r) = \{\exp[-\beta u_{\alpha\gamma}(r)] - 1\} y_{\alpha\gamma}(r) \quad \dots (2)$$

and

$$h_{\alpha\gamma}(r) = y_{\alpha\gamma}(r) + C_{\alpha\gamma}(r) - 1 \quad \dots (3)$$

In Eqs (1)-(3), I is the unit matrix, ρ the molecular number density and β is equal to $1/k_B T$, where k_B is the Boltzmann constant and T is the temperature of the liquid. The function $u_{\alpha\gamma}(r)$ is the site-site interaction potential between site α of one molecule and site γ of another molecule. The function $\hat{\omega}_{\alpha\gamma}(k)$ is defined as

$$\omega_{\alpha\gamma}(k) = \sin(k l_{\alpha\gamma}) / k l_{\alpha\gamma} \quad \dots (4)$$

where $l_{\alpha\gamma}$ is the distance between the sites α and γ in the same molecule. The function $\hat{\omega}_{\alpha\gamma}(k)$ gives the ideal gas structure function for diatomic molecules, which is given by $1 + \hat{\omega}_{\alpha\gamma}(k)$, where the interaction sites α and γ sit at the two atomic centres, in a diatomic molecule.

The site-site pair distribution function $g_{\alpha\gamma}(r)$ is defined as

$$g_{\alpha\gamma}(r) = h_{\alpha\gamma}(r) + 1 \quad \dots (5)$$

The Fourier transform (FT) of $h_{\alpha\gamma}(r)$ is denoted by $\hat{h}_{\alpha\gamma}(k)$.

The RISM Eqs (1) to (3) can be solved numerically by a process of iteration. To start with, the function $y_{\alpha\gamma}(r)$ is taken to be equal to unity, for all r .

If $y'_{\alpha\gamma}(r)$ is defined as

$$y'_{\alpha\gamma}(r) = y_{\alpha\gamma}(r) - 1 \quad \dots (6)$$

then from Eqs (1) and (3), we have

$$\begin{aligned} \hat{y}'_{\alpha\gamma}(k) = & -\hat{C}_{\alpha\gamma}(k) + \{\hat{\omega}(k) \hat{C}(k) \\ & \times [1 - \rho \hat{\omega}(k) \hat{C}(k)]^{-1} \hat{\omega}(k)\}_{\alpha\gamma} \end{aligned} \quad \dots (7)$$

which is used to complete the iterative cycle.

Let $[\hat{y}'_{\alpha\gamma}(k)]_n$ denote the $y'_{\alpha\gamma}(k)$ used in the n th iteration of Eq. (7), and $[\hat{Y}'_{\alpha\gamma}(k)]_n$ denote the right hand side of the same equation after n iterations. Thus, the relationship between $[\hat{y}'_{\alpha\gamma}(k)]_n$ and $[\hat{Y}'_{\alpha\gamma}(k)]_n$ can be written as

$$\begin{aligned} [\hat{y}'_{\alpha\gamma}(k)]_{n+1} = & [\hat{Y}'_{\alpha\gamma}(k)]_n + \Psi \{[\hat{y}'_{\alpha\gamma}(k)]_n \\ & - [\hat{Y}'_{\alpha\gamma}(k)]_n\} \end{aligned} \quad \dots (8)$$

where Ψ is the mixing parameter and is chosen such that a reasonably rapid convergence is obtained for the iterative method.

The site-site potentials used are the hard-sphere potential given by

$$\begin{aligned} u_{\alpha\gamma}(r) = & \infty & r \leq \sigma_{\alpha\gamma} \\ = & 0 & r > \sigma_{\alpha\gamma} \end{aligned} \quad \dots (9)$$

and the repulsive LJ potential given by

$$u_{\alpha\gamma}(r) = 4\epsilon_{\alpha\gamma} \left[\left(\frac{\sigma_{\alpha\gamma}}{r} \right)^{12} - \left(\frac{\sigma_{\alpha\gamma}}{r} \right)^6 \right] + \epsilon_{\alpha\gamma}, \quad r \leq 2^{1/6} \sigma_{\alpha\gamma}$$

$$(r) = 0 \quad r > 2^{1/6} \sigma_{\alpha\gamma} \quad \dots(10)$$

where $\sigma_{\alpha\gamma}$ and $\epsilon_{\alpha\gamma}$ are the diameter and the potential depth respectively.

The function, $n_{\alpha\gamma}(r)$ gives the average number of sites of type γ associated with molecules 2, 3, ..., N that will be found within a sphere of radius r centred on the α th site of molecule 1. Thus,

$$n_{\alpha\gamma}(r) = 4\pi \rho_{\alpha\gamma} \int_0^r g_{\alpha\gamma}(r) r^2 dr \quad \dots(11)$$

When the right hand side of Eq. (11) is integrated over the first co-ordination shell, $n_{\alpha\gamma}(r)$ gives the co-ordination number of γ -sites around an α -site.

The RISM structure function $S(k)$ for homonuclear diatomic molecules is given by

$$S(k) = 1 + \hat{w}_{12}(k) + 2\rho h_{12}(k) \quad \dots(12)$$

3 Results and Discussion

Hsu *et al.*⁴ have applied the fused hard-sphere interaction site model for liquid oxygen. They used both a two-site model and also a three-site model with an auxiliary site at the centre of the molecule. The implications of the use of auxiliary sites have been discussed by them in detail. Johnson and Hazoume's method⁷ allows one to use the more realistic LJ potential for the site-site interaction in this liquid. In our present model for oxygen molecule, we have two interaction sites located at the centre of the oxygen atoms, lying at a distance of 1.20 Å and interacting through a repulsive LJ potential as defined by Eq. (10). Calculations were performed with various sets of potential parameters, i.e. σ_{OO} and ϵ_{OO} (where the subscript O stands for the oxygen atom site) so as to obtain the best possible fit with the experimental

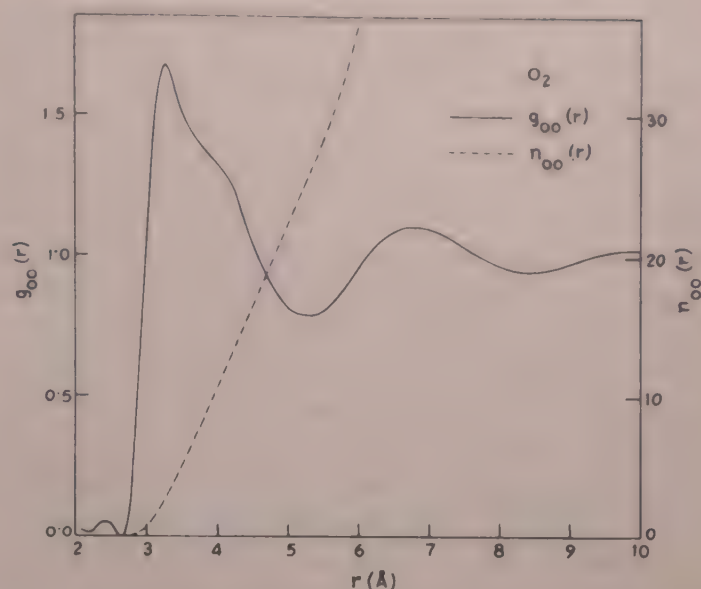


Fig. 2—Site-site pair distribution functions, $g_{\alpha\gamma}(r)$ of liquid oxygen

Table 1—Values of Various Parameters in RISM Calculation for Liquid Oxygen

$T = 84 \text{ K};$	$\rho = 0.02198/\text{\AA}^3$
$l_{OO} = 1.20 \text{ \AA};$	$\sigma_{OO} = 3.00 \text{ \AA}$
$\epsilon_{OO} = 0.75 \times 10^{-14} \text{ erg}$	
$\Psi = 0.8$	

structure factor, $S(k)$ obtained by Dore *et al.*⁸ by neutron diffraction at the same state for the liquid. The best result was obtained for $\sigma_{OO} = 3.00 \text{ \AA}$ and $\epsilon_{OO} = 0.75 \times 10^{-14} \text{ erg}$. The $S(k)$ thus obtained has been compared in Fig. 1 along with the experimental result of Dore *et al.*⁸ and Hsu *et al.*'s result⁴ for a two (hard sphere interaction)-site model. It is clearly seen that the use of repulsive LJ potential improves the result, all throughout the k -space, over the fused hard-sphere sites model. It may be pointed out here that a long-range LJ potential was also tried, but no solution to the RISM equations was found, and hence a cutoff LJ potential defined by Eq. (10) was used. Table 1 gives the various parameters used in the RISM calculation for liquid oxygen.

The RISM pair distribution function for oxygen atoms $g_{OO}(r)$ and the oxygen atom co-ordination number, $n_{OO}(r)$ obtained are plotted in Fig. 2. From this analysis, the number of nearest neighbour oxygen atoms around central oxygen atom has been found to be nearly 26. Hsu *et al.*⁴ also obtained the same result.

Gamertsfelder⁹ has reported the $S(k)$ of liquid chlorine from X-ray diffraction. There being very little information, it will be of interest to see liquid structure of chlorine in the light of RISM theory. While working on liquid bromine, Hsu *et al.*⁴ have concluded that a three-site model with an auxiliary site at the molecular centre (denoted by say, X) improves the result over a simple two-site model with the sites located at the

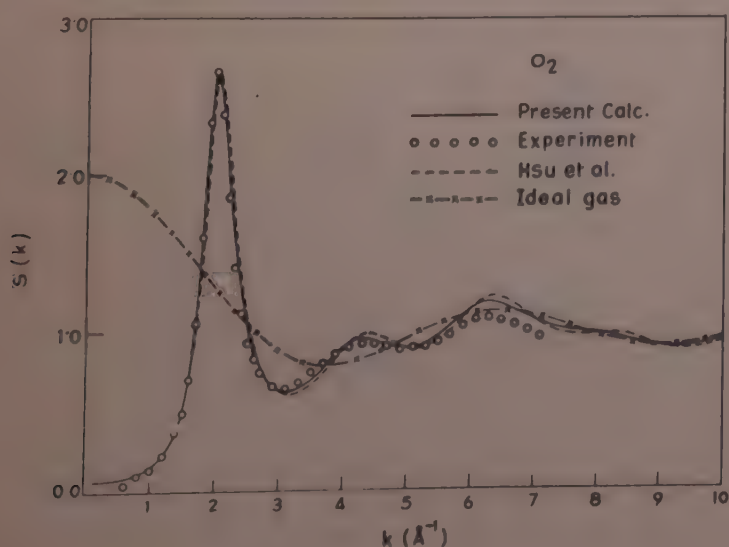


Fig. 1—Structure function, $S(k)$ of liquid oxygen

atomic centres. Thus a two-site model with repulsive LJ interaction sites and a three-site model with HS interaction sites have been used in the liquid chlorine study. The $S(k)$ s obtained from both the models have been plotted in Fig. 3, along with the experimental result of Gamertsfelder⁹. The three-site model predicts better agreement with experiment than the two-site model, though none of the two accounts quantitatively the experimental results. Particularly, the small peak at 5.2 \AA^{-1} , found in the experimental $S(k)$ curve, could not be reproduced from our calculations. However, in the three-site calculation, the third peak in $S(k)$ splits and a shoulder-like peak is obtained at 6.2 \AA^{-1} , which may be corresponding to the experimental peak at 5.2 \AA^{-1} . In the large k region, the fit is very good. Though quantitatively not so good, the theoretical result is in good qualitative agreement with experiment. Further, since the experimental results⁹ are pretty old, the extent of its accuracy is doubtful. The RISM parameters obtained for the best fit to experimental result for liquid chlorine are given in Table 2.

The RISM theory has the advantage of giving all the site-site partial distribution functions and thus give a complete picture of the liquid structure. Fig. 4 shows the three partial pair distribution functions, $g_{\text{Cl-Cl}}(r)$, $g_{\text{X-Cl}}(r)$ and $g_{\text{X-X}}(r)$, where X stands for the auxiliary site at the centre of the molecule. The number of neighbours around a chlorine atom in the first co-ordination shell comes out to be 23. As seen from the $g_{\text{Cl-Cl}}(r)$ curve, the first co-ordination shell around a chlorine atom is quite complex.

It is only very recently that Bosi *et al.*¹⁰ have performed neutron diffraction measurement on liquid iodine at 409 K, to obtain the structure function in the low k region. Liquid iodine shows a distinct split at the first peak of the structure function which is not observed in liquid chlorine, but present in a less conspicuous way in liquid bromine. Hsu *et al.*⁴ explained this feature in liquid bromine taking a three (hard sphere)-site model. For the iodine molecule, we

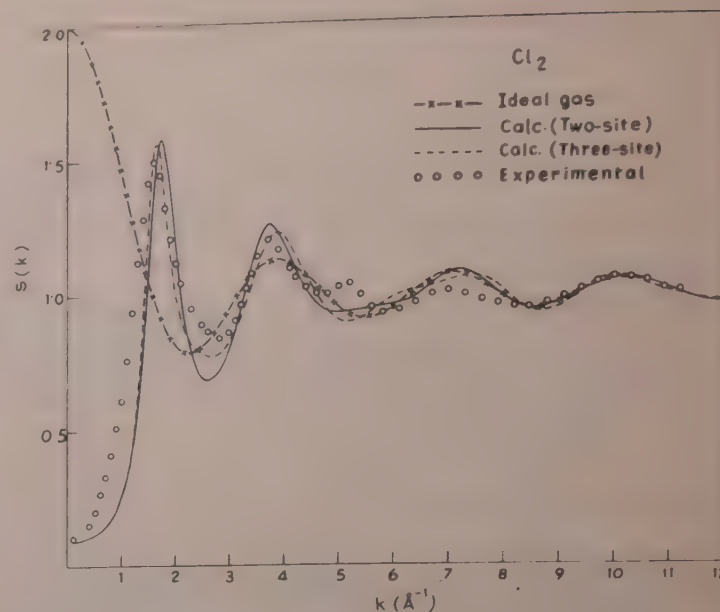
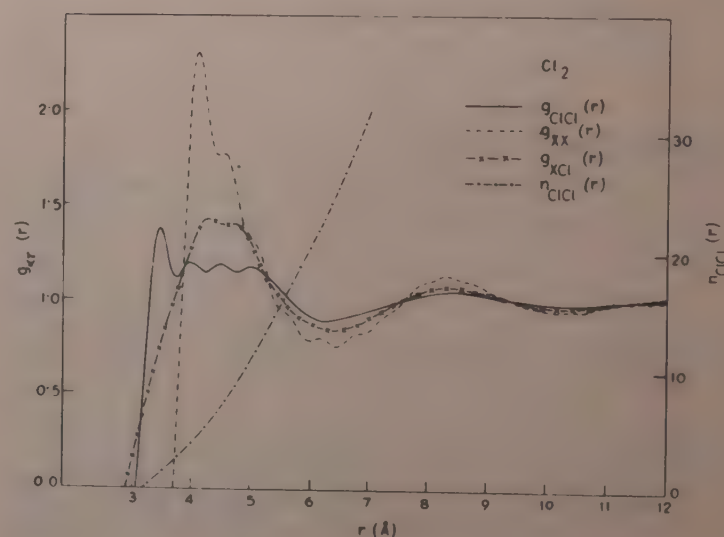
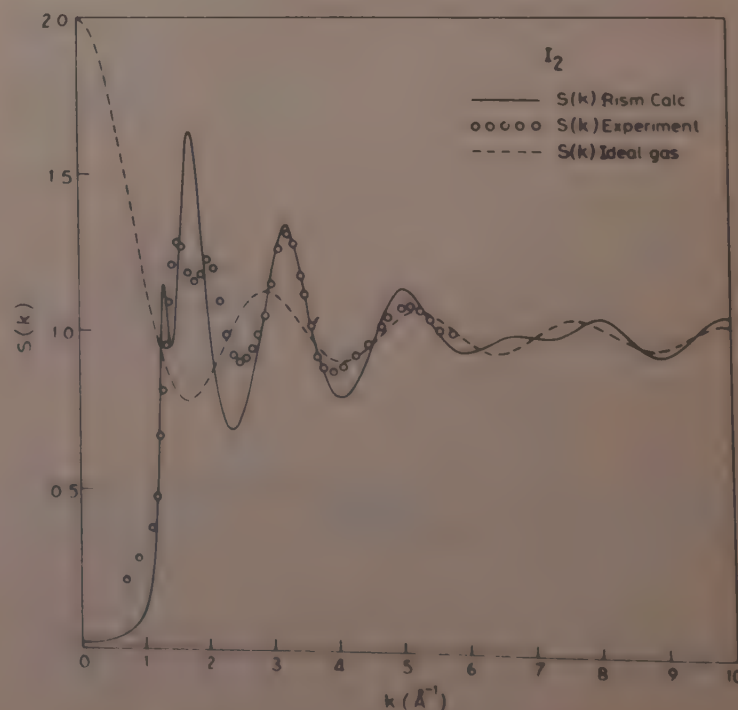

 Fig. 3—Structure function, $S(k)$ of liquid chlorine

 Fig. 4—Site-site pair distribution functions, $g_{ij}(r)$ of liquid chlorine

 Fig. 5—Structure function, $S(k)$ of liquid iodine

Table 2— RISM Parameters for Liquid Chlorine

$T = 298 \text{ K}; \quad \rho = 0.011893 \text{ \AA}^{-3}$	
$l_{\text{Cl-Cl}} = 1.99 \text{ \AA}$	
Two-site model parameters	
$\sigma_{\text{Cl-Cl}} = 3.425 \text{ \AA}$	
$\epsilon_{\text{Cl-Cl}} = 2.22 \times 10^{-14} \text{ erg}$	
$\Psi = 0.6$	
Three-site model parameters	
$\sigma_{\text{Cl-Cl}} = 3.20 \text{ \AA}$	
$\sigma_{\text{Cl-X}} = 2.90 \text{ \AA}$	
$\sigma_{\text{X-X}} = 3.85 \text{ \AA}$	
$\Psi = 0.6$	

take a three hard sphere interaction site model, one each lying on the atomic centres and the third at the centre of the molecule. Various sets of parameters were tried for the $\sigma_{\alpha\gamma}$ s to obtain a good account of the experimental $S(k)$. The best fit was obtained for $\sigma_{II} = 3.80 \text{ \AA}$, $\sigma_{IX} = 3.45 \text{ \AA}$ and $\sigma_{XX} = 5.30 \text{ \AA}$. In Fig. 5, we compare the RISM $S(k)$ function with the neutron diffraction result of Bosi *et al.*¹⁰ The results obtained are only in qualitative agreement with experiment. With the present model, we could obtain the split in the first peak, but the peak heights and positions are not in conformity with experimental results. However, from the second peak onwards the agreement with experiment is better. The various potential parameters, along with other constants are given for liquid iodine in Table 3.

The partial pair distribution functions obtained for liquid iodine are given in Fig. 6, along with the $n_{II}(r)$ function. An iodine atom is seen to have about 17 iodine atoms as its nearest neighbours.

The intermolecular angle-averaged potential function has been calculated for the three liquids from the RISM $S(k)$ obtained, through a method given by Gopala Rao and Joarder¹¹. In Figs 7 and 8, we present these potentials. For liquid chlorine and iodine, a smooth curve of the potential function has been plotted. The oxygen potential does not show a pronounced potential energy depth. This may be

Table 3—Potential Parameters and Other Constants for Liquid Iodine

$T = 409 \text{ K}; \rho = 0.011698/\text{\AA}^3$
$l_{II} = 2.666 \text{ \AA}$
$\sigma_{II} = 3.80 \text{ \AA}$
$\sigma_{IX} = 3.45 \text{ \AA}$
$\sigma_{XX} = 5.30 \text{ \AA}$
$\Psi = 0.9$

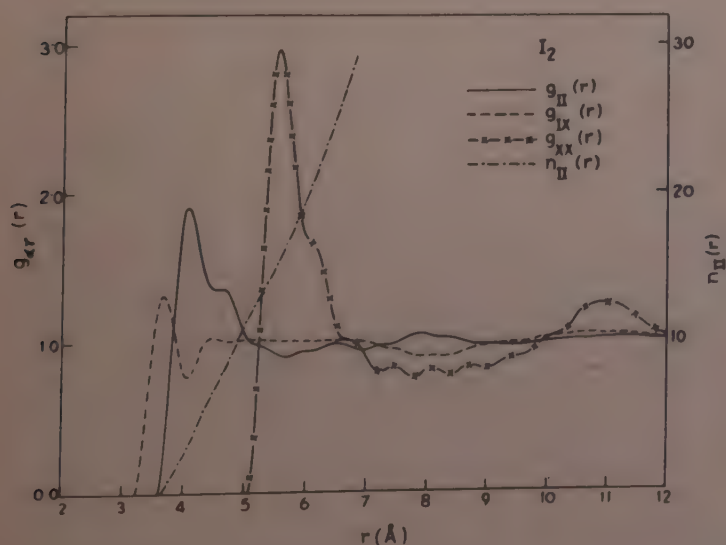


Fig. 6—Site-site pair distribution functions, $g_{\alpha\gamma}(r)$ of liquid iodine

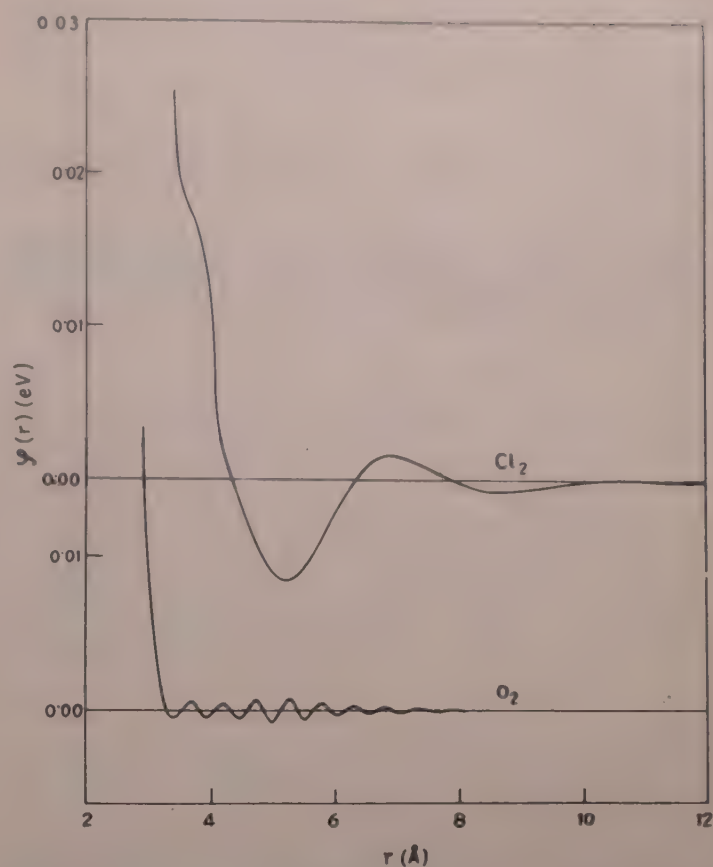


Fig. 7—Intermolecular potential function, $\phi(r)$ of liquid oxygen (84 K) and liquid chlorine (298 K)

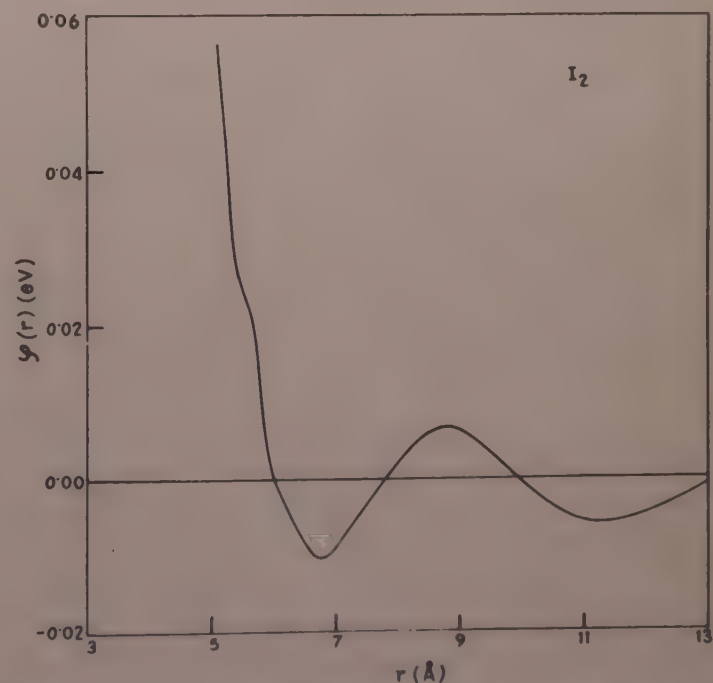


Fig. 8—Intermolecular potential function, $\phi(r)$ of liquid iodine (409 K)

because of the fact that the calculations have been performed near the boiling temperature of the liquid. The liquid chlorine and iodine potentials are alike, each showing a shoulder at the positive side of the potential function curve at the first neighbour distance.

Acknowledgement

One of the authors (BMS) wishes to thank the Department of Science and Technology, Govt of India

for the award of a SRF during the period of this work, and RVGR acknowledges partial financial support from University Grants Commission, New Delhi.

References

- 1 Chandler D & Anderson H C, *J Chem Phys (USA)*, **57** (1972) 1930.
- 2 Lowden L J & Chandler D, *J Chem Phys (USA)*, **59** (1973) 6587.
- 3 Lowden L J & Chandler D, *J Chem Phys (USA)*, **61** (1974) 5228.
- 4 Hsu C S, Chander D & Lowden L J, *Chem Phys (Netherlands)*, **14** (1976) 213.
- 5 Hsu C S & Chandler D, *Mol Phys (GB)*, **36** (1978) 215.
- 6 Murad S & Gubbins K E, *Mol Phys (GB)*, **39** (1980) 271.
- 7 Johnson E & Hazoume R P, *J Chem Phys (USA)*, **70** (1979) 1599.
- 8 Dore J C, Walford G & Page D I, *Mol Phys (GB)*, **29** (1975) 565.
- 9 Gamertsfelder C, *J Chem Phys (USA)*, **9** (1941) 450.
- 10 Bosi P, Cilloco F & Ricci M A, *Mol Phys (GB)*, **40** (1980) 1285.
- 11 Gopala Rao R V & Joarder R N, *Phys Lett A (Netherlands)*, **67** (1978) 71.

Interacting Bosons and Properties of Liquid ^4He II

K M KHANNA & S CHAUBA SINGH*†

Department of Materials Science, National Institute of Foundry & Forge Technology (NIFFT), Hatia, Ranchi 834 003
and

O P SINHA

Department of Applied Physics, Birla Institute of Technology, Mesra, Ranchi 835 215

Received 2 November 1981; revised received 23 January 1982

Properties of interacting bosons have been studied using the Hamiltonian written in terms of the density fluctuation operator ρ_k and the velocity operator v_k . Calculations carried out for the excitation spectrum, structure factor and velocity of sound for a dilute system of bosons using Gaussian potential and Lennard-Jones potential show a marked agreement with the corresponding values obtained experimentally for liquid ^4He for only some definite values of wave number k only. The calculations show that if the transition temperature is large, the depletion is small and vice versa.

1 Introduction

In our previous paper¹, the properties of interacting bosons have been studied using the Hamiltonian written in terms of the density fluctuation operator ρ_k and velocity operator v_k . The calculations done for the Bogoliubov excitation energy spectrum¹ E_k^B showed marked difference between the theoretical and the experimental curves. As shown earlier², this result might improve if we take into account the effect of phonon-phonon interaction in the excitation spectrum. In Ref. 2, it is also mentioned that the best realistic potential to be used for such type of calculation will be that of Lennard-Jones potential.

In an attempt to improve the results obtained earlier¹, we have used both the Lennard-Jones and the Gaussian equivalent of Lennard-Jones potentials in our present calculations. In Ref. 1, the effective mass of helium atom m^* was used in the reaction matrix t_k only. In the present paper, m^* has been introduced in the excitation energies E_k^{L-J} and E_k^G . Studies of both low and high density systems of bosons using hard core followed by an attractive square well potential have already been done by Khanna and Phukan³. These calculations were extended by Khanna *et al.*⁴ for the calculation of energy excitation spectrum and structure factor λ_k using Gaussian equivalent of the Lennard-Jones potential. They obtained good agreement with the experimental curve of Cowley and Woods⁵ for the energy excitation spectrum for a high density system of bosons. However, for a low density system they could not get proper roton dip. It is also seen that at sufficiently low density the roton dip vanishes, as already pointed out by Padmore⁶.

The main purpose of the present paper is to study the elementary excitation spectrum E_k , λ_k and the ground state energy of an assembly of interacting bosons by using the formalism derived earlier² and replacing $v(k)$, the Fourier transform of the interaction potential between helium atoms by t_k . The use of soft core² has no theoretical foundation and as such we have used hard core.

We have done calculations of E_k^B , λ_k and the ground state energy by using both Lennard-Jones potential and Gaussian equivalent of the Lennard-Jones potential. To calculate E_k , we have not used the effect of phonon-phonon interaction, instead we have introduced the effective mass m^* . We replaced the mass of helium atom m by m^* for the calculation of E_k . With the proper choice of m^*/m value we are able to get similar results as obtained by Kebukawa *et al.*² using phonon-phonon interaction. We used in our calculation the value of $m^*/m = 1.18$ which is the same as used by Kumar and Kachhava⁷ for their calculation of E_k using Lennard-Jones potential for a high density system of bosons. It seems that the introduction of phonon-phonon interaction and the calculation replacing m by m^* are equivalent processes since in that case the E_k curve shows a better agreement with the experimental curve.

As for the calculation of λ_k , there is hardly any change in its value with the introduction of m^* . This may be due to the fact that λ_k is a Fourier transform of the pair distribution function which will absorb in its fold the nature of all kinds of interactions that may exist in the system.

We have also done calculations of the transition temperature, the depletion of the ground state and velocity of sound c_1 . Graphs have been drawn for c_1 for different values of wave number k , keeping density

*On leave from the Department of Physics, D M College of Science, Imphal.

constant and also c_1 for different densities in the limit $k \rightarrow 0$.

2 Theoretical Derivation

Let us consider a system of N -bosons enclosed in a volume Ω . It is assumed that the density is held constant even when N and Ω are allowed to approach infinity. The Hamiltonian in terms of ρ_k and v_k is given in Ref. 2 as

$$H = \left\{ \frac{N(N-1)}{2\Omega} v(0) - \frac{N}{2\Omega} \sum_{k \neq 0} v(k) - \frac{\hbar^2}{4m} \sum_k k^2 \right\} + \sum_k \left\{ \frac{1}{2m} v_k \cdot v_{-k} + \left(\frac{\hbar^2 k^2}{8m} + \frac{N}{2} v(k) \right) \rho_k \rho_{-k} \right\} + \sum_{\substack{p, q \\ p+q \neq 0}} \left\{ \frac{1}{2mN^{1/2}} v_p \rho_{p+q} v_q + \frac{\hbar^2}{8mN^{1/2}} (p \cdot q) \rho_p \rho_{-p-q} \rho_q \right\} - O\left(\frac{1}{N}\right) \quad \dots (1)$$

The collective variables ρ_k and v_k can be written as

$$\rho_k = \lambda_k^{1/2} (B_k + B_{-k}^*)$$

and

$$v_k = \frac{\hbar k}{2\lambda_k^{1/2}} (B_{-k} - B_k^*) \quad \dots (2)$$

respectively, where

$$\lambda_k = \frac{k}{\{k^2 + c^2(k)\}^{1/2}} \quad \dots (3)$$

and

$$c^2(k) = \frac{4mN}{\hbar^2 \Omega} v(k) \quad \dots (4)$$

The operators B_k and B_k^* satisfy the commutation relations

$$[B_k, B_k] = [B_k^*, B_k^*] = 0$$

and

$$[B_k, B_k^*] = \delta_{k, k} \quad \dots (5)$$

Introducing Eq. (2) into Eq. (1), we have the Hamiltonian

$$H = H_0 + H_1 \quad \dots (6)$$

where

$$H_0 = E_0^B + \sum_k E_k^B B_k^* B_k$$

and

$$H_1 = \frac{\hbar^2}{8mN^{1/2}} \sum_{\substack{p, q \\ p+q \neq 0}} (p \cdot q) \left(\frac{\lambda_{p+q}}{\lambda_p \lambda_q} \right)^{1/2} (1 + \lambda_p \lambda_q) \times \{ B_p^* B_{p+q}^* B_q + B_p B_{p+q} B_q^* + B_p^* B_q^* B_{p+q} + B_p^* B_{p+q} B_q \}$$

$$- \frac{2\hbar^2}{8mN^{1/2}} \sum_{\substack{p, q \\ p+q \neq 0}} (p \cdot q) \left(\frac{\lambda_{p+q}}{\lambda_p \lambda_q} \right)^{1/2} (1 - \lambda_p \lambda_q) \times \{ B_{-q}^* B_{p+q}^* B_p + B^* B_{p+q} B_{-q} \} \quad \dots (7)$$

where

$$E_0^B = \frac{N(N-1)}{2\Omega} v(0) + \frac{1}{2} \sum_{k \neq 0} \left\{ E_k^B - \frac{\hbar^2 k^2}{2m} - \frac{N}{\Omega} v(k) \right\} \quad \dots (8)$$

and

$$E_k^B = \frac{\hbar^2 k}{2m} \{k^2 + c^2(k)\}^{1/2} \quad \dots (9)$$

The expression E_0^B represents the ground state energy in the lowest order approximation. The energy E_k^B represents the Bogoliubov excitation energy and it does not involve the effect of phonon-phonon interaction H_1 .

The quantities of interest that are to be calculated explicitly are: (1) λ_k given by Eq. (3); (2) E_0^B given by Eq. (8); and (3) E_k^B given by Eq. (9).

The calculation of these quantities requires the evaluation of $v(k)$ which contains hard core as is the case in helium atoms. Fourier transform of an interaction potential containing hard core cannot be evaluated. Moreover, if we only take the matrix element of the interaction potential, the effect of multiple scattering cannot be taken into account. In order to take into account the many-body interactions, $v(k)$ should be replaced by t_k . Thus the quantities λ_k , E_k^B and E_0^B can be written as

$$\lambda_k = k(k^2 + 4mN t_k / \hbar^2)^{-1/2} \quad \dots (10)$$

$$E_k^B = \frac{\hbar^2 k}{2m} (k^2 + 4mN t_k / \hbar^2)^{1/2} \quad \dots (11)$$

and

$$E_0^B = \frac{N(N-1)}{2\Omega} t_{00,00} + \frac{1}{2} \sum_{k \neq 0} \{ E_k^B - \hbar^2 k^2 / 2m - N t_k \Omega \} \quad \dots (12)$$

Following Ref. 1, we have

$$t_k = t_{00,00} \frac{\sin ka}{ka} \quad \dots (13)$$

Introducing Eq. (13) in Eqs (10), (11) and (12) and replacing N/Ω by ρ , we get

$$\lambda_k = k \left(k^2 + \frac{4m \sin ka}{\hbar^2 ka} \rho t_{00,00} \right)^{-1/2} \quad \dots (14)$$

$$E_k^B = \frac{\hbar^2 k}{2m} \left(k^2 + \frac{4m \sin ka}{\hbar^2 ka} \rho t_{00,00} \right)^{1/2} \quad \dots (15)$$

and

$$E_0^B = \frac{N(N-1)}{2\Omega} t_{00,00}$$

$$+ \frac{1}{2} \sum_{k \neq 0} \left\{ E_k^B - \hbar^2 k^2 / 2m - \frac{\sin ka}{ka} \rho t_{00,00} \right\} \dots (16)$$

3 Interaction Potentials

The interaction potentials to be used for our calculations are:

Lennard-Jones potential given by

$$V_{(L-J)}(r) = \begin{cases} +\infty & r \leq a \\ 4\epsilon \left\{ (a/r)^{12} - (a/r)^6 \right\} & r \geq a \end{cases} \dots (17)$$

and Gaussian potential given by

$$V_{(G)}(r) = \begin{cases} +\infty & r \leq a \\ 4\epsilon \left[\exp \left\{ -\left(\frac{r-a}{\mu_R} \right)^2 \right\} - \exp \left\{ -\left(\frac{r-a}{\mu_A} \right)^2 \right\} \right] & r \geq a \end{cases} \dots (18)$$

where μ_R and μ_A are repulsive and attractive ranges after the hard core. The values of the parameters chosen for our calculations for both the potentials are

$$a = 2.1 \text{ \AA}, \quad \epsilon = 14.11 \times 10^{-16} \text{ erg}$$

$$\mu_R^2 = 0.1103 \times 10^{-16} \text{ cm}^2; \quad \mu_A^2 = 0.2206 \times 10^{-16} \text{ cm}^2$$

From Refs 1 and 4 we can write for a dilute system of bosons,

$$t_{00,00} = \frac{B}{m} \{1 + C + D\} + 4\pi \int r^2 V(r) (1 - a/r)^2 dr \dots (19)$$

$$\text{where } B = 4\pi a \hbar^2; \quad C = (8\pi \rho a^3)^{1/2} \text{ and } D = \frac{16}{3} \pi \rho a^3$$

For the Lennard-Jones potential, we have from Ref. 7,

$$t_{00,00} = \frac{B}{m} \{1 + C + D\} - 4\pi (0.1252 \epsilon a^3) \dots (20)$$

and for the Gaussian potential, we have from Refs 3 and 4

$$t_{00,00} = \frac{B}{m} \{1 + C + D\} + 4\pi^{3/2} \epsilon (\mu_R^3 - \mu_A^3) \dots (21)$$

4 Excitation Energy Spectrum E_k

Replacing m by m^* in Eq. (15) and substituting for $t_{00,00}$ from Eqs (20) and (21), we have expressions for E_k as

$$E_k^{(L-J)} = A \left\{ \frac{B}{m^*} (1 + C + D) - 4\pi (0.1252 \epsilon a^3) \right\}^{1/2} \dots (22a)$$

and

$$E_k^{(G)} = A \left\{ \frac{B}{m^*} (1 + C + D) + 4\pi^{3/2} \epsilon (\mu_R^3 - \mu_A^3) \right\}^{1/2} \dots (22b)$$

$$\text{where } A = (\hbar^2 k / 2m^*) \left\{ k^2 + (4m^* / \hbar^2) \frac{\rho \sin ka}{ka} \right\}^{1/2}$$

5 Ground State Energy per Particle

From Eq. (16) the ground state energy per particle is written as

$$E_0^B / N = \frac{1}{2} \rho t_{00,00} + (1/4\pi^2 \rho) \int k^2 \left\{ E_k^B - (\hbar^2 k^2 / 2m) - \frac{\sin ka}{ka} \rho t_{00,00} \right\} dk \dots (23)$$

Inserting the parameters as used in the calculation of E_k^B , E_0^B / N is calculated approximately as:

$$E_0^B / N = -6.10 \times 10^{-16} \text{ erg (using Gaussian potential)}$$

and

$$E_0^B / N = -3.32 \times 10^{-16} \text{ erg (using Lennard-Jones potential)}$$

The value obtained in Ref. 2 with lowest-order approximation is $E_0^B / N = -9.07 \times 10^{-16} \text{ erg}$ whereas the experimental value⁸ is $-9.7 \times 10^{-16} \text{ erg}$.

6 Velocity of Sound

In the limit $k \rightarrow 0$, Landau's relation between the energy E_k of a phonon and its momentum $\hbar k$ is,

$$E_k = c_1 \hbar k \dots (24)$$

where c_1 is the velocity of sound in liquid helium at absolute zero. We have from Ref. 9

$$E_k = \hbar^2 k^2 / 2m^* \lambda_k \dots (25)$$

From Eqs (24) and (25) we get

$$c_1 = \hbar k / 2m^* \lambda_k \dots (26)$$

$$\text{As } k \rightarrow 0, c_1 \rightarrow \left(\frac{\rho}{m^*} t_{00,00} \right)^{1/2} \dots (27)$$

The value of c_1 calculated from Eq. (27) is 259.95 msec^{-1} for the Gaussian potential and 249.96 msec^{-1} for the Lennard-Jones potential as compared to the experimental value of 239 msec^{-1} . We have calculated c_1 for various values of k by using Eq. (26), and also for various values of densities at $k \rightarrow 0$ by using Eq. (27).

7 Depletion of the Ground State

The depletion of the ground state can be calculated by using the relation given in Ref. 1

$$\rho - \rho_0 = (2\pi m k' T_c / \hbar^2)^{3/2} \exp(-\epsilon' / k' T_c) \dots (28)$$

where ρ is the total density of the particles constituting the boson assembly, ρ_0 the number density of particles in the ground state, k' the Boltzmann constant, and \hbar the Planck's constant. We impose the restriction that, since the interaction is weak, the excited state ϵ' will be approximately equal to the energy per particle in the ground state. T_c is the critical temperature of transition and is given by the relation¹

$$T_c = T_0 [1 - 0.256 \exp(-\epsilon' / k' T_0)] \dots (29)$$

where T_0 is the ideal Bose-Einstein condensation temperature and is equal to 3.18 K .

For the Gaussian potential, ϵ' is 6.10×10^{-16} erg,
 $T_c = 2.943$ K, and $\rho_0/\rho = 0.92$... (30)

For the Lennard-Jones potential, $\epsilon' = 3.32 \times 10^{-16}$ erg,
 $T_c = 2.766$ K, and $\rho_0/\rho = 0.87$... (31)

8 Numerical Calculations and Results

Inserting the value of $t_{00,00}$ from Eqs (20) and (21) into Eqs (14), (15) and (16), λ_k , E_k^B , E_0^B/N are calculated and E_k is calculated from Eqs (22a) and (22b) using the following parameters:

$a = 2.1 \text{ \AA}$; $\epsilon = 14.11 \times 10^{-16} \text{ erg}$;
 $m = 6.646 \times 10^{-24} \text{ g}$; $m^* = 1.18 m$;
 $\rho = 2.165 \times 10^{22} \text{ particles cm}^{-3}$;
 $\hbar = 1.054 \times 10^{-27} \text{ erg sec}$;
 $\mu_R^2 = 0.1103 \times 10^{-16} \text{ cm}^2$; and
 $\mu_A^2 = 0.2206 \times 10^{-16} \text{ cm}^2$.

The results of the various calculations are plotted in Figs 1-5. In Fig. 1, E_k^B and E_k are plotted against k using Gaussian potential and E_k' is the experimental curve due to Cowley and Woods⁵. In Fig. 2, E_k^B and E_k are drawn against k using Lennard-Jones potential. In Fig. 3, λ_k is plotted against k using both Gaussian as well as Lennard-Jones potentials. In Fig. 4, the velocity of sound (c_1) is plotted against k , and in Fig. 5 c_1 at various densities is drawn for both the potentials.

9 Discussion

The purpose of all calculations so far has been to see how best the results obtained from theory of interacting

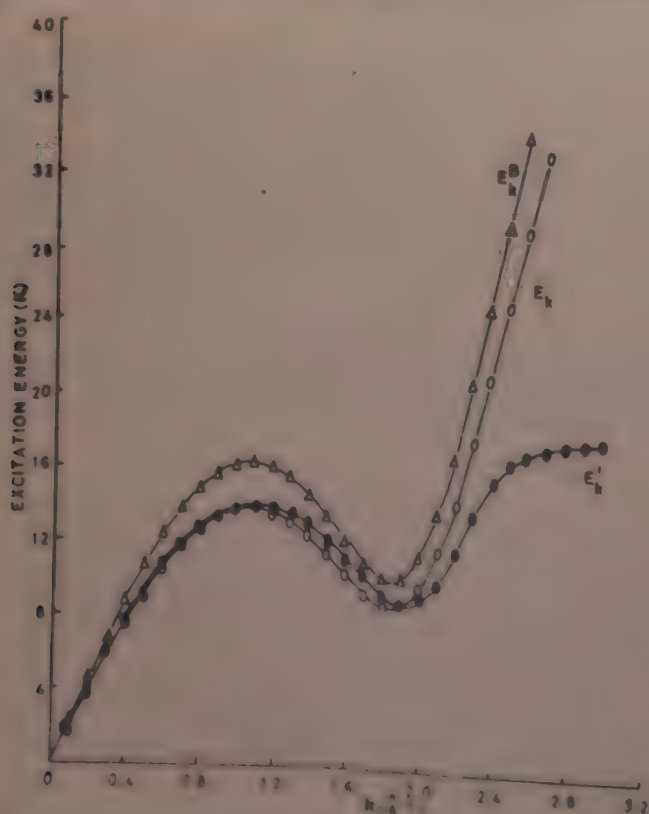


Fig. 1—Excitation energy spectra of liquid ^4He [Curves E_k^B and E_k are drawn for Gaussian potential using Eqs (15) and (22b) respectively; E_k' is the experimental curve due to Cowley and Woods⁵]

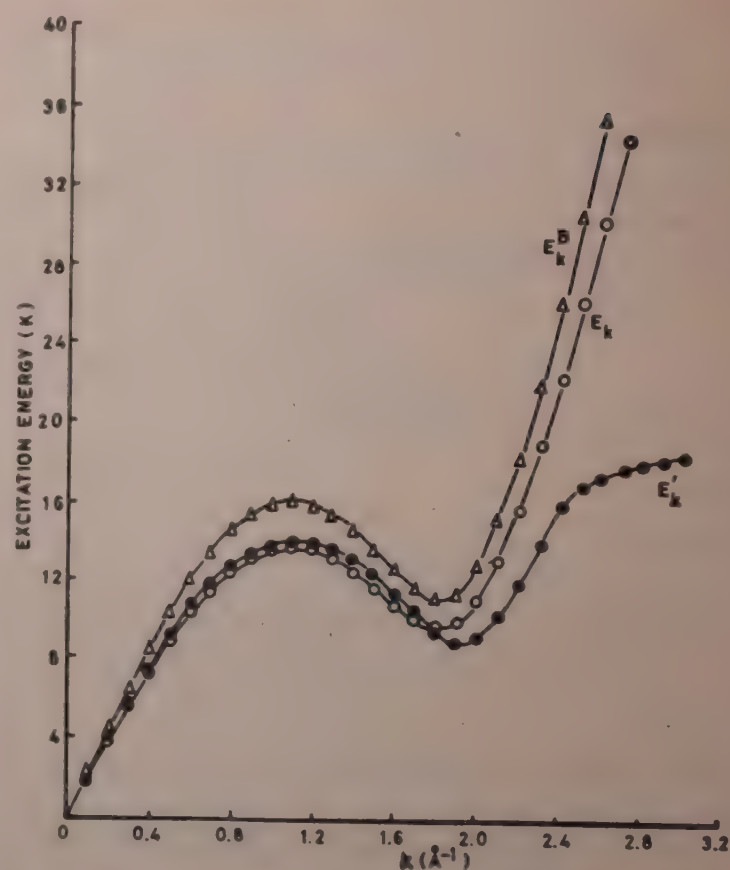


Fig. 2—Excitation energy spectra of liquid ^4He [Curves E_k^B and E_k are drawn for Lennard-Jones potential using Eqs (15) and (22a) respectively; E_k' is the experimental curve⁵]

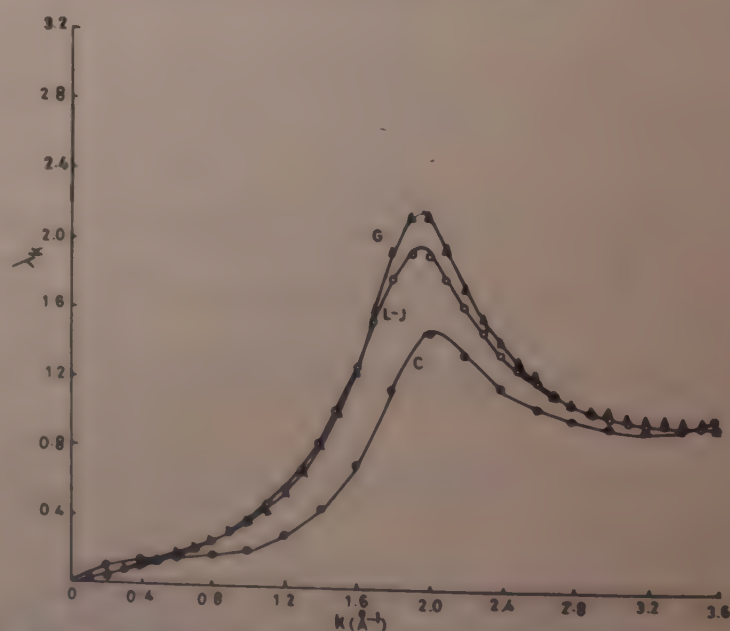


Fig. 3— λ_k versus k graph [Curves G and L—J are drawn for Gaussian and Lennard-Jones potentials respectively using Eq. (14); curve C is the experimental curve due to Henshaw¹⁰.]

bosons can agree with the experimental observations on liquid ^4He . There are only two major hurdles in obtaining an exact agreement. One is the exact form of the interaction potential between the helium particles and the other is the exact relation between E_k and λ_k that should be valid for all values of k . We had built a potential³ that has been used by Lu and Chan¹¹ to obtain a better roton fit. In the present calculation, we have used a few different potentials to see how the results

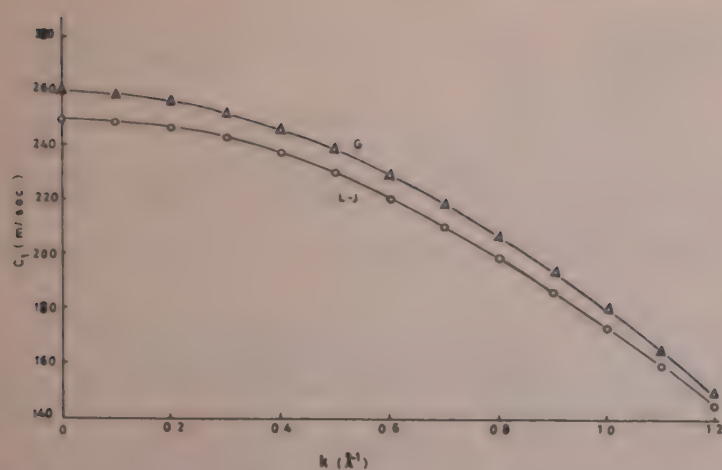


Fig. 4— c_1 as a function of k drawn from Eq. (26) [Curves G and L—J are drawn for Gaussian and Lennard-Jones potentials respectively.]

Table 1—Comparison of Landau Spectrum

Source	$\Delta(k)$ (in K^{-1})	k_0 (in \AA^{-1})	Reference
Neutron Scattering	8.67 ± 0.04	1.936 ± 0.005	Cowley & Woods ⁵
Thermodynamics	9.60	1.95	Landau ¹²
Theoretical	8.452	1.9	Kebukawa <i>et al.</i> ²
-do-	8.60	1.85	Present work (Gaussian potential)
-do-	9.39	1.85	Present work (Lennard-Jones)
-do-	8.78	1.8	Khanna <i>et al.</i> ⁴
-do-	7.92	1.9	Lu & Chan ¹¹

compare with each other. We are still unable to obtain an exact relation between E_k and λ_k , and the old approximate relations available in literature have been used.

Fig. 1 gives the plot of E_k against k for the Gaussian potential and this plot is compared with the experimental E'_k versus k graph for liquid ^4He . The agreement between theory and experiment is very good up to $k = 0.7 \text{ \AA}^{-1}$, and at $k = 0.8 \text{ \AA}^{-1}$ where the phonon region roughly ends, the agreement is excellent, both E_k^G and E_k^{exptl} being 12.65 K. Similarly from $k = 0.9 \text{ \AA}^{-1}$ onwards, the agreement between theory and experiment is fairly good, but at the dip of the roton region at $k = 1.9 \text{ \AA}^{-1}$, the agreement is again excellent with both E_k^G and E_k^{exptl} being 8.70 K.

Such a remarkable agreement between theory and experiment is, however, not available when we use either the Lennard-Jones potential or square well potential after the hard core for interacting bosons. Results obtained by different workers and for different potentials are given in Table 1.

Table 2 gives the ground state energy per particle obtained by different workers using different interaction potentials; the experimentally known value for the same

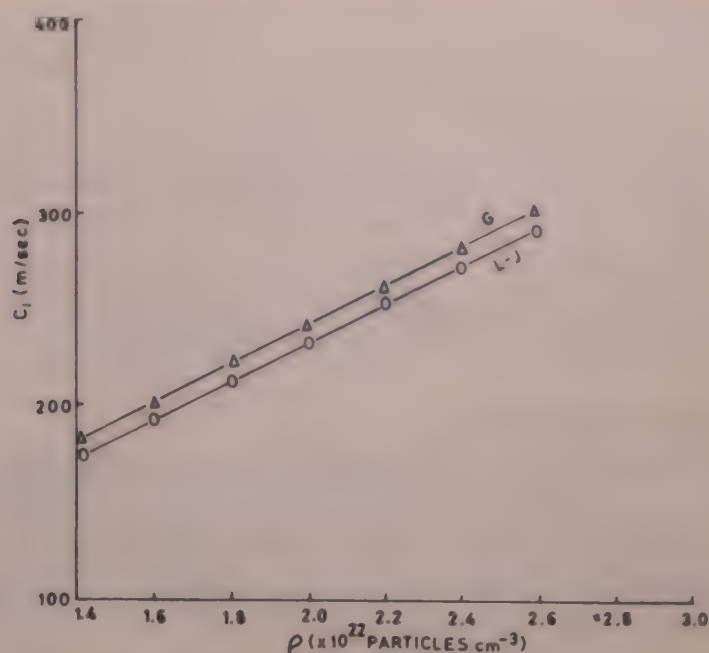


Fig. 5— c_1 versus density at $k \rightarrow 0$ [Curves G and L—J are drawn for Gaussian and Lennard-Jones potentials respectively using Eq. (27)]

Table 2—Ground State Energy per Particle E_0^B/N (in 10^{16} erg^{-1})

$\rho, 10^{22} \text{ particles cm}^{-3}$	E_0^B/N	Reference
2.18	-9.7	Exptl ⁸
2.1834	-9.07	Kebukawa <i>et al.</i> ²
2.165	-6.16	Present work (Gaussian potential)
2.165	-3.32	Present work (L—J potential)

is also given. The comparison shows poor agreement among the various results and hence the need for further work to obtain a result that agrees with the experimental result, is clearly indicated.

The λ_k values are plotted in Fig. 3. There is again a sharp disagreement between theory and experiment; only the qualitative nature of the curve given in Fig. 3 has the form given in the experimental curve.

The value of the velocity of sound c_1 for $\rho = 2 \times 10^{22} \text{ particles cm}^{-3}$ is 243.21 m/sec and is nearest to the experimental value of $239 \pm 2 \text{ m/sec}$.

The transition temperature calculations and the depletion results given in Eqs (30) and (31) show some interesting behaviour. If the T_c is large the depletion is small and vice versa. This will also mean that if the energy gap between the zero momentum state and the first excited state is large, the transition temperature will be large and the depletion will be small and vice versa. This is established from the results in Eqs (30) and (31). However, our T_c values, 2.943 K and 2.766 K, are large compared with the experimental value of 2.176 K for liquid ^4He .

From our work in this field (spread over more than a decade), we have now come to the conclusion that unless

we are able to find an exact relation between E_k and λ_k that is valid for all values of k and not merely in the limit $k \rightarrow 0$, the agreement between theory and experiment will continue to remain poor, although the interaction potential given in Eq. (18) and constructed by us long ago seems to be of the right type. We are now concentrating on obtaining such an exact relation starting from pair distribution function. This will form the subject matter for our future communications.

Acknowledgement

One of the authors (SCS) is thankful to the University Grants Commission, New Delhi, and the Government of Manipur for the award of a teacher fellowship. The authors thank Dr S S Khanna, Director, NIFFT, Ranchi for encouragement.

References

- 1 Khanna K M, Singh S C & Sinha O P, *Indian J Pure & Appl Phys.*, **19** (1981) 985.
- 2 Kebukawa T, Yamasaki S & Sunakawa S, *Prog Theo Phys (Japan)*, **41** (1969) 919; **44** (1970) 565.
- 3 Khanna K M & Phukan A N, *Physica A (Netherlands)*, **58** (1972) 263; **60** (1972) 488.
- 4 Khanna K M, Das B K & Sinha O P, *Physica A (Netherlands)*, **76** (1974) 137.
- 5 Cowley R A & Woods A D B, *Can J Phys (Canada)*, **49** (1971) 177.
- 6 Padmore T C, *Phys Rev Lett (USA)*, **39A** (1974) 826.
- 7 Kumar M & Kachhava C M, *Physica B (Netherlands)*, **101** (1980) 98.
- 8 Koller E W, *Helium-3 and helium-4*, (Plenum Press, New York) 1968, 137.
- 9 Khanna K M & Mehrotra S N, *Physica A (Netherlands)*, **89** (1977) 626.
- 10 Henshaw D G, *Phys Rev (USA)*, **119** (1960) 9.
- 11 Lu P & Chan C K, *Phys Rev B (USA)*, **20** (1979) 3709.
- 12 Landau L D, *J Phys (USSR)*, **5** (1941) 71; **11** (1947) 94.

Bound s-State Energies for Superposed Screened Coulomb Potential in Ecker-Weizel Approximation

A P KAJWADKAR & L K SHARMA*

Department of Applied Physics, Government Engineering College, Jabalpur 482001

Received 5 February 1982; revised received 13 September 1982

Quantum defect, quantum number shift and bound *s*-state eigen energies for *ns* states of a superposed screened Coulomb potential have been obtained. It is also observed that this potential possesses features similar to alkali atoms and alkali-like ions.

1 Introduction

Screened Coulomb potentials have attracted considerable attention on account of their ability to describe adequately the effective interaction in a many-body environment of a variety of fields such as atomic, nuclear, solid state and plasma physics. The normalization screening theory has been applied successfully to explain the anomalously large photo-defect cross-section in molecular hydrogen¹. There are many atomic and nuclear processes which are characterized by the behaviour of an electron wavefunction at the origin. One such phenomenon is the orbital electron capture and in this, only the region of overlap between electron and nuclear wavefunctions is involved.

The screened Coulomb potential has been treated numerically and analytically by various workers using different methods such as the WKB method², the quantum defect method³ and different types of perturbation and non-perturbation methods⁴⁻⁶. But all these methods are not simple and involve many parameters. Ecker and Weizel⁷ solved the radial Schrödinger equation by a simple and approximate method. Using the same standard procedure, Lam and Varshni⁸ and Rogers *et al.*⁹ obtained bound *s*-state energies for the static screened Coulomb potential (SSCP). Ray and Ray¹⁰ obtained *s*-matrix, discrete energies and wavefunctions for the *s*-states of exponential cosine screened Coulomb potential (ECSC) in Ecker-Weizel (EW) approximation. Recently, Dutt¹¹ and Dutt *et al.*¹² calculated bound *s*-state energies of an electron in ECSC potential by the analytical method in EW approximation. They further proposed an extension of EW approximation to treat the non-zero angular momentum bound states of a class of screened Coulomb potential and obtained the energies for Yukawa potential. The Yukawa potential is given by

$$V_I(r) = -\frac{g_1}{r} e^{-\delta r} \quad \dots(1)$$

while the modified screened Coulomb potential has the form

$$V_{II}(r) = -\frac{g_2}{r} e^{-\lambda \delta r} \quad \dots(2)$$

The potential given by Eq. (1) is also called the Debye potential and finds application in plasma physics describing effectively the interaction of a plasma sea on a localized two-particle system. The screening parameter δ is affected by the temperature and density of the plasma sea. At a given density and temperature, the average radius would exceed one half of the average internuclear separation. In this region, the approximation that the electron is bound to a single proton no longer remains valid. One must take into account, therefore, systems in which the electron is bound in screened Coulomb potential having a more general form and potential (2) actually depicts such a situation. Motivated by the above considerations, we have solved the Schrödinger equation for a potential which contains in itself, the possibility of describing most of the above mentioned conditions. We have obtained the bound *s*-state energies for various *ns* state for the potential

$$V(r) = -\frac{(g_1 e^{-\delta r} + g_2 e^{-\lambda \delta r})}{r} \quad \dots(3)$$

These energy values are shown in Table 1. To observe the variation in energy due to the superposition of modified screened Coulomb potential (2) on Yukawa potential (1), the corresponding energy values for the Yukawa potential are also mentioned in Table 1.

2 General Solution

The radial Schrödinger equation for bound *s*-states of potential (3) will then be

$$\left[\frac{1}{2} \frac{d^2}{dr^2} + (g_1 e^{-\delta r} + g_2 e^{-\lambda \delta r}), r - E \right] X(r) = 0 \quad \dots(4)$$

Here the system of units chosen is such that $\hbar = m = c = 1$. Eq. (2) can be converted to the form

Table 1—Energy Eigenvalues as a Function of the Screening Parameter for Various ns States for Potential (3) with $g_1 = g_2 = 1$ and $\lambda = 2$

δ	E_{1s}		E_{2s}	
	A	B	A	B
0.0002	1.9990	0.4998	0.4998	0.1248
0.0005	1.9975	0.4995	0.4995	0.1245
0.001	1.9950	0.4990	0.4990	0.1240
0.002	1.9900	0.4980	0.4980	0.1230
0.005	1.9751	0.4950	0.4901	0.1200
0.01	1.9505	0.4899	0.4802	0.1150
0.02	1.9020	0.4799	0.4610	0.1053
0.04	1.8080	0.4598	0.4239	0.0864
0.06	1.6596	0.4398	0.3880	0.0689
0.08	1.6246	0.4197	0.3539	0.0528
0.1	1.5379	0.3996	0.3215	0.0386
0.2	1.1524	0.3010	0.1855	—
0.4	0.5893	0.1272	0.0295	—

(A, our results and B, Yukawa potential)

$$\frac{d^2\phi}{dr^2} - 2\alpha_n \frac{d\phi}{dr} + \frac{2}{r}(g_1 e^{-\delta r} + g_2 e^{-\lambda\delta r})\phi(r) = 0 \quad \dots(5)$$

by substituting

$$X(r) = \phi(r) e^{-\alpha_n r} \quad \dots(6)$$

in which

$$\alpha_n = \sqrt{2E_n} \quad \dots(7)$$

Now, on changing the variable¹³ from r to $y = 1 - e^{-\delta r}$, one gets from Eq. (4)

$$y(1-y) \frac{d^2\phi}{dy^2} - \beta_n y \frac{d\phi}{dy} - \frac{2y}{\delta} \times \left\{ (g_1 + g_2)(1+y) - y(1+y)(g_1 + g_2\lambda) \right\} \frac{\phi(y)}{\log(1-y)} = 0 \quad \dots(8)$$

where

$$\beta_n = 1 + 2\alpha_n \delta$$

Using Ecker-Weizel approximation⁷, it may be assumed that the last term in Eq. (8) is a slowly varying function and hence may be considered to be constant t given by

$$t = 2\delta(1 - e^{-\delta r})[(g_1 - g_2\lambda) + g_2(1 + \lambda)e^{\delta r}] \delta \bar{r} \quad \dots(9)$$

where r represents an average distance of the bound electron in the appropriate quantum state. Using Eqs (7), (8) and (9) one gets the following for eigen energy of state

$$E_{ns} = \frac{1}{2} \left[\frac{1(1 - e^{-\delta r})}{n} \left\{ g_1 + g_2 e^{-(\lambda-1)\delta r} \right\} - \frac{n\delta}{2} \right]^2 \quad (10)$$

Potential (3) can be easily converted to Hulthén-type potential, i.e.

$$\frac{-V_0 e^{-\delta r}}{1 - e^{-\delta r}}$$

$$\text{with } V_0 = g_1 \delta \left[1 + \frac{g_2}{g_1} e^{-(\lambda-1)\delta r} \right] \quad g_1 \neq 0$$

Since the s -state eigenfunctions for Hulthén potential are obtained in closed form¹¹ the quantity \bar{r} is obtained as

$$\bar{r} = \hbar^2 + \delta/2 + O(\delta^2) \quad \dots(11)$$

We have, therefore, calculated energy eigenvalues for potential (3) with $g_1 = 1$, $g_2 = 1$ and $\lambda = 2$ for \bar{r} given by Eq. (11). The energy eigenvalues for $1s$ and $2s$ states of potential (3) for different values of δ are shown in Table 1. In Fig. 1, we have shown the dependence of energy on $\log D$, D being the screening length. Maximum value of D corresponds to minimum value of screening parameter δ . The curve labelled $E_{R,1s}$ is for the results of Rogers *et al.*⁹ It can be seen from Fig. 1 that weak screening corresponds to maximum energy for the potential (3). The variation of energy with \bar{r} for $1s$ states of potentials (1), (2) and (3) with $g_1 = 1$, $g_2 = 1$ and $\lambda = 2$ is shown in Fig. 2.

The dependence of energy on coupling parameter g_2 and strength of screening λ is shown in Table 2. It can be seen from Table 2 that a small variation in the value of g_2 in potential (3) strongly affects energy E_{ns} but there is no appreciable change in E_{ns} due to gradual variation in the value of λ .

Further, a critical value of the screening parameter δ is found⁸ to exist, above which the binding energy of an electron in that potential becomes zero. The value of the critical screening parameter δ_c for $1s$ state of potential (3) is obtained by solving the following equation:

$$1 - e^{-2\delta_c \bar{r}} - \delta_c^2 \bar{r}/2 = 0 \quad \dots(12)$$

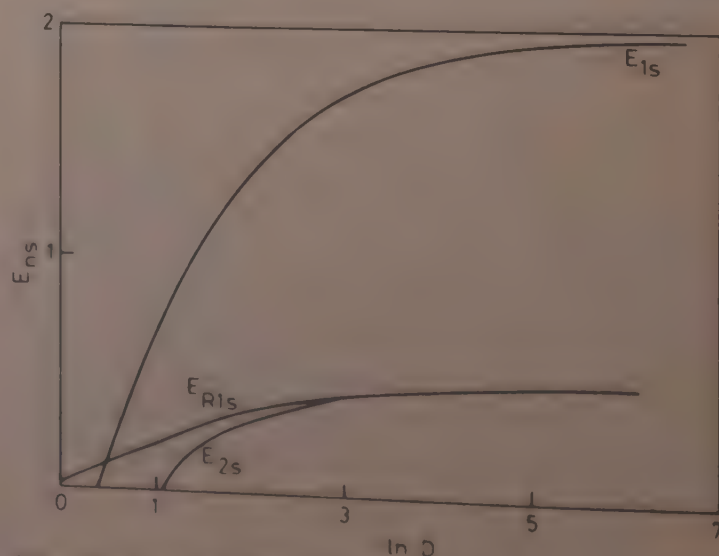


Fig. 1—Plot of E_{ns} versus $\ln D$ (D being the screening length)

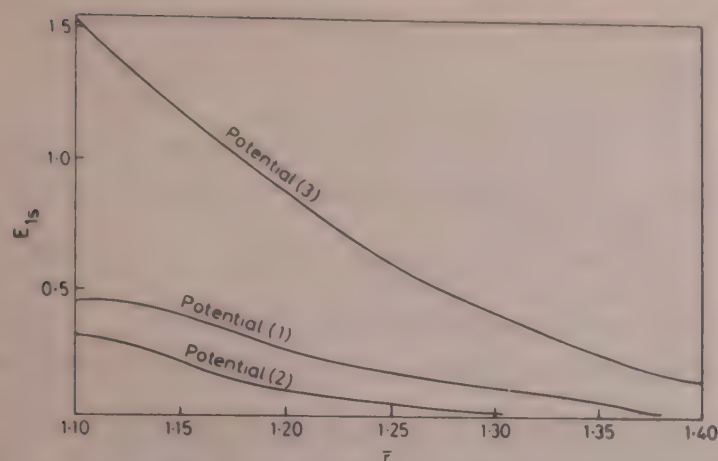


Fig. 2—Variation of energy with \bar{r} in 1s state of potentials (1), (2) and (3) with $g_1 = g_2 = 1$ and $\lambda = 2$

Table 2—Dependence of Energy on Coupling Parameter g_2 and Strength of Screening λ for 1s State for Potential (3)

g_1	g_2	λ	δ	Energy
1	0	2	0.01	0.4905
1	0.5	2	0.01	1.11
1	1.0	2	0.01	1.97
1	1	500	0.01	0.501
1	1	600	0.01	0.497
1	1	700	0.01	0.495

Its solution yields $\delta_c = 0.6375$. It is interesting to note here that due to superposition of Yukawa potential by potential (2), the value of δ_c gets reduced, since for Yukawa potential¹⁴ $\delta_c = 1.2732$. For 2s state of potential (3) one gets $\delta_c = 0.3166$. Also one may obtain values of δ_c from Fig. 1. They show reasonable agreement with values reported by other workers. For example, δ_c obtained from Fig. 1 for results of Rogers *et al.*⁹ is 1.28 while the calculated value¹⁴ is 1.2732. The value of δ_c from Fig. 1 for potential (3) in 1s state is 0.6265 while the calculated value is 0.6375. Similarly for 2s state, δ_c from Fig. 1 is 0.315 while the calculated value is 0.3166.

Now Eq. (6) reads

$$X(r) = \varphi(r) e^{-\alpha_n r}$$

On setting

$$\varphi(r) = k' \varphi(y) \quad \dots (13)$$

where

$$\varphi(y) = \sum_{i=0}^{\infty} C_i y^{i+r} \quad \dots (14)$$

in Eq. (6) and solving Eq. (8) with the help of Eq. (14), one finds $\sigma = 1$.

The normalized wavefunction then has the form:

$$X'(r) = k e^{-\alpha_n r} (1 - e^{\delta r}) \quad \dots (15)$$

where k is the normalization constant given by

$$k = \left[\frac{\alpha_n (1 + 1.5p)}{(1 + 0.75p)} \right]^{1/2} \quad \dots (16)$$

Table 3—Quantum Number Shift and Relative Quantum Defect for ns States of Potential (3) as a Function of Reduced Screening Parameter δ/δ_c

δ/δ_c	1s		2s	
	n	n/n	n	n/n
0.005	-0.4996	-0.4996	-0.9968	-0.4984
0.01	-0.4952	-0.4952	-0.9960	-0.4980
0.02	-0.4925	-0.4925	-0.9815	-0.4907
0.05	-0.4789	-0.4789	-0.9572	-0.4786
0.10	-0.4571	-0.4571	-0.8978	-0.4489
0.15	-0.4333	-0.4333	-0.8406	-0.4203
0.20	-0.4075	-0.4075	-0.7982	-0.3991
0.25	-0.3798	-0.3798	-0.7302	-0.3691
0.30	-0.3497	-0.3497	-0.6568	-0.3284
0.35	-0.3174	-0.3174	-0.5758	-0.2879
0.40	-0.2824	-0.2824	-0.4870	-0.2435
0.45	-0.2442	-0.2442	-0.3680	-0.1840
0.50	-0.2070	-0.2070	-0.2588	-0.1294

with

$$p = \delta/\alpha_n \quad \dots (17)$$

Further, it may be assumed that the bound electron in the potential (3) behaves as if it is under the influence of a modified screened Coulomb potential. One may thus write

$$E_n \approx 1/2n_{\text{eff}}^2 \quad \dots (18)$$

where n_{eff} is the effective quantum number. Using relations (10) and (18) n_{eff} and the quantum number shift $\Delta n = (n_{\text{eff}} - n)$ for different values of the reduced screening parameter δ/δ_c for 1s and 2s states have been calculated. The results for Δn and the relative quantum defect $\Delta n/n$ for various ns states are shown in Table 3.

It is interesting to note that although for a given quantum state, Δn increases with δ/δ_c , the quantity $\Delta n/n$ remains approximately constant and independent of the principal quantum number n at any fixed value of δ/δ_c .

A similar situation has been observed in alkali atoms and alkali-like ions¹¹.

3 Conclusions

1. The critical screening parameter δ_c for the Yukawa potential gets reduced in 1s state when it is superposed by a modified screened Coulomb potential.

2. Normalization constant decreases when screening parameter increases.

3. It is seen that weak screening corresponds to maximum energy. Also there is no appreciable change in maximum energy after a certain screening length.

4. It is seen that a change in magnitude of g_2 strongly affects the energy values while a gradual variation in λ does not appreciably change them.

5. It is observed that there is a sharp fall in energy with increase in \bar{r} (in its lower limit) as compared to its

corresponding decrease in 1s state for potentials (1) and (2) taken separately.

6. The most revealing feature of this is that the quantum defect is independent of the principal quantum number, a feature which is also reported¹⁰ for alkali atoms and alkali-like ions.

References

- 1 Cooper J W, *Phys Rev A (USA)*, **9** (1974) 2236.
- 2 Schiff L I, *Quantum mechanics* (McGraw-Hill, New York), 1958.
- 3 Seaton M J, *Mon Not R Astron Soc (GB)*, **11** (1958) 8504.
- 4 McEannan J, Kissel L & Pratt R H, *Phys Rev A (USA)*, **13** (1976) 532.
- 5 Greene R L & Aldrich C, *Phys Rev A (USA)*, **14** (1976) 2363.
- 6 Mehta C H & Patil S H, *Phys Rev A (USA)*, **17** (1978) 43.
- 7 Ecker G & Weizel W, *Ann Phys (Germany)*, **17** (1956) 126.
- 8 Lam C S & Varshni Y P, *Phys Lett A (Netherlands)*, **59** (1976) 363.
- 9 Rogers F J, Graboske H C & Harwood D J, *Phys Rev A (USA)*, **1** (1970) 1577.
- 10 Ray Pritam P & Ray Aparna, *Phys Lett A (Netherlands)*, **78** (1980) 443.
- 11 Dutt R, *Phys Lett A (Netherlands)*, **73** (1979) 310.
- 12 Dutt R, Ray Aparna & Ray P P, *Phys Lett A (Netherlands)*, **83** (1981) 65.
- 13 Lam C S & Varshni Y P, *Phys Rev A (USA)*, **4** (1971) 1875.
- 14 Totsuji H, *J Phys Soc Jpn (Japan)*, **31** (1971) 584.

Low Energy Spectrum & Directional Correlation Measurements in ^{187}Re

K SINGH, B S GREWAL, RAJ MITTAL & H S SAHOTA*

Physics Department, Punjabi University, Patiala 147 002

Received 18 January 1982; revised received 22 September 1982

The gamma ray spectrum of $23.9\text{h } ^{187}\text{W}$ in the low energy region 0-150 keV has been measured using a high resolution low energy intrinsic Ge detector. The controversial 7.1 keV transition has been confirmed. Also a new transition of energy 125.85 keV has been detected. Gamma-gamma directional correlations are measured for the 72-134 and 552-134 keV cascades. The multipole characters for 72, 134 and 552 keV have been assigned as $E1 + \{2.7(7)\% M2, M1 + (2.9 \pm 0.3)\% E2$ and $E1 + (4.75 \pm 0.75)\% M2$ respectively.

1 Introduction

Level structure of ^{187}Re has been studied in the past by several investigators¹⁻⁵ employing different nuclear techniques. Brenner and Meyer⁵ established a typical decay scheme for the energy levels lower than 900 keV by investigating gamma rays from the decay of ^{187}W . They reported many new lines and levels for the first time. The 16.61, 40.92, 93.22, 100.14, 123.79, 138.50 keV transitions in the energy region 0-150 keV were not placed by them in the ^{187}Re level scheme and assignment to ^{187}W decay was considered tentative. Recently Yamada *et al.*⁶ measured the gamma ray spectrum of $23.9\text{h } ^{187}\text{W}$ using Ge(Li) detector and quoted seven new lines in the energy region 140-1000 keV. They did not find any new line in the low energy region. Very recently Sooch *et al.*⁷ reported on gamma ray energy, intensity and directional correlation measurements in the region 72-880 keV only. The low energy region of the ^{187}Re spectrum has been checked by us with a small-size high-resolution Ge detector with a view to resolving some discrepancies reported in earlier studies. The nature of 72, 134 and 552 keV transitions is still doubtful. From conversion coefficient and directional correlation measurements, Gallagher *et al.*¹ showed for 134 keV transition $\delta_{134} = 0.17(5)$. From nuclear orientation measurements, Krane and Steyer⁸ found $\delta_{134} = 0.160(6)$. From the measurements of the conversion coefficients and the gamma-gamma angular correlations, Yamada *et al.*⁶ quoted $\delta_{134} = 0.184(3)$. These results provide $A_2(134) \approx 0$, giving $A_{22}\{72(134)\}$ and $A_{22}(552-134)$ keV ≈ 0 . But experimentally, this trend has been supported by Keszthelyi and Demesters⁹ only, whereas the results of Michaelis¹⁰, Nigam and Bhattacharya¹¹ and Gupta *et al.*¹² show non-zero values for these cascades. To remove these ambiguities, the angular correlation measurements for 72-134 and 552-134 keV cascades were performed. The nature of the 134 keV transition was examined from the point of view of any

penetration effects using the previous results of conversion electron measurements.

2 Experimental Procedure

The sample of radioactive isotope of ^{187}W was procured from the Bhabha Atomic Research Centre, Bombay, in the form of an aqueous solution. For energy and intensity measurements, the source used was in the solid form (point source on a perspex strip) while for directional correlation measurements, the source used was in the liquid form contained in 2 mm \times 4 mm perspex cylinders.

For gamma-ray singles measurements, an intrinsic Ge detector (active area 200 mm² and sensitive depth 7 mm) having energy resolution of 535 eV at 122 keV gamma ray of ^{57}Co was used.

For gamma-gamma directional correlation measurements, two 2" \times 2" NaI(Tl) crystals covered with graded shields of Al, Cu and Pb and a ND60 multichannel analyser were used. A resolving time of about 30 ns employing the conventional slow-fast assembly was used. The coincidence counts were recorded at 90°, 135° and 180°. The correlation coefficients were corrected for the finite geometry of crystals using correction factors calculated by Yates¹³.

3 Gamma-ray Singles Measurements

The gamma-ray singles spectra were recorded with an intrinsic Ge detector for the 0-150 keV energy region. The experiment was repeated thrice by recording spectra for different times and the intensities of the new lines were found to follow the half-life of $23.9\text{h } ^{187}\text{W}$ in comparison with well known 72 and 134 keV gamma rays of this decay. A typical spectrum is shown in Fig. 1, and the resulting energies and intensities are listed in Table 1.

The lines at energies 40.92, 93.22, 100.14, 123.79 and 138.5 keV reported by Brenner and Meyer⁵ were observed in all three independent runs. Out of these,

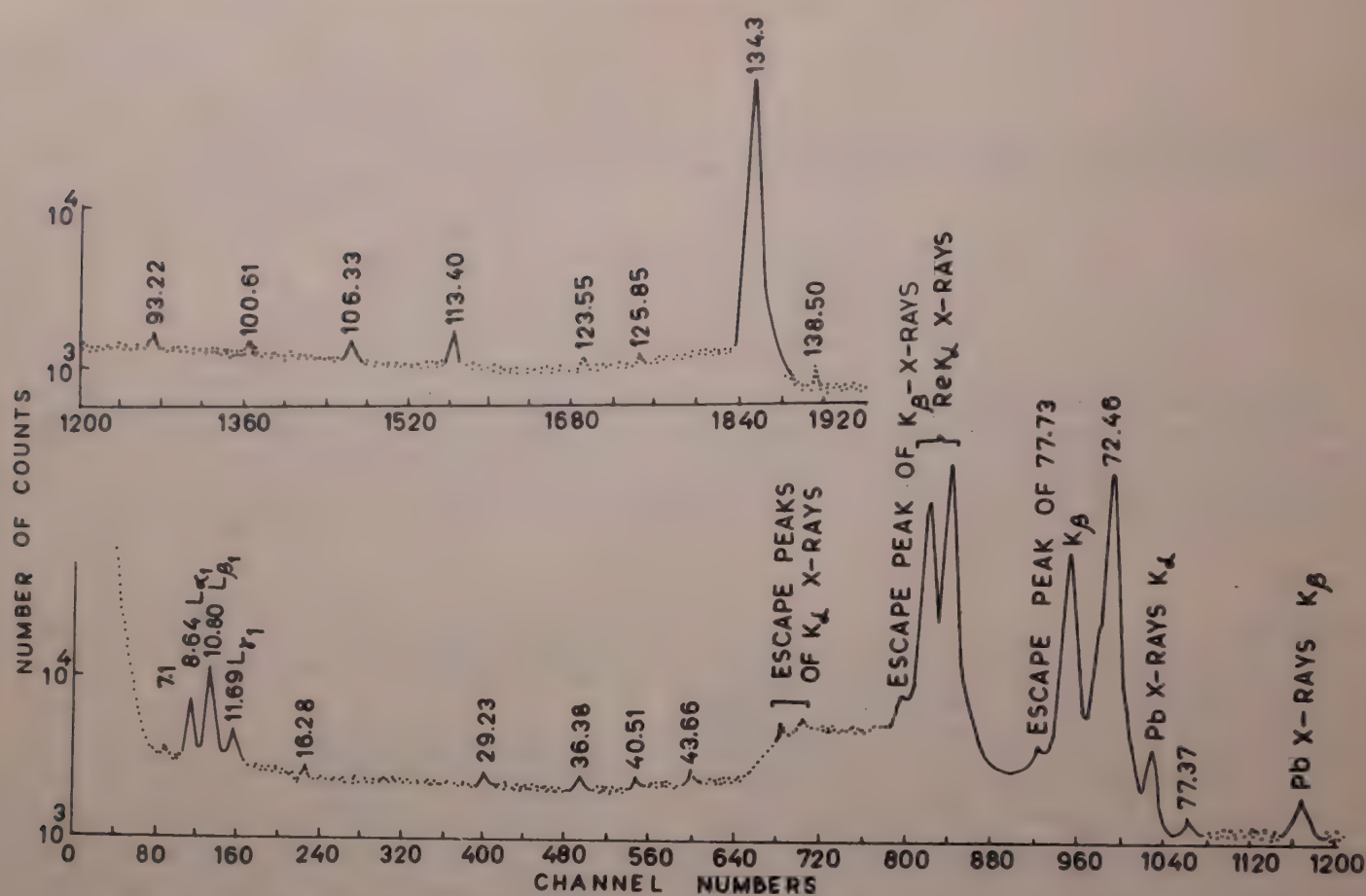


Fig. 1—Single gamma ray spectrum of ^{187}W observed with a $200\text{ mm}^2 \times 7\text{ mm}$ intrinsic Ge detector

Table 1—Energies (in keV) and Relative Intensities of Gamma Transitions Associated with the Decay of ^{187}W

Present study	Brenner & Meyer ⁶	Present study	Brenner & Meyer ⁵	Brabec et al. ¹⁸
7.1(3)	—	0.043(21)	—	—
16.28(2)	16.61(2)	0.073(8)	0.069(9)	—
29.23(4)	29.23(3)	0.070(11)	0.042(9)	—
36.38(3)	36.38	0.202(12)	0.246	—
40.51(6)	40.92(5)	0.025(8)	0.019(9)	—
43.66(7)	43.66(6)	0.024(8)	0.019(9)	—
72.46(1)	72.46(1)	124.88(162)	125.96(78)	130.56(13)
77.37(5)	77.37(5)	0.077(18)	0.079(19)	0.072(23)
93.22(4)	93.22(5)	0.050(8)	0.069(9)	—
100.61(2)	100.14(2)	0.098(12)	0.101(14)	—
106.59(2)	106.59(1)	0.296(7)	0.288(7)	0.461(70)
113.75(2)	113.75(2)	0.866(15)	0.869(20)	0.78(11)
123.55(10)	123.79(11)	0.028(6)	0.029(9)	—
125.85(7)	—	0.022(7)	—	—
134.22(1)	134.22(1)	100	100	100
138.50(7)	138.50(6)	0.052(16)	0.049(19)	—

only 40.92 keV satisfying the Ritzs combination principle has been placed in decay scheme of ^{187}W . The 7.1 keV transition reported by Widemann and Sebillé¹⁴ and confirmed by Herman et al.¹⁵ using a coincidence technique has been seen in the present singles measurements for the first time. A new line of energy 125.85 keV has been seen which can be satisfactorily placed between 772.88 and 647.30 keV levels (Fig. 2). A preliminary report on this assignment was reported at the Silver Jubilee Physics Symposium, Bombay, by Raj Mittal et al.¹⁶

4 Gamma-Gamma Directional Correlation Measurements

The 72-134 keV cascade—Because of poor energy resolution of NaI(Tl) detectors, the 72 keV gamma ray was not resolved from the intense Re K X-rays. As reported by Michaelis¹⁰, these K X-rays are in coincidence with the 134 keV gamma ray and contribute an isotropic component with interesting results. To get rid of this interference, 61 keV energy peak was suppressed relative to 72 keV using Gd absorber, in the form of a foil of thickness 0.028 cm (as

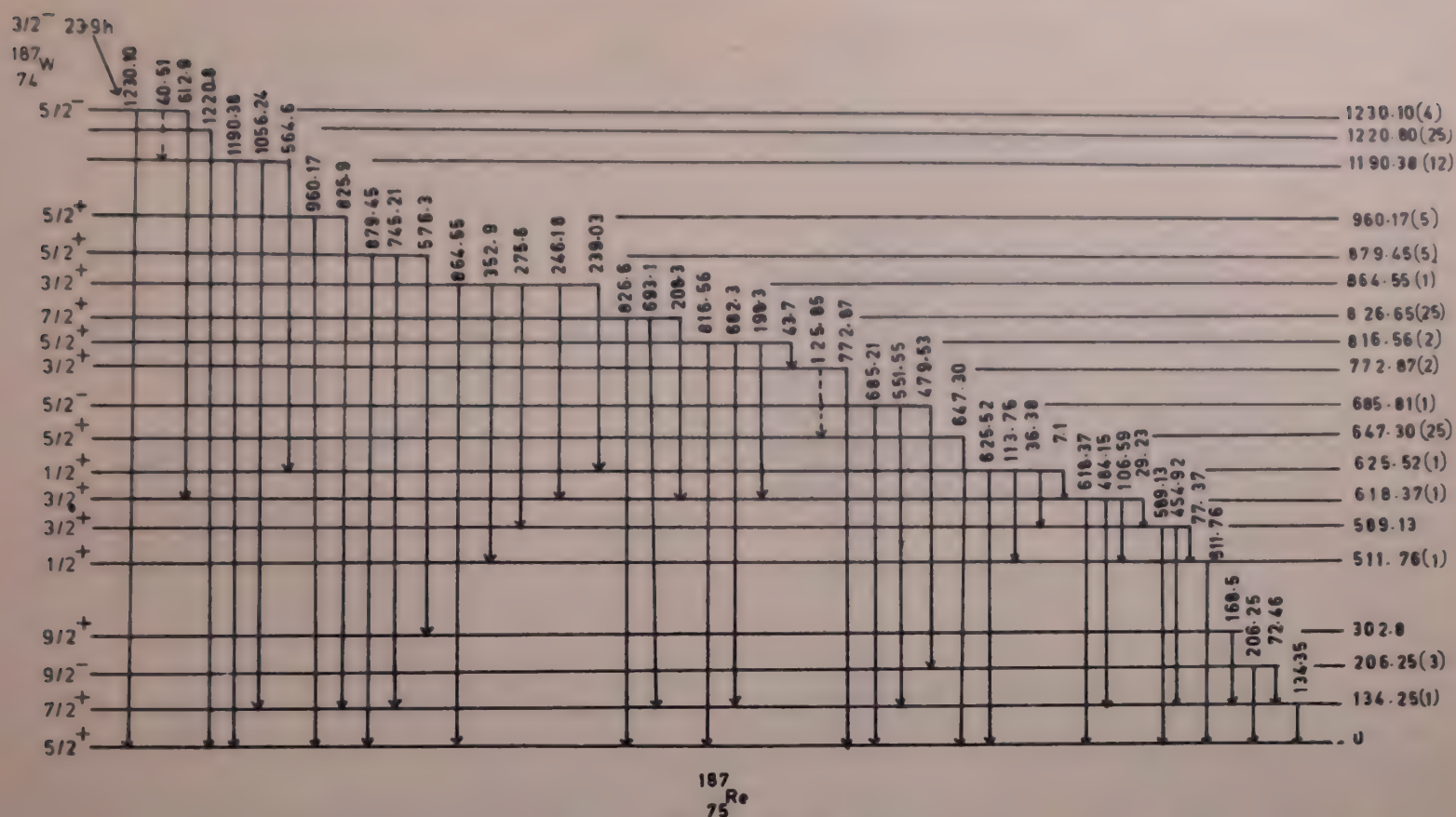


Fig. 2—Decay scheme of ^{187}W

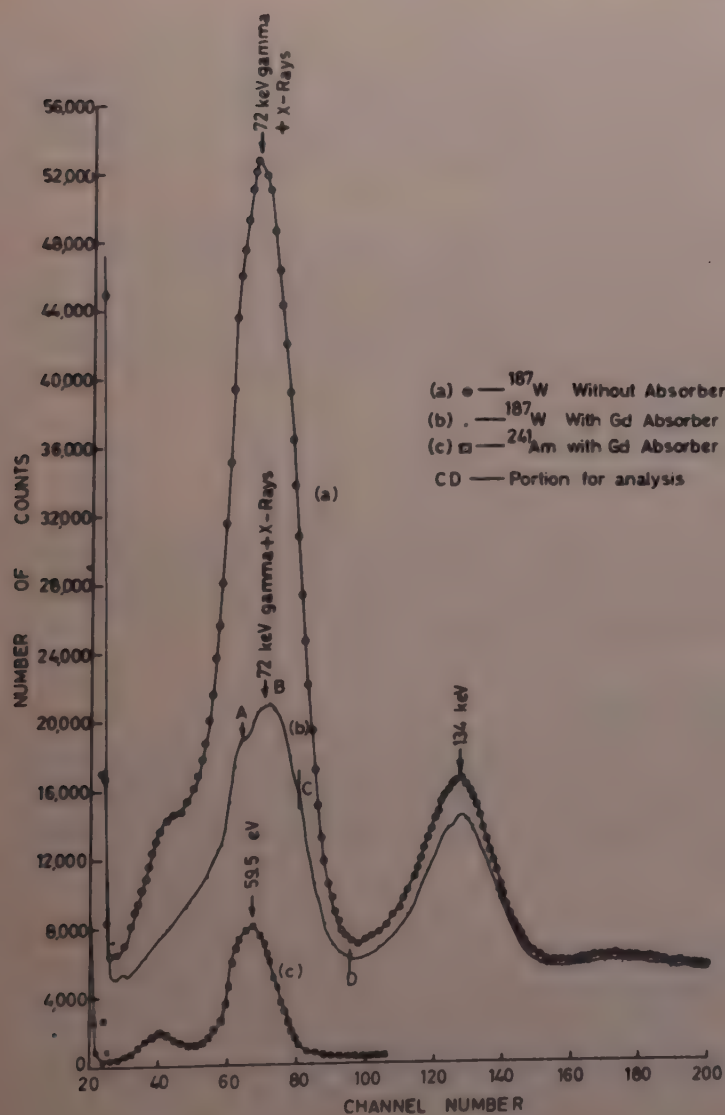


Fig. 3—Use of K-absorption edge of Gd to suppress the 61 keV K X-rays relative to 72 keV gamma in 72-134 keV correlation measurements

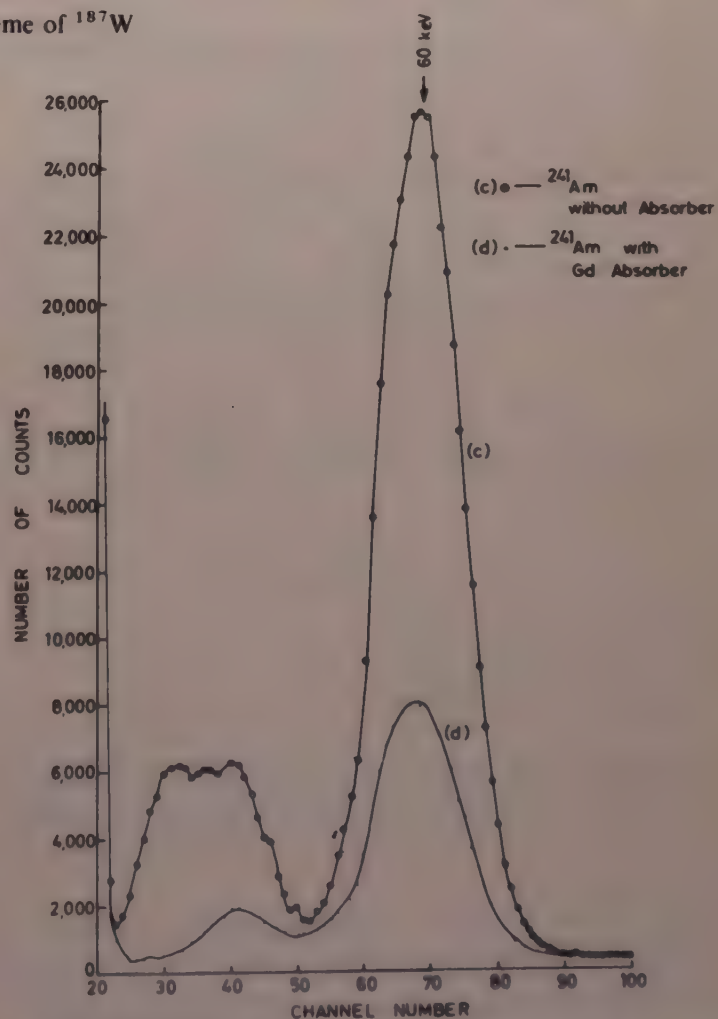


Fig. 4—Suppression of 60 keV gamma ray of ^{241}Am with required thickness of Gd absorber

its K absorption edge is at 58 keV). The singles spectra of ^{187}W and ^{241}Am (60 keV) with and without Gd absorber are shown in Figs 3 and 4 respectively. It is clear (Fig. 3) that portion CD of curve b is free from 61

keV energy contribution and is enriched with that of 72 keV.

The weighted average of calculated correlation coefficients corrected for solid angle corrections are:

$$A_{22} = -0.066 \pm 0.011; \quad A_{44} = 0.030 \pm 0.023$$

These results agree with those obtained by Michaelis¹⁰ and Nigam and Bhattacharya¹¹, but are slightly higher than those of Gupta *et al.*¹² and entirely differ from those of Keszthelyi and Demesters⁹.

The present results are more accurate as justified from the following explanation. The results were obtained by selecting counts under the composite peak in three different ways and the values of correlation coefficients are as follows.

(i) full peak (containing full contributions of both 61 and 72 keV):

$$A_{22} = -0.022 \pm 0.005; \quad A_{44} = -0.018 \pm 0.008$$

(ii) Half of the composite peak on the higher energy side (containing half contribution of 72 keV and less than half that of 61 keV):

$$A_{22} = -0.030 \pm 0.007; \quad A_{44} = -0.011 \pm 0.012$$

(iii) Quarter of composite peak on the higher energy side (containing only contribution of 72 keV):

$$A_{22} = -0.050 \pm 0.015; \quad A_{44} = -0.016 \pm 0.024$$

This shows that the isotropic contribution of 61 keV Re K X-rays lowers the values of correlation coefficients. It seems that in their measurements, Gupta *et al.*¹² and Keszthelyi and Demesters⁹ might not have taken complete care of the contribution of Re K X-rays.

The character of 134 keV transition was re-investigated from sub-shells ratio analysis (Fig. 5). This analysis yields

$$\lambda = 0 \pm 3.5 \text{ and } \delta_{134} = \pm 0.172 \pm 0.007$$

Further $\delta_{134} = -0.172 \pm 0.007$ gives

$$A_2(134) = 0 \pm 0.013 \text{ while}$$

$$\delta_{134} = 0.172 \pm 0.007 \text{ gives}$$

$$A_2(134) = 0.631 \pm 0.014$$

On the basis of present experimental results, only $\delta_{134} = -0.172 \pm 0.007$ was entertained and used to assign the multipole characters to the 552 and 72 keV transitions.

The 552-134 keV cascade—This cascade is practically free from interfering effects. The correlation coefficients after applying solid angles corrections are:

$$A_{22} = -0.058 \pm 0.019; \quad A_{44} = -0.023 \pm 0.039$$

Using the present A_{22} 552-134 keV correlation coefficients, $A_2(552)$ was obtained to be -0.092 ± 0.032 . The mixing ratio analysis¹³ yields two values of Q , the quadrupole content in the 552 keV transition, $Q_{552} = 1$ and $0.004 \leq Q_{552} \leq 0.055$

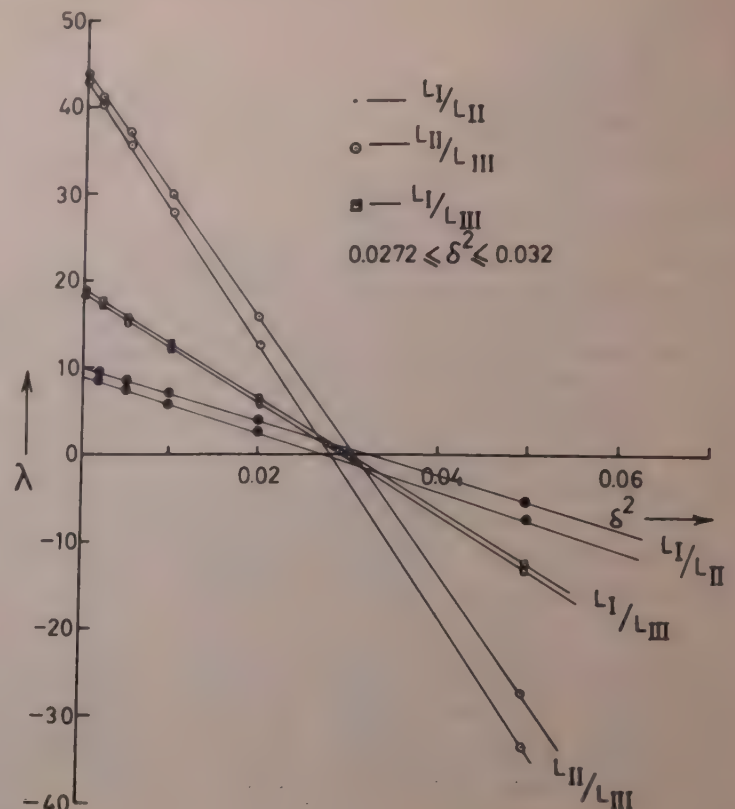


Fig. 5— L -subshell ratio analysis for penetration effects in the 134.22 keV transition

The higher value of $Q_{552} = 1$ is rejected on the basis of conversion coefficients and nuclear orientation measurements. Thus 552 keV transition is assigned as $E1 + (4.75 \pm 0.75)\%$ $M2$ and is slightly higher than listed by Ellis⁴.

The analysis of A_{22} (72-134) keV cascade for $\delta_{134} = -0.172(7)$ yields $A_2(72) = -0.105(32)$. Taking into consideration these results, the mixing ratio analysis gives two values of Q , the quadrupole content in 72 keV transition

$$0.02 \leq Q_{72} \leq 0.035; \quad 0.92 \leq Q_{72} \leq 0.95$$

The higher value of Q is rejected on the basis of internal conversion measurements of Gallagher *et al.*¹ Therefore, the mixing ratio of the 72 keV transition is predominantly $E1$ with $2.7(7)\%$ $M2$.

Acknowledgement

The authors are grateful to Prof. C S Khurana, Head of the Physics Department, for necessary facilities for this work and the CSIR, New Delhi, for a research grant.

References

- 1 Gallagher C J, Edwards W F & Manning G, *Nucl Phys (Netherlands)*, **19** (1960) 18.
- 2 Bashandy E, Migahed M, Sayed E L G M & EL-Aassar M R, *Nuovo Cimento (Italy)*, **39** (1965) 1017.
- 3 Bisgard K M, Olesen K & Estergard P, *Nucl Phys (Netherlands)*, **33** (1962) 126.
- 4 Ellis Y A, *Nucl Data Sheets (USA)*, **14** (1975) 347.
- 5 Brenner D S & Meyer R A, *Phys Rev. (USA)*, **C13** (1976) 1288.

- 6 Yamada S, Sud S P, Miyatake Y & Hayashi T, *Nucl Phys A (Netherlands)*, **332** (1979) 317.
- 7 Sooch S S, Kaur Ravinder, Singh Nirmal & Trehan P N, *Nucl Phys & Solid State Phys Symp (India)*, **24B** (1981) 35.
- 8 Krane K S & Steyert W, *Phys Rev (USA)*, **C7** (1973) 1243.
- 9 Keszthelyi L & Demesters I, *Acta Phys (Poland)*, **32** (1972) 187.
- 10 Michaelis W, *Nucl Phys (USA)*, **45** (1963) 573.
- 11 Nigam A K & Bhattacharya R, *Nucl Phys A (Netherlands)*, **164** (1971) 411.
- 12 Gupta S L, Bajaj M M & Saha N K, *Proc Natl Inst Sci (India)*, **32A** (1966) 281.
- 13 Yates M J L, in *alpha, beta and gamma-ray spectroscopy*, Ed. K Siegbahn (North-Holland Publishing Co, Amsterdam), 1965.
- 14 Widemann F & Seville C, *Port Phys (Portugal)*, **4** (1966) 215.
- 15 Herman A W, Heighway E A & Mac-Auther J D, *Can J Phys (Canada)*, **48** (1970) 1040.
- 16 Mittal Raj, Singh K & Sahota H S, *Nucl Phys & Solid State Phys Symp (India)*, **24B** (1981) 155.
- 17 Arns R G & Wiedenbeck M L, *Nucl Phys (Netherlands)*, **111** (1958) 1631.
- 18 Brabec V, Maly L & Vobecky M, *Bull Acad Sci Phys Ser (USSR)*, **35** (1971) 1424.

Vibrational Spectra of Phosphotungstate Ion— $\text{PW}_{12}\text{O}_{40}^{3-}$

S SHEIK SALEEM & G ARULDHAS*

Department of Physics, University of Kerala, Kariavattom 695 581

Received 5 September 1981; accepted 2 November 1982

The infrared and Raman spectra of phosphotungstic acid have been recorded. The factor group analysis has been carried out using the site group approach for the phosphotungstate ion, $\text{PW}_{12}\text{O}_{40}^{3-}$ of T_d symmetry. Based on group vibrations and factor group analysis a vibrational assignment has been proposed for the $\text{PW}_{12}\text{O}_{40}^{3-}$ ion.

1 Introduction

Heteropoly compounds have been of interest since the description of ammonium phosphomolybdate by Berzelius¹. The heteropoly compounds are formed when one atom of elements such as P, Si, As, B, Al, etc., is combined with a number of atoms of W or Mo, together with a relatively large number of oxygen atoms. They are widely used in analytical chemistry^{2,3} and as solid electrolytes for fuel cells⁴. Heteropoly acids are classified according to the ratio of the number of the two types of cations present. 12-Heteropoly acids, $\text{H}_n^+(X\text{W}_{12}\text{O}_{40})^{n-}$ where X is the heteroatom, exist in two forms α and β . The stable α -form has the Keggin structure⁵. 12-Phosphotungstic acid, $\text{H}_3\text{PW}_{12}\text{O}_{40} \cdot n\text{H}_2\text{O}$ crystallizes in four crystal systems, viz. triclinic ($n=14$), trigonal ($n=24$), rhombohedral ($n=21$) and cubic ($n=6, 29$) depending on the number of water molecules present in them⁶. The infrared spectra of heteropolymolybdates and tungstates⁷⁻¹⁴ and the Raman spectra of heteropolymolybdates¹³⁻¹⁵ have already been reported. A comparative investigation of heptamolybdate, molybdophosphates and molybdoarsenates¹⁶ and a study of heteropolymolybdate species in aqueous solutions¹⁷ have also been reported. The force field analysis of 12-molybdophosphate ion has been worked out by Lyhamn *et al.*¹⁸ In the present investigation, the infrared and Raman spectra of phosphotungstic acid have been recorded and a vibrational assignment proposed for the $\text{PW}_{12}\text{O}_{40}^{3-}$ ion.

2 Experimental Details

Commercially available phosphotungstic acid (Veb product) was used for the investigation. The infrared spectrum was recorded in a Perkin Elmer 599 spectrophotometer using KBr pellet. A Spex Ramalog 1401 spectrophotometer equipped with a Spectra-Physics model 165 argon ion laser was used to obtain the Raman spectrum (Fig. 1) of the powdered samples placed in a capillary tube. The spectra were obtained in the Stokes region of the blue line 4880 Å. Plasma lines

of the laser were used for calibration of the instrument. Spectral slit widths of 300-100 μ were employed for different regions of the spectrum.

3 Factor Group Analysis

The complete acidic anion $\text{PW}_{12}\text{O}_{40}^{3-}$ has an overall tetrahedral symmetry, T_d . It consists of a central regular PO_4 tetrahedron surrounded by 12 deformed tungsten oxygen octahedra as a shell, linked together by shared oxygen atoms (Fig. 2). The ion can be alternatively thought of as consisting of a central atom P with four ligands of W_3O_{13} units, which are interconnected by sharing oxygen atoms to form $\text{P}(\text{W}_3\text{O}_{10})_4$. Each W_3O_{13} unit (Fig. 3) of C_{3v} symmetry is formed by three oxygen-sharing WO_6 deformed octahedra. There are six sets P, W, O_a , O_b , O_c , O_d of symmetrically equivalent atoms with their site positions at T_d , C_s , C_{3v} , C_s , C_s , C_s respectively⁵. The factor group analysis can be done either by correlating the site symmetry of W_3O_{13} and PO_4 units to the factor group or by correlating the site group of each atom individually to the factor group. Both will give the same total number of modes for each symmetry species. The normal

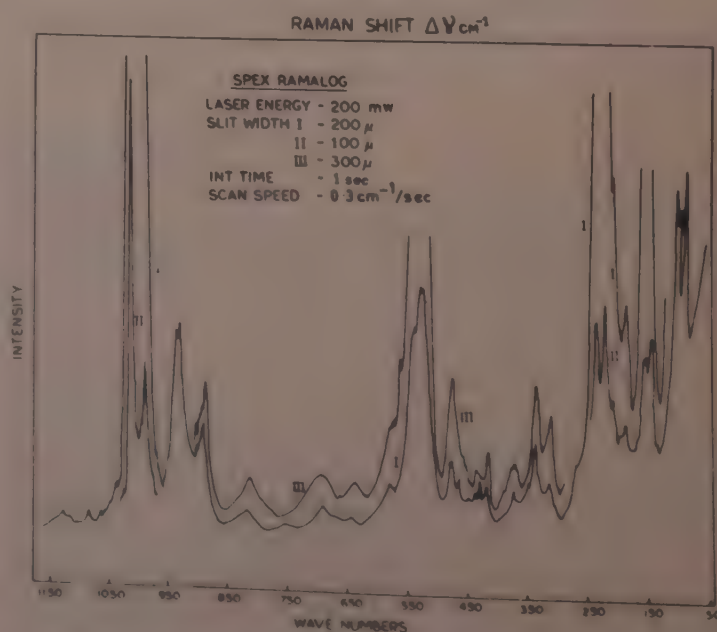


Fig. 1—Raman spectrum of phosphotungstic acid

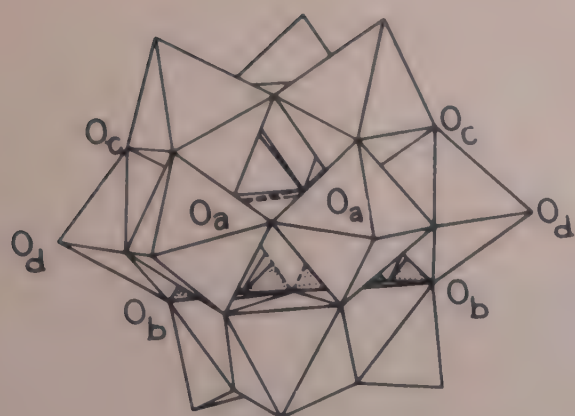
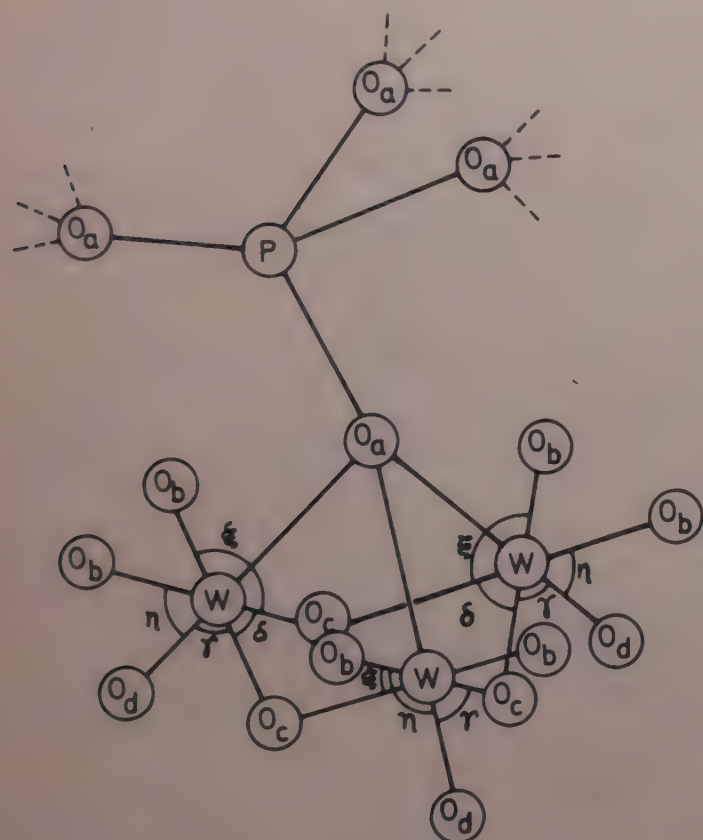

 Fig. 2—Structure of the Keggin anion, $PW_{12}O_{40}^{3-}$ (from Ref. 23)

 Fig. 3— PO_4 tetrahedra with one W_3O_{13} unit

 Table 1—Classification of Normal Modes of $PW_{12}O_{40}^{3-}$ Ion

Type of vibration	Network	Symmetry of network	Normal modes of network	Correlated modes under T_d symmetry
Framework	PO_4	T_d	$A_1 + E + 2F_2$	$A_1 + E + 2F_2$
Ligand	W_3O_7	C_{3v}	4.6 A_1 4.2 A_2 4.8 E	6 $A_1 + 6F_2$ $2A_2 + 2F_1$ $8E + 8F_1 + 8F_2$
Interligand	$W_3O_3^*$	C_{3v}	4.2 A_1 4 A_2 4.3 E	$2A_1 + 2F_2$ $A_2 + F_1$ $3E + 3F_1 + 3F_2$
Framework ligand coupling				$A_2 + E + 2F_1 + 2F_2$

* For the interligand, the normal mode is not 12 since the tungsten atoms are shared with the ligands.

modes of $PW_{12}O_{40}^{3-}$ ion can be classified under four headings, viz. framework vibrations, ligand vibrations, framework-ligand couplings and interligand vibrations¹⁸. These classified normal modes are shown in Table 1 and the correlation table of the site groups to the factor group is shown in Table 2.

4 Assignments and Discussion

Out of the 64 ($9A_1 + 4A_2 + 13E + 16F_1 + 22F_2$) normal modes predicted for the phosphotungstate ion, 44 ($9A_1 + 13E + 22F_2$) are active in Raman and 22 ($22F_2$) in IR. As the anion is complex, random degeneracies are expected and hence it may not be possible to observe all the predicted vibrations. Based on normal coordinate analysis, Lyhamn *et al.*¹⁸ have calculated the frequencies for the corresponding molybdate ion. The frequencies for the phosphotungstate ion are expected to be higher by 10 to 15 wavenumbers¹⁹.

In the phosphotungstate ion, different groups of atoms can be isolated, the vibrations of which depend

 Table 2—Factor Group Analysis of $PW_{12}O_{40}^{3-}$ Ion (T_d symmetry)

Correlation of the P atom with site symmetry T_d					$Z = 1$
f^v	t^v	Site	Correlation	Crystal	
		T_d	T_d	$\Gamma_P = F_2$	
3	3	F_2	F_2	F_2	
Correlation of the O_a atom with site symmetry C_{3v}					$Z = 4$
f^v	t^v	C_{3v}	T_d		
4	1	A_1	A_1	E	
				F_1	
				F_2	
8	2	E	E	F_1	
				F_2	
Correlation of the O_b, O_c, O_d and W atoms with site symmetry C_s					$Z = 12$
f^v	t^v	C_s	T_d		
24	2	A'	A_1	A_2	
			E	F_1	
			F_2	F_2	
12	1	A''	F_1	F_2	
10					

$$\Gamma_{O_b} = 2A_1 + A_2 + 3E + 4F_1 + 5F_2$$

Total normal modes $9A_1 + 4A_2 + 13E + 16F_1 + 22F_2$

Raman active modes $9A_1 + 13E + 22F_2$

IR active modes $22F_2$

t^v = the number of translation in a site species
 $f^v = n \cdot t^v$ = degrees of vibrational freedom present in each site species
 n = number of atoms in the site

Table 3—Vibrational Assignments of $PW_{12}O_{40}^{3-}$ Ion

IR freq. (cm^{-1})		Raman freq. (cm^{-1})		Symmetry		Assignments
Present study		From Ref. 13	Present study	Calc. values from Ref. 18		
1080	s	1080	1117 1075 1009	1107 F_2 A_1	P—O _a P—O _a W—O _d	asymm. stret. " symm. stret.
990	sh					----
979	sh	985	985	980	A_1 & F_2	symm. stret. asymm. stret.
			934	941	F_2 or E	symm. stret.
			928 903			----
885	m	887	890	885	F_2	asymm. stret.
810	s	807	814 690 635	799 688	F_2 A_1	W—O _c —W W—O _a
590	w, br	598		582 572 558 538		lib. H ₂ O? -do- -do- combination
518	s	525	520	528	F_2	asymm. bending
483	sh	480	471	469	E	PO ₄ PO ₄ symm bending
420	w	425	430	460 422	F_2	----
377	s	382	372	425		$\xi + \xi'$ combination
330	m	338	336	327	F_2	-do- η deformation
280	w	278				
			313	309	A_1	O—W—O $\eta + \delta + \xi$ mixed deformation
230	w		235	233	F_2	O—W—O $\delta + \gamma$ -do-
210	w	207	220 208	219	F_2	----
			186	174	E	$\delta + \gamma$ mixed deformation
			152, 143	154	E	lattice modes
			102, 88			

s, strong; m, medium; w, weak; sh, shoulder; br, broad and all other notations used are explained in Fig. 3.

negligibly on the vibrations of other atoms. In the anion, there are 12 terminal multiple W—O_d bonds, 12 almost linear W—O_b—W bonds, 12 angular W—O_c—W bonds, and 12 W—O_a single bonds in which the oxygen atoms are common to three W atoms and the central atom P.

The assignments have been made using the principle of group vibrations. The tungsten-oxygen stretchings usually occur in the region 700-1000 cm^{-1} , and the deformations of the angular and linear tungsten-oxygen-tungsten bridges will fall below 500 cm^{-1} . The vibrations of the tetrahedral anion PO₄ appear in the region 800-1100 cm^{-1} (A_1 and F_2) and 400-600 cm^{-1} (F_2 and F_2)²⁰. Due to the complexity of the anion, mixing occurs and a line of demarcation may not be possible.

Of the Raman active $9A_1 + 13E + 22F_2$ modes, $5A_1 + 6E + 11F_2$ are stretching vibrations and $4A_1 + 7E + 11F_2$ are bending vibrations. The stretching vibrations can be further classified as W—O_a = W—O_d = $A_1 + E + 2F_2$; W—O_b = W—O_c = $A_1 + 2E + 3F_2$; P—O = $A_1 + F_2$ and the bending vibrations as OPO = $E + F_2$ and OWO = $4A_1 + 6E + 10F_2$.

4.1 Stretching Vibrations

The terminal oxygen O_d is having the shortest bond length of W—O_d = 1.693 Å. Consequently, the strong

band at 1009 cm^{-1} has been assigned to the symmetric pulsation vibration (A_1 type) of all the 12 $\text{W}-\text{O}_d$ bonds. This is supported by the absence of bands $\sim 1000\text{ cm}^{-1}$ in the infrared. The fairly strong band at 985 cm^{-1} has been assigned to the asymmetric vibration of symmetry F_2 , since there is a corresponding band in the infrared at 799 cm^{-1} . However, the normal coordinate analysis of Lyhamn *et al.*¹⁸ ascribes this band to the symmetric $\text{P}-\text{O}$ stretching. Hence, it seems reasonable to assume that the A_1 vibration of the PO_4 tetrahedra coincides with the asymmetric vibration of the $\text{W}-\text{O}_d$ bonds. Further, the A_1 vibration of a free PO_4^{3-} ion is 936 cm^{-1} (Ref. 21) and there is no other observed frequency above 936 cm^{-1} except the one at 985 cm^{-1} . The strong broad band centred at 1080 cm^{-1} in infrared is due to the asymmetric stretching vibration (F_2) of the PO_4 tetrahedra, and in Raman they are at 1075 and 1117 cm^{-1} . The bands in Raman are very weak which is usually the case²². The bands at 928 and 934 cm^{-1} may be due to either the vibrations of linear and angular $\text{W}-\text{O}-\text{W}$ bridges (F_2 or E type) or the vibrations of the $\text{W}-\text{O}_a$ bonds. The two bands at 890 and 814 cm^{-1} with the former having a shoulder at 903 cm^{-1} have been assigned to the asymmetric stretching vibrations of the linear and angular $\text{W}-\text{O}-\text{W}$ bonds. The intensities of these bands are not equal, although the number of bonds responsible for these vibrations is the same. The broad band at 690 cm^{-1} has been assigned to the symmetric stretching of the $\text{W}-\text{O}_a$ bonds. The low value of this vibration is suggestive of a bending vibration interacting with this stretching vibration.

4.2 Bending Vibrations

The strong band at 520 cm^{-1} and the medium band at 471 cm^{-1} with splittings have been assigned respectively to the asymmetric (F_2) and symmetric (E) deformations of the PO_4 tetrahedra. The assignment of the F_2 vibration is supported by the presence of a strong broad absorption centred at 518 cm^{-1} in infrared. The fairly high intensity and its splittings indicate that there is some mixing up of this vibration with the vibrations of $\text{W}-\text{O}-\text{W}$ bonds. A free PO_4^{3-} ion has its ν_4 deformation $\sim 570\text{ cm}^{-1}$ (Ref. 21). In the $\text{PW}_{12}\text{O}_{40}^{3-}$ ion, each oxygen of the PO_4 tetrahedra is covalently bonded to W_3O_{10} units resulting in the

lowering of the PO_4 deformation by $\sim 50\text{ cm}^{-1}$ and enhancing the PO_4 stretching frequencies by $\sim 45\text{ cm}^{-1}$. The vibrations below 450 cm^{-1} are due to the mixed deformations of the linear and angular metal-oxygen-metal bridges. The assignments of these lines are shown in Table 3.

Acknowledgement

The authors are thankful to Prof P S Narayanan, Indian Institute of Science, Bangalore for making available the Spex Ramalog for recording the spectrum. One of the authors (SSS) is grateful to the CSIR, New Delhi for the award of a fellowship and to Prof P S Narayanan for his hospitality at Bangalore.

References

- 1 Berzelius J J, *Prog Ann (Germany)*, **6** (1826) 369, 380.
- 2 Charlot G, *Colorimetric determination of elements* (Elsevier, New York) 1964.
- 3 Mitchell P C H, *The chemistry and uses of molybdenum*, edited by P C H Mitchell (Climax Molybdenum Co., New York) 1974.
- 4 Nakamura O, Kodama T, Ogino I & Miyake Y, *Chem Lett (Netherlands)*, (1979) 17.
- 5 Keggin J F, *Proc R Soc London Ser A (GB)*, **144** (1934) 75.
- 6 Kraus O, *Z Krist (Germany)*, **100** (1939) 394; **94** (1936) 256.
- 7 Flynn C M & Pope M T, *Inorg Chem (USA)*, **10** (1971) 2754, 2524; **11** (1972) 1950.
- 8 Weakley T J R, *Struct & Bonding (Germany)*, **18** (1974) 131.
- 9 Tsigdinos G A & Hallada C J, *Inorg Chem (USA)*, **7** (1968) 437.
- 10 Sharpless N E & Munday J S, *Anal Chem (USA)*, **29** (1957) 1619.
- 11 Brown D H, *Spectrochim Acta (GB)*, **19** (1963) 585.
- 12 Lange G, Hahn H & Dehnicke K, *Z Naturforsch b (Germany)*, **24** (1969) 1498.
- 13 Thouvenot R, Rocchiccioli-Deltcheff C & Souchay P, *C.R. Hebd Seanc Acad Sci Paris Ser C (France)*, **278** (1974) 455.
- 14 Rocchiccioli-Deltcheff C, Thouvenot R & Franck R, *C.R. Hebd Seanc Acad Sci Paris Ser C (France)*, **280** (1975) 751.
- 15 Kazanskii L P, Torchenkova E A & Spitsyn V, *Dokl Akad Nauk SSSR (USSR)*, **209** (1973) 141.
- 16 Lyhamn L & Petterson L, *Chem Scr (Sweden)*, **12** (1977) 142.
- 17 Kasprzak M S, Crouch S R & Leroi G E, *Appl Spectrosc (USA)*, **32** (1978) 537.
- 18 Lyhamn L, Cyvin S J, Cyvin B N & Brunvoll J, *Z Naturforsch a (Germany)*, **31** (1976) 1589.
- 19 Matte S R, Bierbusse H & Fuchs J, *Z Anorg Allg Chem (Germany)*, **385** (1971) 230.
- 20 Herzberg G, *Infrared and Raman spectra*, (D Van Nostrand, New York) 1945.
- 21 Chapman A C, Long D A & Jones D T L, *Spectrochim Acta (GB)*, **24** (1965) 633.
- 22 Casciani F & Condrate R A, *J Solid State Chem (USA)*, **34** (1980) 385.
- 23 Allmann R & D'Amour H, *Z Krist (Germany)*, **141** (1975) 161.

Crystallization of Amorphous Mercury Selenide Films

K N SHARMA[†] & K BARUA*

Department of Physics, Dibrugarh University, Dibrugarh 786 004

Received 7 January 1982; accepted 12 November 1982

The crystallization of amorphous mercury selenide (a-HgSe) films has been studied as a function of annealing temperature ($343\text{ K} < T < 365\text{ K}$). The crystallization process was found to be gradual, which took place at any finite temperature and was thermally activated with an activation energy of 0.963 eV. The characteristic time associated with the microscopic reaction between the neighbouring atoms was $1.273 \times 10^{-10}\text{ s}$.

It is well known that amorphous materials undergo irreversible transformation to crystalline state when heated to a relatively high temperature. Crystallization of amorphous materials has been studied by a number of workers¹⁻⁷. They have observed that large thermal energy was required to initiate a very quick crystallization process in which an amorphous material would switch over to a polycrystalline state. Loma *et al.*⁸ have reported that HgSe films, when deposited on unheated cleaved mica substrate, showed no trace of crystallinity when examined using the reflection electron diffraction technique. The study of crystallization process is essential to the experimental physicists wishing to anneal and also to determine the maximum time allowed for a measurement at a particular temperature on the films of amorphous materials, while preserving most of the amorphous characters. We report in this note our study on the crystallization of HgSe films of thicknesses of $\sim 4080\text{ \AA}$.

a-HgSe films were prepared by vacuum evaporation of the compound (99.999%, Koch Light, England) on to glass substrates held at -2 to -5°C . The predeposition pressure was of $\sim 10^{-5}$ torr, while during deposition the pressure remained at 4×10^{-5} torr. The source-to-substrate distance was 15 cm.

Samples of size $0.5 \times 1\text{ cm}^2$ were obtained either by cutting a single large area ($2.5 \times 7\text{ cm}^2$) of the film or by using masks of proper dimensions on smaller glass slides. Electrical contacts were established using conducting silver paint in a planar configuration. The contact was found to be ohmic up to an applied field 10^3 V/cm . Evaporated indium contacts were also found to be ohmic. The films studied were red in colour,

electrically continuous and dry air-annealed at a temperature of $\sim 300\text{ K}$.

For crystallization, the sample was placed in position on a cradle inside a vacuum jacket which was evacuated ($\sim 10^{-3}$ torr). The jacket was then inserted into a furnace which was preheated to a specific temperature. The furnace temperature was pre-calibrated with the help of a chromel-alumel thermocouple, fixed on the cradle without the sample, to a temperature of $\pm 0.5^\circ\text{C}$ of annealing temperature. This was tested for about 2 hr for every sample at different constant temperatures.

The sample current was noted by measuring the potential drop across a standard resistance using an electronic meter (Philips PK 2505). The voltage across the film was measured using an electrometer amplifier (ECIL EA813). The temperature and sample current for a fixed voltage were then noted with time. The zero of the time was taken when the film attained the pre-determined temperature.

The optical transmission of the film was measured using a spectrophotometer (Systronics type 105). The transmission micrographs and diffraction patterns were taken with the help of an electron microscope

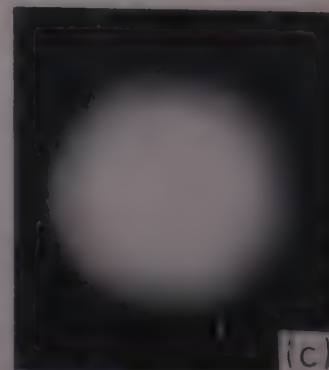
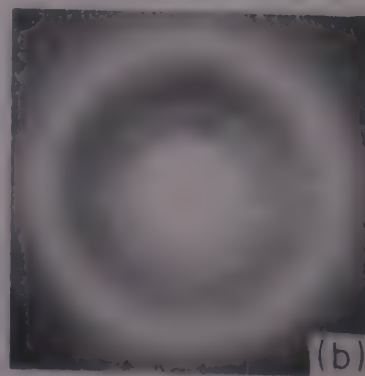
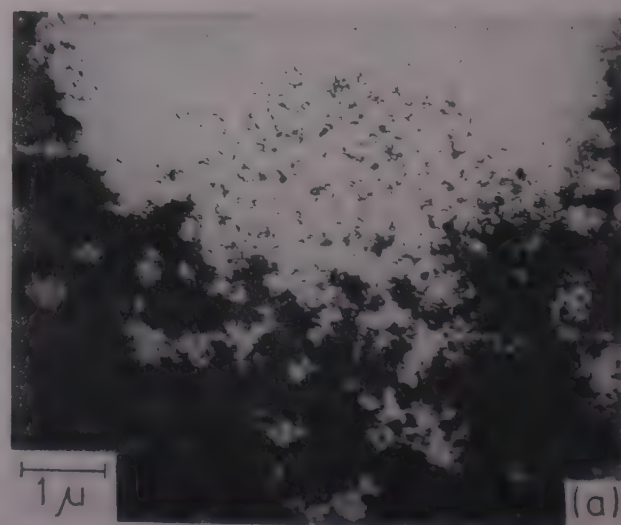


Fig. 1 (a) Electron micrograph of a-HgSe film; (b) electron diffraction pattern showing haloes and (c) electron diffraction pattern showing weak rings

[†]Present address: Department of Physics, Government D M College of Science, Imphal 795 001

(Philips EM200). The film thickness was measured using the multiple-beam interference method.

The resistivity of the film, within the thickness range of 1000-3500 Å, was found to be very high and the current measurement was not possible because of noise. Electron diffraction patterns and micrographs for the films of 3880-4300 Å thickness, showed the presence of both the amorphous and microcrystalline regions as evident from the haloes and weak rings as seen from Figs 1(b) and (c). We have studied these films

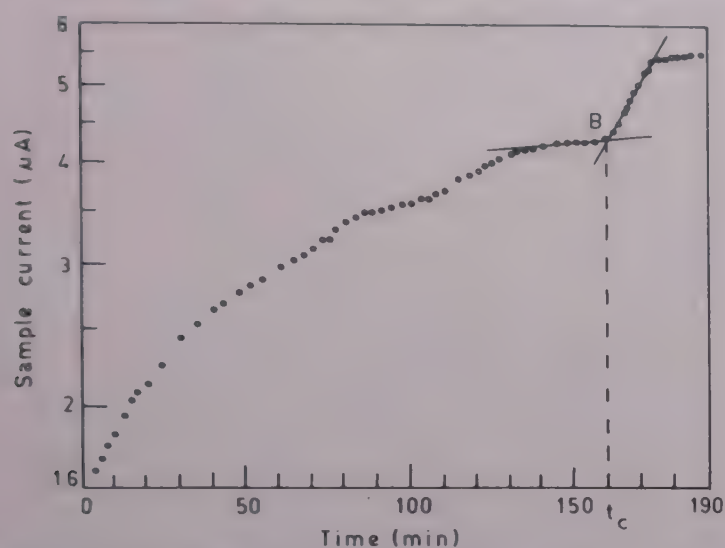


Fig. 2—Log (sample current) versus time for a fixed annealing temperature of 350 K

assuming the presence of microcrystallites embedded in an amorphous matrix as one of the three types of disorders which may be found in any amorphous material⁹.

Fig. 2 shows the film current against time at a constant annealing temperature of 350 K. It is seen that at the beginning the current increases exponentially and then remains constant for a short interval of time and then increases linearly with time reaching a final constant value. The annealed films, when examined under optical microscope, were found to develop microcracks and at the same time the colour of the film changed from red to dark red. The transmittance was also found to reduce from 63-70% to 20-23% when measured at the maximum transmittance wavelength 960 nm. The time at which the current increases suddenly was taken as the crystallization time (t_c). The value of t_c was found to decrease with the increase of annealing temperature. It was interesting to note that when the films were heated at 97°C, the rate of change of current at constant voltage was very fast and t_c was 8-12 min.

Fig. 3 shows a micrograph and the corresponding diffraction pattern for a film annealed above t_c . The

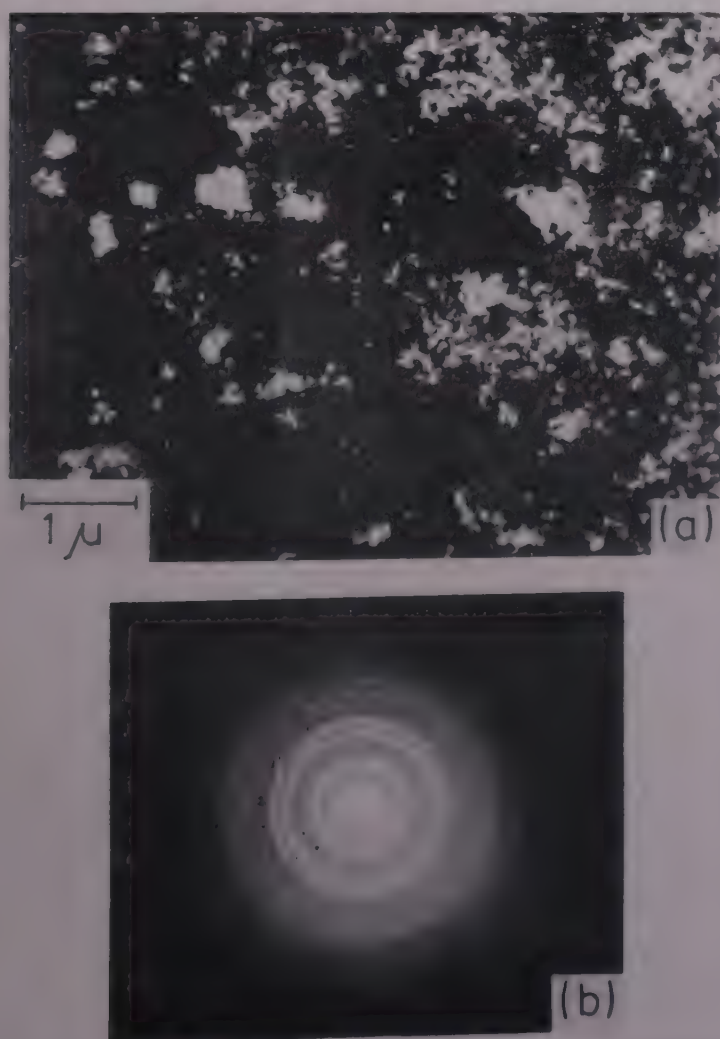


Fig. 3—(a) Electron micrograph and (b) corresponding diffraction pattern for a crystallized HgSe film

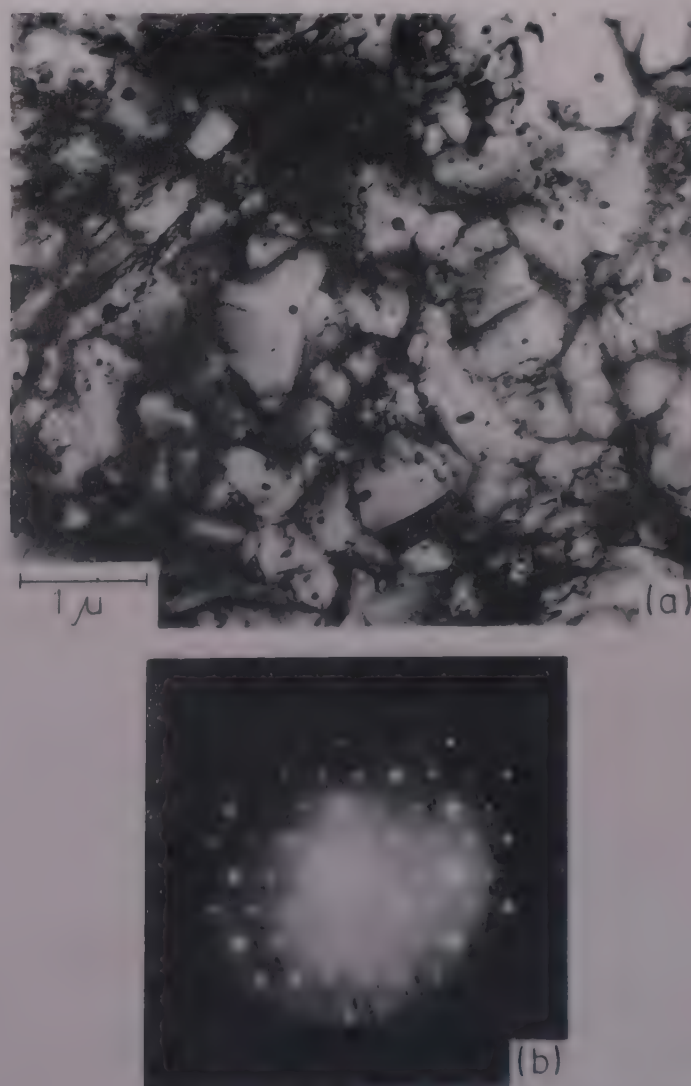


Fig. 4—(a) Electron micrograph and (b) electron diffraction pattern for a film deposited on glass at 97°C

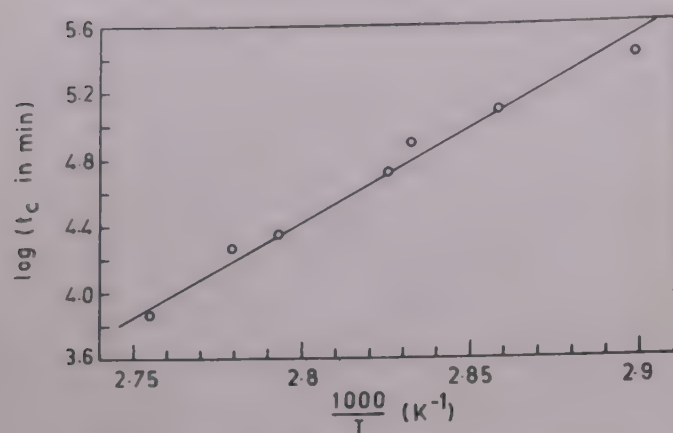


Fig. 5—Log t_c versus $1000/T$ for a-HgSe films

diffraction pattern showed sharp rings indicating polycrystalline nature of the film. It has already been mentioned that at an annealing temperature of 97°C , the process of crystallization was very fast. We have deposited HgSe on glass slides at 97°C , and the micrographs and diffraction patterns revealed the monocrystalline nature of the deposit. Fig. 4 shows the micrograph (a) and corresponding diffraction pattern (b) for a film deposited on glass substrate at 97°C . Hence it can be concluded that the observed behaviour was due to polymorphic transformation excluding nucleation¹⁰.

The activation energy E_0 , between the metastable amorphous and stable crystalline state, the characteristic time τ associated with the microscopic reaction between the neighbouring atoms and annealing temperature T are related to the crystallization time t_c by³

$$t_c = \tau \exp(E_0/kT) \quad \dots (1)$$

Thus a plot of $\log t_c$ versus $1/T$ would yield a straight line (Fig. 5). The straight line (Fig. 5) has been drawn, following the regression method. The value of E_0 was determined by equating the slope to E_0/k , and was found to be 0.963 eV. The value of τ was calculated using this value of E_0 in Eq. (1) and was found to be 1.273×10^{-10} s. The crystallization time t_c at room temperature (26°C) was calculated to be 27.2 days.

The authors are thankful to Dr O N Srivastava, Department of Physics, Banaras Hindu University for providing electron microscopy facilities. One of the authors (KNS) is thankful to the University Grants Commission, New Delhi, for the award of a teacher research fellowship.

References

- 1 Bagley B G & Bair H E, *J Non-Cryst Solids (Netherlands)*, **2** (1970) 155.
- 2 Barna A, Barna P B & Pocza J F, *J Non-Cryst Solids (Netherlands)*, **8** (1972) 36.
- 3 Blum N A & Feldman C, *J Non-Cryst Solids (Netherlands)*, **11** (1972) 242.
- 4 Chaudhari P & Herd S R, *J Non-Cryst Solids (Netherlands)*, **8** (1972) 56.
- 5 Chik K P & Pin-co-him, *Thin Solid Films (Switzerland)*, **35** (1976) 45.
- 6 Moss S C & De Neufville J P, *J Non-Cryst Solids (Netherlands)*, **8** (1972) 45.
- 7 Webb J B & Brodie D E, *Can J Phys (Canada)*, **53** (1975) 2481.
- 8 Lomas R A, Tomlinson R D & Hampshire M J, *Thin Solid Films (Switzerland)*, **13** (1972) S2.
- 9 Jonscher A K & Walley P A, *J Vac Sci & Technol (USA)*, **6** (1969) 662.
- 10 Christian J W, *Theory of transformation in metals and alloys*. (Pergamon Press, London) 1965.

Viscosity of Binary Liquid Mixtures in Hard-Sphere Approximation

HARMINDER*

Physics Department, College of Home Science, Punjab Agricultural University, Kaoni, Punjab 152 031

Received 22 December 1981

Argon-krypton binary liquid mixture has been simulated as a hypothetical hard-sphere fluid, for its viscosity through conformal solution theory. The agreement between the experimental data and calculated values using Enskog theory is found to be excellent.

Hard sphere approach has proved to be highly successful in interpreting the equilibrium and transport properties of simple dense liquids¹. This approach has not been intensively used in the study of the properties of binary liquid mixtures, in particular the transport properties. Jhunjunwala *et al.*² have studied the shear viscosity of argon-krypton liquid mixture in the hard-sphere model. The purpose of this study was to judge the appropriateness, in representing the observed viscosity of a simple liquid mixture as the viscosity of a hypothetical hard-sphere fluid mixture. The agreement of the values of viscosity calculated through the Thorne extension of Enskog theory, with the observed values is highly encouraging. Protopapas and Parlee³ have studied the shear viscosity of the binary liquid alloys in the hard-sphere approximation. The comparison between the experimental and calculated set of values, studied by these authors, is satisfying. On the basis of the success of hard-sphere model for simple liquids and the above mentioned studies, it is reasonable to expect that single hard-sphere approach may also be appropriate for the binary liquid mixtures.

An attempt has been made to simulate a simple liquid mixture as a hypothetical one-component hard-sphere fluid, against the two-component hard-sphere fluid mixture as suggested by Jhunjunwala *et al.*², for its shear viscosity behaviour. The objective of this study is to gather information about the appropriateness of using the single hard sphere model for the binary liquid mixtures. Further, it is intended to find the relative applicability of the single hard-sphere model over the binary hard-sphere model, for binary liquid mixtures. Ready availability of the experimental data for the shear viscosity^{4,5} and highly simple liquids which constitute the mixture have been the criteria, leading to the choice of argon-krypton mixture in this work.

Since it is intended to simulate the binary liquid mixture as a one-component hard-sphere fluid, the

shear viscosity of the hard sphere can be obtained through the use of Enskog theory. The shear viscosity η , of a hard sphere fluid having effective hard-sphere diameter σ , mass m , number density n at a temperature T , is given as,

$$\eta = (5/16 \sigma^2)(mkT/\pi)^{1/2} [g(\sigma)^{-1} + 0.8b\rho + 0.7614b^2\rho^2 g(\sigma)], \quad \dots(1)$$

with

$$b\rho = (2/3)\pi n\sigma^3 \quad \dots(2)$$

The contact radial distribution function $g(\sigma)$ through P-Y theory can be written as

$$g(\sigma) = [1 + (\pi n\sigma^3/12)]/[1 - (\pi n\sigma^3/6)]^2 \quad \dots(3)$$

In order to use Eq. (1) for the calculation of shear viscosity of argon-krypton mixture, the values of σ , m and n , which are functions of composition of the mixture, must be known over the whole composition of the mixture. The values of n are obtainable from the available molar volumes of the mixture. For obtaining the values of σ and m , at different compositions, the use of conformal solution theory is made.

It has been established⁶ that the pair potentials for argon and krypton liquids can be represented by 6, 12 Lennard-Jones potential. The potential parameters for pure species are taken as the ones used by Jhunjunwala *et al.*² The dissimilar pair potential parameters are obtainable through the use of Lorentz-Berthelot rules. The diameters for the hypothetical hard-spheres for argon and krypton are obtained by fitting the experimental values of shear viscosities for pure liquids to Eqs (1) to (3). The ratios of the effective hard-sphere diameter to the Lennard-Jones diameter, β , are 1.0256 and 1.1119, respectively, for argon and krypton.

The essential requirement for the application of conformal solution theory, namely that the pair interactions in the mixture are of the same functional form, is satisfied for the present mixture. The conformal solution theory for the transport properties⁷ of liquid mixture has proposed various mixing rules. The mixing rule pertinent to the potential contributions for the shear viscosity, which is dominating at liquid densities, is used for obtaining the Lennard-Jones diameter and mass for the hypothetical Lennard-Jones fluid. The mixing rule is

$$\begin{aligned} \sigma_x^3 &= \sum x_\alpha x_\beta \sigma_{\alpha\beta}^3 \\ \epsilon_x \sigma_x^3 &= \sum x_\alpha x_\beta \epsilon_{\alpha\beta} \sigma_{\alpha\beta}^3 \\ \epsilon_x \sigma_x^4 \mu_x^{1/2} &= \sum x_\alpha x_\beta \epsilon_{\alpha\beta} \sigma_{\alpha\beta}^4 \mu_{\alpha\beta}^{1/2} \end{aligned} \quad \dots(4)$$

Table 1—Shear Viscosities of Ar-Kr Mixtures at 100 K

Mole fraction of argon	Shear viscosities (in mP)		
	Exptl.	Present study (Calc.)	Jhunjhunwala <i>et al.</i> ² (Calc.)
0.0	6.9	6.9	6.9
0.2	—	5.178	5.361
0.411	3.917	3.878	4.049
0.6	3.022	3.019	3.144
0.8	2.274	2.331	2.401
1.0	1.81	1.81	1.81

where x specifies the composition of the mixture and μ is the reduced mass. Now the effective hard-sphere diameter for the hard-sphere is obtained through a relation for β . It is suggested that β can be written as,

$$\beta = \sum x_\alpha \beta_\alpha \quad \dots (5)$$

The shear viscosity of argon-krypton mixture at 100 K is calculated over the whole range of composition using Eqs (1) to (3) in conjunction with Eqs (4) and (5). In Table 1 the presently calculated values along with the

experimental values for the mixture are tabulated. The calculated values due to Jhunjhunwala *et al.*² are also given in Table 1, which reveals that the presently calculated values are in excellent agreement with the observed values. Further, significantly these calculated values are in closer agreement with the experimental values than the calculated values of Jhunjhunwala *et al.*² Therefore, it can be reasonably concluded that the single-component hard-sphere approach may be appropriate for the transport properties of the binary liquid mixtures.

References

- 1 Andersen H C, Chandler D & Weeks J D, *Adv Chem Phys (USA)*, **34** (1976) 106.
- 2 Jhunjhunwala N, Boon J P, Frisch H L & Lebowitz J L, *Physica (Netherlands)*, **41** (1969) 536.
- 3 Protopapas P & Parlee N A D, *Chem Phys (Netherlands)*, **11** (1975) 201.
- 4 Boon J P & Thomaes G, *Physica (Netherlands)*, **28** (1962) 1074.
- 5 Boon J P, Legros J C & Thomaes G, *Physica (Netherlands)*, **33** (1967) 547.
- 6 Verlet L, *Phys Rev (USA)*, **159** (1967) 98.
- 7 Mo K C & Gubbins K E, *Mol Phys (GB)*, **31** (1976) 825.

Force Field Study of Some Non-linear XY₂-type Molecules

S MOHAN*, S GUNASEKARAN & K G RAVIKUMAR

Division of Applied Sciences, Anna University, Madras Institute of Technology, Madras 600 044

Received 18 March 1982

The most probable force fields of the non-linear XY₂-type molecules like SO₂, ClO₂ and CF₂ have been fixed by a parametric method. The centrifugal distortion constants are used as additional data to fix the potential constants unambiguously.

The determination of an unambiguous set of potential constants from vibrational spectral data alone is not possible because the number of potential constants exceeds the number of fundamental frequencies. Therefore, one is forced to turn to other sources for the determination of a unique set of potential constants. The centrifugal distortion constants form a very important set of molecular data as they are essential for an accurate knowledge of the rotational energy levels of the molecules. If the experimental values of the centrifugal distortion constants are available accurately, the values can serve well as additional data to fix the harmonic force field in the molecules. A parametric approach is presented, in this note, to the analysis of the centrifugal distortion constants to fix the unique force field of some of the XY₂ bent-type molecules, namely SO₂, ClO₂ and CF₂.

Theory—The general theory of centrifugal distortion in the rotational spectra of asymmetric rotor molecules has been formulated by various authors¹⁻³. The distortion constants are defined as:

$$\tau_{\alpha\beta\gamma\delta} = -(2I_{\alpha\alpha}^e I_{\beta\beta}^e I_{\gamma\gamma}^e I_{\delta\delta}^e)^{-1} \sum_{i,j} J_{\alpha\beta,s}^i J_{\gamma\delta,s}^j N_{ij} \quad \dots(1)$$

where I_{xx}^e , I_{yy}^e and I_{zz}^e [$\alpha, \beta, \gamma, \delta = x, y$ (or) z] are the principal moments of inertia at equilibrium and $J_{\alpha\beta,s}^i$ represent partial derivatives at equilibrium of the instantaneous inertia tensor components with respect to the symmetric co-ordinates. Here, N_{ij} is the appropriate element of the compliance matrix⁴. The partial derivatives appearing in Eq. (1) may be evaluated following the general method proposed by Kivelson and Wilson⁵. Kivelson and Wilson's theory of centrifugal distortion has been reformulated by several authors⁶⁻¹¹. The formulation suggested by Cyvin⁸⁻¹¹, extensively employing matrix notation, is

found to be the most convenient one for the calculation of centrifugal distortion constants.

A new quantity $t_{\alpha\beta\gamma\delta}$ is defined as

$$t_{\alpha\beta\gamma\delta} = -2I_{\alpha\alpha}^e I_{\beta\beta}^e I_{\gamma\gamma}^e I_{\delta\delta}^e \tau_{\alpha\beta\gamma\delta} \\ = \sum_{i,j} J_{\alpha\beta,s}^i J_{\gamma\delta,s}^j N_{ij} \quad \dots(2)$$

Eq. (2) may be written, in matrix notation as

$$t = J_s' N J_s \quad \dots(3)$$

Substituting

$$J_{\alpha\beta,s} = G^{-1} T_{\alpha\beta,s} \\ t = \tilde{T}_s \tilde{G}^{-1} N G^{-1} T_s \quad \dots(4)$$

The elements of the matrix T_s can be calculated for a given molecular model from the equilibrium position vector of atoms and Wilson's S vectors¹². G^{-1} is the kinetic energy matrix of Wilson¹².

Writing t in L -matrix notation

$$t = \tilde{T}_s \tilde{L}^{-1} \Lambda^{-1} L^{-1} T_s \quad \dots(5)$$

In the parametric method, the L -matrix is written as

$$L = L_0 A \quad \dots(6)$$

where A is an orthogonal matrix.

Thus

$$t = \tilde{L}_0^{-1} \tilde{T}_s A \Lambda^{-1} \tilde{A} L_0^{-1} T_s \quad \dots(7)$$

By varying the values of the parameters in A -matrix, it is possible to find all the t values that fit the observed frequencies. Then, using the expression

$$F = \tilde{L}_0^{-1} A \Lambda \tilde{A} L_0^{-1} \quad \dots(8)$$

the force field corresponding to each of the A matrix can be obtained.

Results and discussion—This procedure has been applied to three molecules, namely SO₂, CF₂ and ClO₂ in the present investigation. The A matrix used here is of the form

$$A = \begin{pmatrix} 1 & a & 0 \\ \frac{1}{\sqrt{1+a^2}} & \frac{a}{\sqrt{1+a^2}} & 0 \\ -\frac{a}{\sqrt{1+a^2}} & \frac{1}{\sqrt{1+a^2}} & 0 \\ 0 & 0 & 0 \end{pmatrix}$$

Expansion of Eq. (7) gives t_{xxxx} , t_{yyyy} , t_{zzzz} , t_{xxyy} , t_{xxzz} , t_{yyzz} and t_{yzxz} . But Kivelson and Wilson have already shown⁵ that the t_{yyyy} , t_{yyxx} and t_{yyzz} are dependent quantities for the molecule under consideration. Hence it is sufficient to map t_{xxxx} , t_{zzzz} and t_{xxzz} with A .

A horizontal line is drawn on the Y -axis ($\tau_{\alpha\beta\gamma\delta}$ -axis) corresponding to the experimental values of $\tau_{\alpha\beta\gamma\delta}$. The intersection point of the line with the curves mentioned earlier gives the value of A . Hence we obtain three

Table 1—Values of $\tau_{\alpha\beta\gamma\delta}$ Elements and Parameter A

Molecule	$\tau_{\alpha\beta\gamma\delta}$ element and its value (MHz)	A
SO ₂	τ_{zzzz} 9.809 (Ref. 13)	0.006
ClO ₂	τ_{xxxx} 8.529 (Ref. 14)	0.012
CF ₂	τ_{xxxx} 11.2778 (Ref. 15)	0.02

Table 2— F_{ij} Elements (10^5 dyne/cm)

F_{ij}	SO ₂		ClO ₂		CF ₂	
	PW	EW (Ref. 16)	PW	EW (Ref. 17)	PW	EW (Ref. 15)
$F_{11}(A_1)$	10.2441	10.0793	7.2274	7.1590	8.7481	7.796
$F_{22}(A_1)$	0.8305	0.8086	0.6895	0.6885	1.1176	1.373
$F_{12}(A_1)$	0.4330	0.2513	0.2644	—	1.1250	0.7713

PW, present work; EW, earlier work

values for A , each corresponding to τ_{xxxx} , τ_{zzzz} and τ_{xxzz} . The best suitable value for A is the one which is closer to zero. This is because A -matrix is always nearly equal to unity.

The following are the best A values corresponding to $\tau_{\alpha\beta\gamma\delta}$ for the molecules under investigation:

SO₂—The best A value is corresponding to τ_{zzzz}

CF₂—The best A value is corresponding to τ_{xxxx}

ClO₂—The best A value is corresponding to τ_{xxxx}

The experimentally observed values of the $\tau_{\alpha\beta\gamma\delta}$ elements and the A values obtained in the present

investigation are given in Table 1. Table 2 deals with the evaluated force constants in the present investigation along with the values reported in the literature.

References

- 1 Wilson E B (Jr), *J Chem Phys (USA)*, **4** (1936) 526; **5** (1937) 617.
- 2 Wilson E B (Jr) & Howard J B, *J Chem Phys (USA)*, **4** (1936) 260.
- 3 Nielson H H, *Rev Mod Phys (USA)*, **23** (1951) 90.
- 4 Decius J C, *J Chem Phys (USA)*, **38** (1963) 241.
- 5 Kivelson D & Wilson E B (Jr), *J Chem Phys (USA)*, **20** (1952) 1575; **21** (1953) 1229.
- 6 Pulay P & Sawodny W, *J Mol Spectrosc (USA)*, **26** (1968) 150.
- 7 Klauss K & Strey G, *Z Naturforsch a (Germany)*, **23** (1968) 1308.
- 8 Cyvin S J & Hagen G, *Chem Phys Lett (Netherlands)*, **1** (1968) 645.
- 9 Cyvin S J, Cyvin B N & Hagen G, *Z Naturforsch a (Germany)*, **23** (1968) 1649.
- 10 Cyvin B N, Elvebredd I & Cyvin S J, *Z Naturforsch a (Germany)*, **24** (1969) 139.
- 11 Sorensen G O, Hagen G & Cyvin S J, *J Mol Spectrosc (USA)*, **35** (1970) 489.
- 12 Wilson E B (Jr), Decius J C & Cross P C, *Molecular vibrations* (McGraw-Hill, New York) 1955.
- 13 Bauer A & Bellet J, *J Phys (France)*, **25** (1964) 805.
- 14 Brand J C D & Redding R W, *J Mol Spectrosc (USA)*, **34** (1970) 399.
- 15 Kirchoff W H, Lide D R (Jr) & Powell F X, *J Mol Spectrosc (USA)*, **47** (1973) 491.
- 16 Ramaswamy K & Srinivasan R, *Acta Phys Pol A (Poland)*, **51** (1977) 139.
- 17 Venkateswarlu K & Thanalakshmi R, *Indian J Pure and Appl Phys*, **1** (1963) 377.

Dipole Moments of Dichlorotoluenes in Benzene Solution

JAI PRAKASH*, BASHISHTH RAI & RAHUL

Department of Physics, University of Gorakhpur, Gorakhpur 273 001

Received 19 April 1982; revised received 29 October 1982

Dielectric constant, density and refractive index of 2,4-; 2,6- and 3,4-dichlorotoluenes have been determined at 35°C using benzene as a non-polar solvent. These data have been utilized for evaluating their respective dipole moments using Palit's method. The dipole moment has been found to be 1.78, 0.65 and 2.29 D respectively for 2,4-; 2,6- and 3,4-dichlorotoluenes.

Different methods¹⁻⁸ are being employed for the determination of the dipole moment of a polar solute molecule in a non-polar solvent. It has been observed that these methods incorporate some simplifying assumptions and can be derived from the simple Debye equation^{9,10}. The method suggested by Palit¹¹ is, however, free from any assumption. Further, Guggenheim's method⁸ and Higasi's method⁴ can also be derived¹² from Palit's method. Hence, Palit's method proves to be the most general procedure for the determination of the dipole moment of a polar solute molecule in a non-polar solvent^{11,12}. Dipole moments of dichlorotoluenes in benzene solution were evaluated by the authors using Higasi's Guggenheim's and Palit's methods and the results are reported in this note.

Samples of dichlorotoluenes (purum grade) were procured from M/s Fluka A G, Switzerland and AR grade benzene from M/s BDH, India. These chemicals were further fractionally distilled just before use. The experimental procedures are essentially the same as described elsewhere^{13,14}. Dielectric constant (ϵ_0), density (d) and refractive index (n_D) of different dilute solutions of 2,4-; 2,6- and 3,4-dichlorotoluenes were measured at 35°C using benzene as a non-polar solvent.

According to Palit¹¹ the dipole moment (μ) of a polar solute molecule in a non-polar solvent can be evaluated with the help of the equation:

$$P_{2\mu} = \frac{3M_2(\epsilon_{01} - n_{D1}^2)}{d_1(\epsilon_{01} + 2)(n_{D1}^2 + 2)} \left(1 - \frac{\beta_{0w}}{d_1}\right) \frac{3M_2\alpha_{0w}}{d_1(\epsilon_{01} + 2)^2} - \frac{6M_2n_{D1}\gamma_{0w}}{d_1(n_{D1}^2 + 2)^2} \quad \dots(1)$$

where $P_{2\mu}$ is the orientation polarization of the solute molecule expressed as:

$$P_{2\mu} = \frac{4\pi N\mu^2}{9kT} \quad \dots(2)$$

In Eq. (1), M is the molecular weight, d the density, w the concentration in weight fraction and subscripts 1, 2 and 12 stand for the solvent, solute and solution respectively; α_{0w} , β_{0w} and γ_{0w} are the limiting slopes defined as

$$\alpha_{0w} = \left(\frac{\partial \epsilon_{012}}{\partial w_2}\right)_{w_2 \rightarrow 0}$$

$$\beta_{0w} = \left(\frac{\partial d_{12}}{\partial w_2}\right)_{w_2 \rightarrow 0} \quad \text{and} \quad \gamma_{0w} = \left(\frac{\partial n_{D12}}{\partial w_2}\right)_{w_2 \rightarrow 0}$$

It has been shown¹¹ that for $\epsilon_{01} = n_{D1}^2$ or $\beta_{0w} = d_1$, Eq. (1) reduces to Guggenheim's equation:

$$\mu^2 = \frac{9kT}{4\pi N} \frac{3}{(\epsilon_{01} + 2)^2} \frac{M_2}{d_1} \left(\frac{\Delta}{w_2}\right)_{w_2 \rightarrow 0} \quad \dots(3)$$

where

$$\left(\frac{\Delta}{w_2}\right)_{w_2 \rightarrow 0} = \left[\left(\frac{\partial \epsilon_{012}}{\partial w_2}\right)_{w_2 \rightarrow 0} - 2n_{D1} \left(\frac{\partial n_{D12}}{\partial w_2}\right)_{w_2 \rightarrow 0}\right]$$

Further, Eq. (2) can also be rearranged^{9,15} to yield Higasi's equation

$$\mu = \beta \left(\frac{d\epsilon_{012}}{df_2}\right)^{1/2} \quad \dots(4)$$

where β is a constant and is equal to 0.828 D for benzene as a non-polar solvent¹³.

Dipole moments of 2,4-; 2,6- and 3,4-dichlorotoluenes have been evaluated using Eqs (1)-(4).

Measured values of ϵ_{012} , d_{12} and n_{D12} of different dilute solutions using benzene as a non-polar solvent are presented in Table 1. It has been observed that ϵ_{012} , d_{12} and n_{D12} vary linearly with the concentration. The corresponding values of limiting slopes are also included in Table 1.

The values of $P_{2\mu}$ evaluated from Palit's method using Eq. (1) are presented in Table 2. It is apparent that 2,6-dichlorotoluene has the lowest value of $P_{2\mu}$ out of the set presented in Table 2. It is expected also because of the structural considerations.

Dipole moments of 2,4-; 2,6- and 3,4-dichlorotoluenes evaluated following Eqs (1)-(4) are presented in Table 2. It is apparent that μ evaluated from Guggenheim's method using Eq. (3) is in close agreement with those evaluated from Palit's method. Also, μ evaluated from Higasi's method using Eq. (4) is significantly far off, particularly in the case of 2,6-dichlorotoluene. This discrepancy is due to the fact that Higasi's method, although a quick procedure for the determination of μ , is valid only for gases or very dilute binary liquid mixtures of a polar solute in a non-polar solvent. Higasi's method should, therefore, be

Table 1—Dielectric Constant, Density & Refractive Index of 2,4-, 2,6- and 3,4-Dichlorotoluenes in Benzene Solution at 35°C

Mole fraction f_2	Weight fraction w_2	Dielectric constant measured at 450 KHz ϵ_{012}	Density d_{12} g/cc	Refractive index n_{D12}
2,4-Dichlorotoluene				
0.0000	0.0000	2.268	0.8628	1.4914
0.0079	0.0161	2.279	0.8674	1.4918
0.0151	0.0306	2.317	0.8719	1.4924
0.0308	0.0614	2.400	0.8801	1.4934
0.0445	0.0883	2.457	0.8874	1.4937
0.0596	0.1155	2.529	0.8941	1.4953
0.0623	0.1204	2.558	0.8976	1.4953
0.0736	0.1407	2.586	0.9035	1.4959
0.0838	0.1586	2.632	0.9068	1.4964
0.0954	0.1786	2.674	0.9135	1.4969
0.1080	0.1998	2.712	0.9173	1.4977
$\alpha_{0m} = 4.348; \beta_{0m} = 0.532; \gamma_{0m} = 0.059$ $\alpha_{0w} = 2.285; \beta_{0w} = 0.265; \gamma_{0w} = 0.028$				
2,6-Dichlorotoluene				
0.0000	0.0000	2.268	0.8628	1.4914
0.0081	0.0166	2.277	0.8699	1.4926
0.0152	0.0309	2.277	0.8725	1.4926
0.0251	0.0504	2.285	0.8774	1.4933
0.0381	0.0755	2.296	0.8827	1.4940
0.0464	0.0911	2.302	0.8905	1.4947
0.0624	0.1206	2.312	0.8960	1.4955
0.0752	0.1436	2.330	0.9057	1.4959
0.0834	0.1580	2.336	0.9077	1.4969
0.0940	0.1761	2.344	0.9137	1.4972
0.1058	0.1961	2.351	0.9215	1.4990
0.1150	0.2113	2.358	0.9262	1.4995
$\alpha_{0m} = 0.762; \beta_{0m} = 0.550; \gamma_{0m} = 0.071$ $\alpha_{0w} = 0.375; \beta_{0w} = 0.261; \gamma_{0w} = 0.033$				
3,4-Dichlorotoluene				
0.0000	0.0000	2.268	0.8628	1.4914
0.0048	0.0098	2.306	0.8650	1.4916
0.0078	0.0159	2.316	0.8685	1.4917
0.0129	0.0263	2.352	0.8720	1.4925
0.0185	0.0374	2.408	0.8738	1.4928
0.0247	0.0497	2.481	0.8773	1.4934
0.0358	0.0710	2.581	0.8848	1.4945
0.0460	0.0904	2.688	0.8908	1.4950
0.0583	0.1131	2.842	0.8976	1.4959
0.0678	0.1304	2.947	0.9027	1.4967
0.0816	0.1547	3.035	0.9090	1.4978
0.0834	0.1579	3.045	0.9090	1.4979
$\alpha_{0m} = 7.500; \beta_{0m} = 0.592; \gamma_{0m} = 0.080$ $\alpha_{0w} = 3.635; \beta_{0w} = 0.284; \gamma_{0w} = 0.40$				

Table 2—Dipole Moment of Dichlorotoluenes in Benzene Solution at 35°C by Different Methods

Substance	Orientation polarization $P_{2\mu}$ cc	Dipole moment (D)		
		Palit's method	Guggenheim's method	Higasi's method
2,4-Dichlorotoluene	63.28	1.78	1.78	1.73
2,6-Dichlorotoluene	8.36	0.65	0.63	0.72
3,4-Dichlorotoluene	104.31	2.29	2.29	2.27

used in the cases where one is interested to have a rough estimate of the dipole moment.

It can be concluded that Palit's method should invariably be used for the determination of the dipole moment of a polar solute molecule in a non-polar solvent. However, when either $\epsilon_{01} = n_{D1}^2$ or $\beta_{0w} = d_1$, Guggenheim's method can as well be used for the determination of μ . In situations when one is interested to have an estimate of dipole moment, Higasi's method should be preferred.

The authors are thankful to Prof. N K Sanyal for valuable suggestions. Two of the authors (B R & Rahul) are thankful to CSIR, New Delhi, for financial assistance.

References

- 1 Debye P, *Polar molecules* (Chemical Catalog Co., New York) 1929.
- 2 Hill N E, Vaughan W E, Price A H & Davies M, *Dielectric properties and molecular behaviour* (Van Nostrand Reinhold Co, London) 1969.
- 3 Halverstadt I F & Kumler W D, *J Am Chem Soc (USA)*, **64** (1942) 2988.
- 4 Higasi K, *Bull Inst Phys Chem Res Tokyo (Japan)*, **22** (1943) 805.
- 5 Le Fevre R J W, *Trans Faraday Soc (GB)*, **46** (1950) 1.
- 6 Smith J W, *Trans Faraday Soc (GB)*, **46** (1950) 394.
- 7 Everard K B, Hill R A W & Sutton L E, *Trans Faraday Soc (GB)*, **46** (1950) 417.
- 8 Guggenheim E A, *Trans Faraday Soc (GB)*, **47** (1951) 573.
- 9 Prakash J, *Indian J Pure & Appl Phys*, **11** (1973) 901.
- 10 Prakash J, *Indian J Phys*, **49** (1975) 84.
- 11 Palit S R, *J Am Chem Soc (USA)*, **74** (1952) 3952.
- 12 Prakash J, *Indian J Pure & Appl Phys*, **14** (1976) 571.
- 13 Mehrotra V K & Prakash J, *Indian J Pure & Appl Phys*, **5** (1967) 528.
- 14 Chandra S & Prakash J, *J Chim Phys (France)*, **68** (1971) 1128; *J Phys Chem (USA)*, **75** (1971) 2616; *J Chem Phys (USA)*, **54** (1971) 5366.
- 15 Srivastava S C & Charandas P, *J Chem Phys (USA)*, **30** (1959) 816.

Uranium Estimation in Mussoorie Phosphorites using Solid State Nuclear Track Detector

SURINDER SINGH & H S VIRK*

Department of Physics, Guru Nanak Dev University, Amritsar

Received 23 June 1982; revised received 6 September 1982

A fission track analysis has been used to estimate the uranium concentration in phosphorite deposits of Mussoorie syncline in the lesser Himalayan region of Uttar Pradesh. The uranium content in these deposits has been found to vary from 0.01 to 0.06 %.

It is an established fact that sedimentary type of uranium deposits are generally more enriched in uranium than precambrian metamorphic complexes¹⁻³. The concentration of uranium in phosphorite deposits of Mussoorie syncline has been measured using homogenized fission track technique developed by Fisher⁴.

The phosphorite deposits in Mussoorie outcrop along the periphery of a double plunging syncline for some 120 km. The syncline axis extends in a NW-SE direction for about 20 km. The phosphorite horizon occurs at the transition zone between the underlying Krol limestone and the overlying Tal shales and sandstones and has intercalations of chert and black shales.

Experimental technique—The experimental technique for uranium estimation is the same as reported elsewhere⁵⁻⁷. Sample powder (50 mg) was mixed with 100 mg of methyl cellulose powder used as a binding material. The mixture was pressed into a pellet of 1.3 cm diameter and 1 mm thickness. One such pellet was made of standard glass having a uranium concentration of 12 ppm. The pellets covered with Lexan discs on both sides were enclosed in an aluminium capsules and were irradiated from CIRUS Reactor of Bhabha Atomic Research Centre, Trombay, with a total integral thermal neutron dose of 5×10^{15} (nvt), where nv represents the thermal neutron flux available for irradiation in the reactor (5×10^{12} n cm² sec for IC-1 position of CIRUS Reactor) and t is the irradiation time. The Lexan discs were etched in 6N NaOH at a temperature of 70 C for 30 min. The induced fission track density on Lexan discs was recorded using Olympus binocular research microscope with a magnification of $\times 600$. Density of fission tracks was measured on surfaces showing uniform distribution of uranium. In order to avoid errors due to the external contamination, only the inner portions of the discs were scanned.

Uranium concentration in the rock sample was measured by comparison between track densities registered on Lexan detectors around the sample pellet and that of the standard glass pellet⁵⁻⁷, from the relation:

$$C_{\text{ppm}}(\text{sample}) = \frac{\rho_{\text{(sample)}}}{\rho_{\text{(standard)}}} \times C_{\text{ppm}}(\text{standard}) \quad \dots (1)$$

where ρ is the induced fission track density and C_{ppm} denotes the U content.

In order to establish the correlation between uranium, phosphorus and magnesium in phosphorites, the magnesium content was determined complexometrically using EDTA titrations and phosphorus content was measured gravimetrically by precipitating phosphate as phosphomolybdate. U, Mg and P₂O₅ contents estimated are summarized in Table I.

Results and discussion—The present investigations are based on the uranium estimation in phosphorite samples collected from Durmala, Maldeota and Parritibba deposits of Mussoorie syncline. The uranium content varies from 0.01 to 0.06 %. Phosphorite sample from Parritibba mine has yielded maximum uranium content of 0.06 % which is significant from the prospecting and exploration angle.

Udas and Mahadevan³ have reported an average uranium content of 0.03 % in the phosphorite horizon of Mussoorie syncline on the basis of geochemical investigation by Sarswat *et al.*⁸ Thus results obtained here corroborate the earlier findings⁸. From the data (Table I) it is evident that there is no direct correlation between uranium, magnesium and phosphorous contents of these phosphorites. The absence of correlation seems to be due to the fact that chemogenic precipitation of phosphates is possible under a much wider range of Eh-pH conditions than uranium³.

The authors are thankful to the Managing Director, Pyrites, Phosphates and Chemicals Ltd, Dehra Dun.

Table I—U, Mg and P₂O₅ Contents (in ppm) in Mussoorie Phosphorites (Number of samples studied in each case is three)

Sample location	U (Mean)	Mg	P ₂ O ₅
Maldeota	124.55 ± 0.99*	1.90	31.20
Durmala	143.82 ± 1.69	2.70	24.70
Parritibba	612.11 ± 1.16	2.30	33.40

*Standard error of the mean $S_{\bar{u}} = \left[\frac{1}{N(N-1)} \sum_{i=1}^N (X_i - \bar{X})^2 \right]^{1/2}$

U.P. for facilities extended to our teams during sample collection. They also thankfully acknowledge the help of Mr P S Suri and Dr Pritam Singh in the collection and analysis of the samples.

References

- 1 Alder H H, *Proceedings of a Symposium on the Formation of Uranium Ore Deposits*, held in Athens, Greece, 6-10 May 1974, (IAEA, Vienna) 1974, 141.
- 2 Barthel F H, *Proceedings of a Symposium on the Formation of Uranium Ore Deposits*, held in Athens, Greece, 6-10 May, 1974 (IAEA, Vienna) 1974, 277.
- 3 Udas G R & Mahadevan T M, *Proceedings of a Symposium on the Formation of Uranium Ore Deposits*, held in Athens, Greece, 6-10 May, 1974 (IAEA, Vienna) 1974, 425.
- 4 Fisher D E, *Anal Chem (USA)*, **42** (1970) 414.
- 5 Nagpal M K & Nagpal K K, *Chayanica Geologica (India)*, **2** (1976) 156.
- 6 Virk H S & Koul S L, *C R Hebd Seances Acad Sci Ser B (France)*, **284** (1977) 295.
- 7 Koul S L & Virk H S, *Czech J Phys Sect B (Czechoslovakia)*, **30** (1980) 778.
- 8 Sarswat A C, Sankaran A V, Varadarajan H N, et al., *Geochemical Data on the Uraniferous Phosphorites of Mussoorie, Dehra Dun District, U.P., India*, Unesco-Ecafe session on "Geochemical Prospecting", Colombo, Ceylon, 1970.

Electronic Spectral Study of Praseodymium(III) Complexes with Cysteine & Diols

ASHOK KOTHARI, SUDHINDRA N MISRA* & M P BHUTRA**

Department of Chemistry, University of Jodhpur, Jodhpur

Received 1 May 1982; accepted 1 October 1982

The electronic spectra of the complexes of praseodymium(III) with cysteine and diols have been studied and the values of Slater-Condon (F_k), Lande' spin-orbit interaction (ζ_{4f}), oscillator strength (P) and Judd-Ofelt intensity parameter (T_λ) have been calculated. The calculated values of the nephelauxetic ratio β and bonding parameter $b^{1/2}$ suggest covalent character of these complexes.

The structural studies of the lanthanide coordination compounds in solutions have been carried out recently by observing nephelauxetic band shift in different environments¹⁻⁴. The characteristics of the spectrum such as position, intensity and shape of the bands are helpful in studying the mechanism of the intermolecular interaction, viz. interelectronic repulsion, spin-orbit interaction, nephelauxetic effect and bonding in the complexes.

Misumi *et al.*⁵ have studied the amino acid binary complexes of Pr^{3+} and Nd^{3+} in alkaline environment, and the oxygen and nitrogen donor mixed ligand complexes of praseodymium have been studied by us^{6,7}.

The present note reports the electronic spectral study of ten ternary complexes of Pr^{3+} having cysteine as primary ligand and diols as secondary ligands. The values of various energy parameters like Slater-Condon (F_k), Lande' spin-orbit interaction (ζ_{4f}) and intensity parameter like oscillator strength (P), Judd-Ofelt (T_λ), nephelauxetic ratio (β) and bonding ($b^{1/2}$) have been calculated from the observed spectra by partial multiple regression method. The results have been used to interpret the bonding and structure of the complexes.

L-Cysteine and diols obtained from Fluka AG (Switzerland) and BDH Ltd (England), praseodymium chloride (99.9% pure) from Indian Rare Earths (Alwayee, Kerala), were used.

The complexes have been synthesized by the method^{8,9} reported earlier and were characterized by elemental analysis. The absorption spectra were taken

on Carl-Zeiss VSU-2 Spectrophotometer in the region 380-650 nm in methanol (Fig. 1).

Energy parameters—By assuming hydrogenic radial function for Pr^{3+} the values of ΔF_2 and $\Delta\zeta_{4f}$ have been computed using the free ion energy levels¹⁰ by partial-multiple regression method on the basis of the equation:

$$E_{\text{obs}} = E_{0j} + \sum_{k=2,4,6} \left(\frac{\partial E_j}{\partial F_k} \right) \Delta F_k + \left(\frac{\partial E_j}{\partial \zeta_{4f}} \right) \Delta \zeta_{4f}$$

where the various letters have their usual meaning.

The nephelauxetic ratio β is given by the equation:

$$\beta = \frac{F_2^c}{F_2^f}$$

where the superscripts c and f refer to complex and free ion values.

Henrie and Choppin have introduced another parameter b known as mixing coefficient signifying the amount of the bonding of the $4f$ orbital and ligand group orbital and is related to β through the following relation:

$$b^{1/2} = \left(\frac{1 - \beta}{2} \right)^{1/2}$$

The observed and calculated energy values for various transitions of $\text{Pr}(\text{Cyst})$ (diol), $\text{Pr}(\text{Cyst})_2$ (diol) and $\text{Pr}(\text{Cyst})(\text{diol})_2$ ternary complexes are reported in Table 1.

The rms deviation between observed and calculated energy lies between 87 to 125. The high value of rms deviation seems to be due to the assumption of radial wavefunction being hydrogenic. The energy of a transition does not change appreciably due to change of ligand in a set of complexes which shows that the

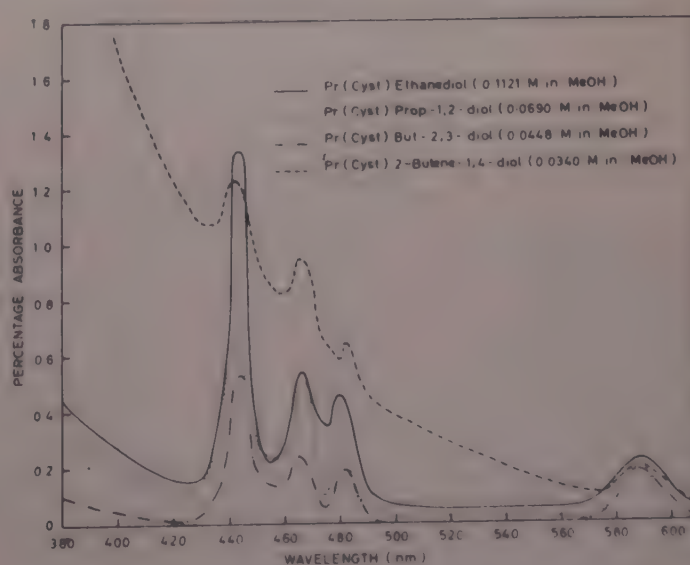


Fig. 1—Absorption spectra of ternary complexes (MLL)

*Department of Chemistry, M S University of Baroda, Baroda.

**Department of Physics, University of Jodhpur, Jodhpur.

coordination environment around metal ion in the inner sphere complexation remains unaltered due to change in ligand.

The decrease in Slater-Condon parameter (F_2 , F_4 , F_6) and Lande' parameter (ζ_{4f}) from that of free ion on complexation (Table 2) indicates the expansion of central metal ion on complexation. The increase in the value of $b^1/2$ suggests that the covalency of the complexes increases as the diols are changed in the order: ethanediol, propane-1,2-diol, butane-2,3-diol

and 2-butane-1,4-diol which forms a nephelauxetic series in the present complexes.

Intensity parameter—The values of oscillator strength (P) for all the four peaks in each complex have been computed by using the following relationship:

$$P = 4.6 \times 10^{-9} \times \epsilon_m \times \Delta\nu_{1/2}$$

where ϵ_m and $\Delta\nu_{1/2}$ are the molar extinction coefficient and half band width and are given in Tables 3 along with the values of T_λ parameters which have been

Table 1—Computed Values of Energies (in cm^{-1}) of the Bands of Pr(III) Complexes with Cysteine and Diols

Complex	3P_2		3P_1		3P_0		1D_2		rms deviation (σ)
	E_{exptl}	E_{calc}	E_{exptl}	E_{calc}	E_{exptl}	E_{calc}	E_{exptl}	E_{calc}	
Pr(Cyst)(ethanediol)	22523	22487	21413	21333	20790	20832	16978	17160	103
Pr(Cyst)(prop-diol)	22573	22533	21413	21376	20790	20730	17007	17171	89
Pr(Cyst)(but-diol)	22472	22514	21413	21356	20747	20826	17007	17144	87
Pr(Cyst)(butene-diol)	22548	22525	21413	21339	20704	20764	16978	17157	102
Pr(Cyst) ₂ (ethanediol)	22548	22494	21413	21334	20747	20804	16949	17149	114
Pr(Cyst) ₂ (prop-diol)	22573	22537	21459	21360	20747	20801	16978	17176	115
Pr(Cyst) ₂ (butene-diol)	22548	22494	21413	21321	20704	20770	16920	17135	124
Pr(Cyst)(ethanediol) ₂	22573	22465	21413	21324	20790	20833	16978	17151	113
Pr(Cyst)(prop-diol) ₂	22573	22537	21459	21360	20747	20801	16978	17176	115
Pr(Cyst)(butene-diol) ₂	22573	22557	21505	21374	20747	20789	16978	17186	125

Propane-1,2-diol = prop-diol; butane-2,3-diol = but-diol

2-butene-1,4-diol = butene-diol

Table 2—Computed Values of Various Spectroscopic Parameters (F_k , ζ_{4f} , β , $b^1/2$, $\% \delta$) of Pr(III) Complexes

Complexes	F_2 (cm^{-1})	F_4 (cm^{-1})	F_6 (cm^{-1})	ζ_{4f} (cm^{-1})	β	$b^1/2$	$\% \delta$
Pr ³⁺ (free ion)	322.09	44.46	4.87	741.00	—	—	—
Pr(Cyst)(ethanediol)	311.77	43.04	4.71	680.59	0.9679	0.1265	3.32
Pr(Cyst)(prop-diol)	311.40	42.98	4.70	693.24	0.9668	0.1288	3.43
Pr(Cyst)(but-diol)	310.80	42.90	4.69	695.18	0.9649	0.1323	3.64
Pr(Cyst)(butene-diol)	309.58	42.73	4.67	716.30	0.9611	0.1393	4.05
Pr(Cyst) ₂ (ethanediol)	310.76	42.90	4.69	694.74	0.9648	0.1326	3.65
Pr(Cyst) ₂ (prop-diol)	310.25	42.83	4.68	714.56	0.9632	0.1355	3.82
Pr(Cyst) ₂ (butene-diol)	309.87	42.77	4.68	716.30	0.9620	0.1377	3.95
Pr(Cyst)(ethanediol) ₂	311.53	43.00	4.70	688.12	0.9672	0.1280	3.39
Pr(Cyst)(prop-diol) ₂	310.40	42.85	4.69	709.00	0.9637	0.1347	3.77
Pr(Cyst)(butene-diol) ₂	310.29	42.83	4.69	714.21	0.9633	0.1355	3.81

Table 3—Computed Values of T_λ & Oscillator Strength of Pr(III) Complexes

Complexes	$T_\lambda \times 10^9$			3P_2		3P_1		3P_0		1D_2		rms deviation $P \times 10^6$
	$T_2 \times 10^9$	$T_4 \times 10^9$	$T_6 \times 10^9$	P_{exptl}	P_{calc}	P_{exptl}	P_{calc}	P_{exptl}	P_{calc}	P_{exptl}	P_{calc}	
Pr(Cyst)(ethanediol)	4.90	0.84	4.15	13.30	13.30	3.65	3.09	2.47	3.03	3.69	3.69	0.40
Pr(Cyst)(prop-diol)	35.06	1.41	3.83	14.78	14.78	8.68	5.16	2.04	5.07	3.94	3.94	1.69
Pr(Cyst)(but-diol)	61.55	1.45	5.06	16.63	16.63	5.20	5.33	5.35	5.22	8.52	8.52	0.09
Pr(Cyst)(butene-diol)	55.91	1.64	5.41	17.88	17.88	9.92	5.90	2.08	6.03	7.72	7.72	2.72
Pr(Cyst) ₂ (ethanediol)	52.71	1.26	4.40	14.47	14.47	4.35	4.60	4.73	4.51	6.56	6.56	0.17
Pr(Cyst) ₂ (prop-diol)	25.84	1.24	4.88	15.94	15.94	5.15	4.53	3.85	5.03	5.81	5.81	0.67
Pr(Cyst) ₂ (butene-diol)	2.87	0.79	5.84	18.50	18.50	3.67	2.88	2.05	2.83	5.49	5.49	1.39
Pr(Cyst)(ethanediol) ₂	26.40	0.45	4.10	12.92	12.92	2.88	1.66	0.43	1.19	2.58	2.58	0.85
Pr(Cyst)(prop-diol) ₂	6.70	0.57	4.21	13.36	13.36	3.47	2.09	0.70	2.05	3.59	3.59	0.96
Pr(Cyst)(butene-diol) ₂	15.32	0.92	5.40	17.29	17.29	3.48	3.40	3.25	3.32	5.71	5.71	0.04

computed from the four equations obtained by using the Judd-Ofelt relationship:

$$P_{\text{obs}} = [U^{(2)}]^2 \nu \times T_2 + [U^{(4)}]^2 \nu \times T_4 + [U^{(6)}]^2 \nu \times T_6$$

In the computation of T_λ , the values of matrix elements $[U^{(\lambda)}]^2$ as reported by Carnall *et al.*¹¹ have been used.

The rms deviation between observed and calculated values of oscillator strength varies from 0.04×10^{-6} to 2.72×10^{-6} (Table 3). The low rms deviations suggest the suitability of Judd-Ofelt relation used for computing the intensity of a transition for the present set of complexes.

The ratio of the parameters T_4 and T_6 is fairly constant in a set of complexes which indicates that the symmetry of complexes in solution remains invariant due to change of ligand. The parameter T_2 which is sensitive to the environment¹¹ changes appreciably when the ligands are changed. The negative value of T_2 has no special physical significance. This may be due to the appearance of a $f \leftrightarrow d$ transition in the visible region.

Thanks are due to the University Grants Commission, New Delhi for providing with a fellowship to one of us (AK). The authors are also thankful to Prof. R C Kapoor, Department of Chemistry and Prof. A N Nigam, Department of Physics, University of Jodhpur, Jodhpur, for providing necessary facilities during the work.

References

- 1 Henrie D E & Choppin G R, *J Chem Phys (USA)*, **43** (1968) 477.
- 2 Peacock R D, *Structure and bonding* (Springer-Verlag-Berlin & Heidel, New York) **22** (1975) 88.
- 3 Wybourne B G, *Spectroscopic properties of rare-earths* (Interscience, New York), 1965.
- 4 Megh Singh, Bhutra M P, Vaishnava P P & Misra S N, *Bull Chem Soc Jpn (Japan)*, **51** (1978) 1241.
- 5 Misumi S, Kida S, Isobe F & Inazumi A, *Bull Chem Soc Jpn (Japan)*, **41** (1968) 25.
- 6 Joshi G K, Bhutra M P & Misra S N, *J Inorg Nucl Chem (GB)*, **43** (1981) 525.
- 7 Kothari A, Jain R K, Ahmed A & Misra S N, *J Inorg Nucl Chem (GB)*, **43** (1981) 2905.
- 8 Oki H, *Bull Chem Soc Jpn (Japan)*, **50** (1977) 680.
- 9 Yasoi T, *Bull Chem Soc Jpn (Japan)*, **50** (1977) 2632.
- 10 Carnall W T, Field P R & Wybourne B G, *J Chem Phys (USA)*, **42** (1965) 3797.
- 11 Bhutra M P & Gupta A K, *Indian J Pure & Appl Phys*, **20** (1982) 954.

Spectroscopic Studies of Oxovanadium(IV) Complexes of Biguanide, Dibiguanides & *o*-Methyl-1-amidinourea

A SYAMAL*

Chemistry Department, Regional Engineering College, Kurukshetra
132 119

Received 6 February 1982; revised received 6 October 1982

The ESR [in diamagnetic nickel(II) complex matrix], IR and electronic spectra of oxovanadium(IV) complexes of biguanide; ethylene-, trimethylene-, tetramethylene-, hexamethylene-, piperazine-dibiguanides and of *o*-methyl-1-amidinourea are recorded. The ESR spectra of all these complexes exhibit 8 perpendicular and 8 parallel lines. The ESR parameters for a typical complex, viz. $\text{VO}(\text{OH}_2)(\text{biguanide})_2$, are determined as $g_{\perp} = 1.99$, $A_{\perp} = 54$, $g_{\parallel} = 1.94$, $A_{\parallel} = 154$. The ESR parameters are very similar in the oxovanadium (IV) complexes of biguanide, *o*-methyl-1-amidinourea and dibiguanides indicating the similarity of bonding in these complexes. This fact is further confirmed from the dipolar term $|A_{\perp} - A_{\parallel}|$ which is essentially constant. The observed low values of $\nu(\text{V}=\text{O})$ ($\sim 940 \text{ cm}^{-1}$) are consistent with the strong out-of-plane $d\pi\text{-}p\pi$ bonding. These complexes exhibit three electronic spectral bands due to $d_{xy} \rightarrow d_{xz}$, d_{yz} , $d_{xy} \rightarrow d_{x^2 - y^2}$ and $d_{xy} \rightarrow d_{z^2}$ transitions.

Biguanides, dibiguanides and *o*-alkyl-1-amidinoureas are regarded as strong-field ligands which have produced metal complexes of very high formation-constant values. They have stabilized a large number of uncommon oxidation states of transition metal ions [e.g. Ni(III), Co(I), Mn(IV), Ag(III), Au(III), Mo(III), Ir(IV), etc.] and the metal complexes show aromatic character^{1,2}. We report in this note the ESR, IR and electronic spectral studies of oxovanadium (IV) complexes of biguanide, ethylenedibiguanide (endibig), trimethylenedibiguanide (tndibig), tetramethylenedibiguanide (tetramedibig), hexamethylenedibiguanide (hexamedibig), piperazinedibiguanide (piperazinedibig) and *o*-methyl-1-amidinourea (OMAU).

Experimental details— $\text{VO}(\text{OH}_2)(\text{biguanide})_2$ and $\text{VO}(\text{OH}_2)(\text{endibig})$ were prepared according to the already known procedure¹. The complexes $\text{VO}(\text{OH}_2)(\text{tndibig})$, $\text{VO}(\text{OH}_2)(\text{tetramedibig})$, $\text{VO}(\text{OH}_2)(\text{hexamedibig})$ and $\text{VO}(\text{OH}_2)(\text{piperazinedibig})$ were prepared by following a procedure similar to $\text{VO}(\text{OH}_2)(\text{biguanide})_2$, and gave a satisfactory vanadium and nitrogen (V, N) analysis. $\text{VO}(\text{OH}_2)(\text{OMAU})_2$ was prepared by the known method². Oxovanadium(IV)-doped samples of diamagnetic NiL_2 or NiL' (where $L = \text{biguanide}$ or *o*-methyl-1-amidinourea; $L' = \text{endibig}$, tndibig, tetramedibig,

hexamedibig or piperazinedibig) were prepared by following similar procedures for the synthesis of corresponding oxovanadium(IV) complexes but using a solution of nickel (II) nitrate hexahydrate containing 5-10% of $\text{VOSO}_4 \cdot \text{H}_2\text{O}$.

The ESR spectra were measured using a Varian V 4502-12 X-band spectrometer with 100 kc/s modulation and a 9" electromagnet. A minute powdered sample of diphenylpicrylhydrazide (Aldrich Chemical Co, USA) free radical was used as a *g*-marker in dual channel cavity and the frequency was monitored with the help of a frequency meter. The *g* values were calculated from the *H* values using a second-order correction: $H = H_{4,5} + 31A^2/4H_{4,5}$ where $H_{4,5}$ is the field at the middle of the separation between the fourth and fifth lines; *A*, the vanadium nuclear hyperfine splitting constant. Electronic spectra were recorded in nujol mull with a Cary-14 recording spectrophotometer. The IR spectra were recorded in nujol mull on a Perkin-Elmer-621 spectrophotometer calibrated with polystyrene film.

Results and discussion—The oxovanadium(IV) complexes of these ligands were doped into the corresponding diamagnetic nickel(II) complexes in order to obtain magnetic dilution and the ESR data are presented in Table 1. The pure polycrystalline samples at room temperature exhibited a single exchange-narrow line at $g = \sim 1.97$. But magnetic dilution to the corresponding diamagnetic nickel(II) complexes results in the resolution of vanadium(IV) nuclear hyperfine splitting; consequently, the ESR spectrum consists of 8 parallel and 8 perpendicular lines. A typical ESR spectrum is presented in Fig. 1. Nitrogen-14 superhyperfine splitting could not be located in the ESR spectra at 77 K and at room temperature as the nitrogen superhyperfine coupling constants in oxovanadium(IV) complexes are very small³. It is interesting to note that nitrogen superhyperfine components are detectable in the ESR spectrum⁴ of $\text{Cu}(\text{biguanide})_2$. Although V and Cu nuclei have quadrupole moments giving rise to the line-broadening, the quadrupole moment of V is twice that of Cu; hence it may not be possible to locate the nitrogen superhyperfine components in vanadium(IV) complexes as these are small. The ESR data indicated that $g_{\perp} > g_{\parallel}$ and $A_{\perp} < A_{\parallel}$ are according to the expectations. The ESR spectra of the complexes in dilute acetic acid (25% glacial acetic acid-water by volume) exhibit 8 line spectra and reveal decom-

Table 1—ESR Data of Oxovanadium(IV) Complexes

Complex	Medium	$g_{av}^{(a)}$	g_{\perp}	g_{\parallel}	$\langle A \rangle^{(b)}$	A_{\perp}	A_{\parallel}
VO(OH ₂)(biguanide) ₂	Ni(II) complex	1.97	1.99	1.94	87	54	154
	25% Glacial acetic acid-water by volume	1.97	—	—	101	—	—
VO(OH ₂)(OMAU) ₂	Ni(II) complex	1.97	1.99	1.94	87	50	160
	25% Glacial acetic acid-water by volume	1.97	—	—	101	—	—
VO(OH ₂)(endibig)	Ni(II) complex	1.97	1.99	1.94	88	55	153
VO(OH ₂)(tndibig)	Ni(II) complex	1.97	1.99	1.94	88	56	152
VO(OH ₂)(tetramedibig)	Ni(II) complex	1.97	1.99	1.94	87	53	155
VO(OH ₂)(hexamedibig)	Ni(II) complex	1.97	1.99	1.94	87	53	155
VO(OH ₂)(piperazinedibig)	Ni(II) complex	1.97	1.99	1.94	87	54	154
VO(phthalocyanine) ⁶	Free ligand	—	1.989	1.966	—	56	158
VO(tetraphenylporphine) ⁷	CHCl ₃	1.979	1.989	1.961	88.2	51.7	161.2

^(a) $g_{av} = \frac{1}{3}(g_{\parallel} + 2g_{\perp})$ except for VO(OH₂)(biguanide)₂ and VO(OH₂)(OMAU)₂ in dilute acetic acid

^(b) $\langle A \rangle = \frac{1}{3}(A_{\parallel} + 2A_{\perp})$ except for spectra in dilute acetic acid. The $\langle A \rangle$, A_{\perp} and A_{\parallel} are in units of 10^{-4} cm^{-1}

Table 2—Electronic Spectral Data of Oxovanadium(IV) Complexes

Complex	Medium	$\nu_{\max} \text{ cm}^{-1}$
VO(OH ₂)(biguanide) ₂	Nujol	16700, 23200,
	50% Glacial acetic acid-water by volume	25500, 13000, 16500
VO(OH ₂)(OMAU) ₂	Nujol	14900, 17200,
	50% Glacial acetic acid-water by volume	26700, 13200, 16100
VO(OH ₂)(endibig)	Nujol	16730, 23230, 25550
VO(OH ₂)(tndibig)	Nujol	16700, 23200, 25600
VO(OH ₂)(tetramedibig)	Nujol	16650, 23200, 25500
VO(OH ₂)(hexamedibig)	Nujol	16700, 23200, 25600
VO(OH ₂)(piperazinedibig)	Nujol	16680, 23200, 25500

position of the complexes to aquo-acetato species. This is reflected in the increase in the average vanadium nuclear hyperfine splitting, $\langle A \rangle$. The electronic spectral data (Table 2) also support the decomposition of the complexes in dilute acetic acid solutions.

The ESR spectrum of oxovanadium(IV) complexes in tetragonal symmetry is described by the following spin-Hamiltonian⁵:

$$H = g_{\parallel} \beta H_z S_z + g_{\perp} \beta (H_x S_x + H_y S_y) + A_{\parallel} I_z S_z + A_{\perp} (I_x S_x + I_y S_y) \quad \dots (1)$$

A comparison of the dipolar term $|A_{\perp} - A_{\parallel}|$ for oxovanadium(IV) complexes of phthalocyanine⁶, tetraphenylporphine⁷ and the present ligands indicates that it is almost constant and emphasizes the similarity of bonding in the complexes of these ligands. It has

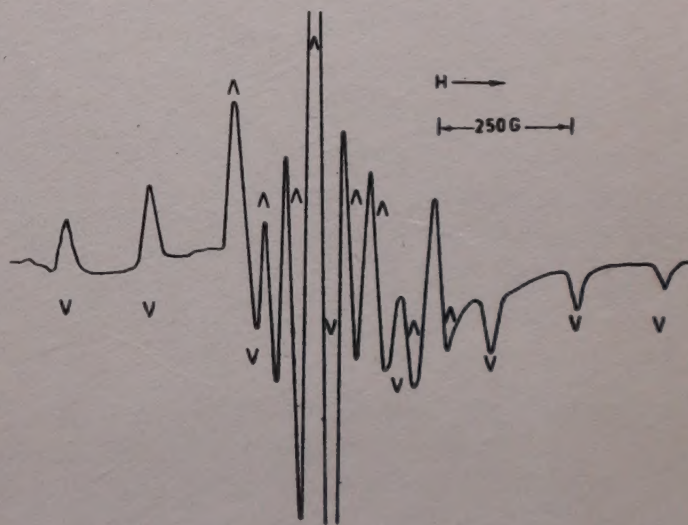


Fig. 1—A typical ESR spectrum

been observed that $\langle A \rangle$ decreases as the ligand field strength increases. A comparison of $\langle A \rangle$ values with other oxovanadium(IV) complexes indicates that the present ligands rank as strong-field ligands³. The ratio of axial charge to equatorial charge (ρ) is obtained from the relation:

$$\rho = \frac{3[\Delta E(d_{xy} \rightarrow d_{z^2})] - 4[\Delta E(d_{xy} \rightarrow d_{xz, yz})]}{2[\Delta E(d_{xy} \rightarrow d_{x^2 - y^2})]} - \frac{1}{2} \quad \dots (2)$$

The values of ρ for the present complexes have been found to vary from 0.096 to -0.291. From an empirical $\langle A \rangle$ versus ρ relation⁸, $\langle A \rangle$ is estimated to be 113 G when $\rho = -0.290$. For VO(OH₂)(biguanide)₂, $\langle A \rangle$ is 95 G and this lack of correlation is indicative of the significant metal-ligand covalency⁸. The ESR study thus indicates that the nature of bridging group in

dibiguanides has little effect on the bonding parameters.

These complexes exhibit three electronic spectral bands (Table 2) around 17000, 23000 and 25000 cm^{-1} due to $d_{xy} \rightarrow d_{xz}$, d_{yz} , $d_{xy} \rightarrow d_{x^2-y^2}$ and $d_{xy} \rightarrow d_{z^2}$ transitions respectively, according to the Ballhausen-Gray scheme⁹. The red shift of the bands occurs in the dilute acetic acid solution of the complexes and this indicates decomposition of the complexes in dilute acetic acid solution.

A very strong band around 940 cm^{-1} in the IR spectra of the complexes is assigned to $\nu(\text{V}=\text{O})$ stretch. This value is remarkably lower than those for other oxovanadium(IV) complexes and this is consistent with the presence of strong out-of-plane metal-ligand $d\pi \rightarrow p\pi$ bonding which accounts for the decrease in $\nu(\text{V}=\text{O})$ stretch.

This work is supported by the University Grants Commission, New Delhi.

References

- 1 Ray P, *Chem Rev (USA)*, **61** (1961) 313.
- 2 Dutta R L & Syamal A, *Coord Chem Rev (Netherlands)*, **2** (1967) 441.
- 3 Selbin J, *Coord Chem Rev (Netherlands)*, **1** (1966) 293.
- 4 Wasson J R & Zacharopoulos P, *J Inorg & Nucl Chem (GB)*, **31** (1969) 3881.
- 5 O'Reilly D E, *J Chem Phys (USA)*, **29** (1958) 1188.
- 6 Assour J M, Goldmacher J & Harrison S E, *J Chem Phys (USA)*, **43** (1965) 159.
- 7 Assour J M, *J Chem Phys (USA)*, **43** (1965) 2477.
- 8 Kuska H A & Rogers M T, *Inorg Chem (USA)*, **5** (1966) 313.
- 9 Ballhausen C J & Gray H B, *Inorg Chem (USA)*, **1** (1962) 111.

THE WEALTH OF INDIA

An Encyclopaedia of Indian Raw Materials and Industrial Products, published in two series:
(i) **Raw Materials**, and (ii) **Industrial Products**.

RAW MATERIALS

The articles deal with Animal Products, Dyes & Tans, Essential Oils, Fats & Oils, Fibres & Pulps, Foods & Fodders, Drugs, Minerals, Spices & Flavourings, and Timbers and other Forest products. Names in Indian languages, and trade names are provided.

For important crops, their origin, distribution, evolution of cultivated types, and methods of cultivation, harvesting and storage are mentioned in detail. Data regarding area and yield and import and export are provided. Regarding minerals, their occurrence and distribution in the country and modes of exploitation and utilization are given. The articles are well illustrated. Adequate literature references are provided.

Eleven volumes of the series covering letters A – Z have been published.

Vol. I(A-B) Rs. 80.00; Vol. II (C) Rs. 95.00; Vol. III (D-E) Rs. 40.00; Vol. IV (F-G) Rs. 65.00; Vol. IV: Suppl. Fish & Fisheries Rs. 40.00; Vol. V (H-K) Rs. 75.00; Vol. VI (L-M) Rs. 90.00; Vol. VI: Suppl. Livestock Rs. 60.00; Vol. VII (N-Pc) Rs. 30.00; Vol. VIII (Ph-Re) Rs. 86.00; Vol. IX (Rh-So) Rs. 104.00; Vol. X (Sp-W) Rs. 152.00; Vol. XI (X-Z) Rs. 102.00.

INDUSTRIAL PRODUCTS

Includes articles giving a comprehensive account of various large, medium and small scale industries. Some of the major industries included are: Acids, Carriages, Diesel Engines, Fertilizers, Insecticides & Pesticides, Iron & Steel, Paints & Varnishes, Petroleum Refining, Pharmaceuticals, Plastics, Ship & Boat-building, Rubber, Silk, etc.

The articles include an account of the raw materials and their availability, manufacturing processes, and uses of products, and industrial potentialities. Specifications of raw materials as well as finished products and statistical data regarding production, demand, exports, imports, prices, etc., are provided. The articles are suitably illustrated. References to the sources of information are provided.

Nine volumes of the series covering letters A – Z have been published.

Part I (A-B) Rs. 54.00; Part II (C) Rs. 64.00; Part III (D-E) Rs. 25.00; Part IV (F-H) Rs. 25.00; Part V (I-L) Rs. 30.00; Part VI (M-Pi) Rs. 28.00; Part VII (Pl-Sh) Rs. 60.00; Part VIII (Si-Ti) Rs. 66.00; Part IX (To-Z) Rs. 80.00.

HINDI EDITION: BHARAT KI SAMPADA—PRAKRITIK PADARTH

Vols. I to VI and two supplements of Wealth of India—Raw Materials series in Hindi already published.

Published Volumes:

Vol. I (अ-औ) Rs. 38; Vol. II (क) Rs. 36; Vol. III (ख-न) Rs. 36; Vol. IV (प) Rs. 83; Vol. V (फ-मेरे) Rs. 60; Vol. VI (मेल-रु) Rs. 80.

Supplements:

Fish & Fisheries (Matsya & Matsyaki) Rs. 49; Liverstock (*Pashudhan aur Kukkut Palan*) Rs. 34.

Vols. VII to XI under publication.

Please contact:

Manager (Sales & Advertisement)

PUBLICATIONS & INFORMATION DIRECTORATE, CSIR

Hillside Road, New Delhi 110012

CSIR PUBLICATIONS

WEALTH OF INDIA

An encyclopaedia of the economic products and industrial resources of India issued in two series

RAW MATERIALS SERIES—contains articles on plant, animal and mineral resources

	Rs	\$	£
Vol. I (A-B)	80.00	30.00	13.00
Vol. II (C)	95.00	33.00	17.00
Vol. III (D-E)	40.00	12.00	4.00
Vol. IV (F-G)	65.00	27.00	12.00
Supplement (Fish & Fisheries)	40.00	16.00	7.00
Vol. V (H-K)	75.00	28.00	12.50
Vol. VI (L-M)	90.00	34.00	15.00
Supplement (Livestock)	60.00	18.00	6.00
Vol. VII (N-Pe)	30.00	9.00	3.00
Vol. VIII (Ph-Re)	86.00	32.00	14.00
Vol. IX (Rh-So)	104.00	35.00	19.00
Vol. X (Sp-W)	152.00	65.00	23.00
Vol. XI (X-Z)	102.00	42.00	20.00

INDUSTRIAL PRODUCTS SERIES—

deals with major, small-scale and cottage industries

Part I (A-B)	54.00	20.00	9.00
Part II (C)	64.00	24.00	11.00
Part III (D-E)	25.00	7.50	2.50
Part IV (F-H)	25.00	7.50	2.50
Part V (I-L)	30.00	9.00	3.00
Part VI (M-Pi)	28.00	8.00	2.80
Part VII (Pi-Sh)	60.00	18.00	6.00
Part VIII (Si-Ti)	66.00	27.00	10.00
Part IX (To-Z)	80.00	34.00	12.00

BHARAT KI SAMPADA (Hindi Edition of Wealth of India, Raw Materials)

Vol. I (अ-औ)	38.00	16.00	6.50
Vol. II (क)	36.00	15.00	6.00
Vol. III (ख-न)	36.00	15.00	6.00
Vol. IV (प)	83.00	34.00	16.00
Vol. V (फ-मेरे)	60.00	22.00	10.00
Vol. VI (मेल-ह)	80.00	27.00	13.00
Livestock (Kukkut Palan)	34.00	15.00	6.00
Fish & Fisheries (Matsya aur Matsyaki)	49.00	21.00	8.00
A Dictionary of Generic & Specific Names of Plants and Animals Useful to Man with their English and Latin pronunciation in Devanagari	30.00	11.00	5.00

OTHER PUBLICATIONS

Proceedings seminar on primary communications in Science & Technology in India by Sh. R.N. Sharma & S. Seetharama	52.00	17.50	9.00
Flora of Delhi by J.K. Maheshwari	28.00	8.00	2.80
Indian Fossil Pteridophytes by K.R. Surange	23.00	8.00	2.30
Indian Thysanoptera by T.N. Ananthakrishnan	26.00	8.00	2.60
The Millipede Thyropygus by G. Krishnan	12.00	3.50	1.20
Drug Addiction with special reference to India by R.N. Chopra & I.C. Chopra	12.00	3.50	1.20
Glossary of Indian Medicinal Plants by R.N. Chopra & I.C. Chopra	35.00	13.00	6.00
Fluidization & Related Processes	12.00	4.00	1.20
Evolution of Life by M.S. Randhawa, A.K. Dey, Jagjit Singh & Vishnu Mitre	22.50	7.00	2.25
Collected Scientific Papers of Meghnad Saha	30.00	9.00	3.00
Proteaceae by C. Venkata Rao	34.00	11.00	3.40
Pinus by P. Maheshwari & R.M. Konar	30.00	11.00	5.00
Cellulose Research I	3.00	0.90	0.30
Cellulose Research II	6.00	1.75	0.60
Chemical Process Design	9.00	2.50	0.90
Low Temperature Carbonization of Non-coking Coals & Lignites & Briquetting Coal Fines:			
Vol. I	17.50	5.50	1.75
Vol. II	17.50	5.50	1.75
Nucleic Acids	10.00	3.00	1.00
IGY Symposium: Vol. I	9.00	2.50	0.90
IGY Symposium: Vol. II	9.00	2.50	0.90
CNS Drugs	16.50	5.00	1.65
Kinetics of Electrode Processes & Null Points of Metals	2.50	0.75	0.25
Indian Sardines by R.V. Nair	22.00	7.00	2.20
Termite Problems in India	9.00	3.00	0.90
Loranthaceae by B.M. Johri & S.P. Bhatnagar	32.00	11.00	3.20
Abies and Picea by K.A. Chowdhury	14.00	6.00	2.10
Gnetum by P. Maheshwari and Vimla Vasil	20.00	6.00	2.00
Aquatic Angiosperms by K. Subramanyam	20.00	6.00	2.00
Supplement to Glossary of Indian Medicinal Plants by R.N. Chopra, I.C. Chopra & B.S. Varma	18.00	7.00	3.00
Herbaceous Flora of Dehra Dun by C.R. Babu	144.00	60.00	22.00
Diosgenin and Other Steroid Drug Precursors by Y.R. Chadha & Miss L.V. Asolkar	36.00	13.00	6.00
Research & Development Management by Inder Dev	25.00	10.00	—
Rural Development and Technology—A Status Report-cum Bibliography by P.R. Bose & V.N. Vashist	100.00	38.00	17.00

Packing and Postage extra

Please contact:

Manager (Sales & Advertisement)
PUBLICATIONS & INFORMATION DIRECTORATE, CSIR
Hillside Road, New Delhi 110012